Failure processes in elastic fiber bundles

Srutarshi Pradhan*

Department of Physics, Norwegian University of Science and Technology, NO-7491 Trondheim, Norway and SINTEF Petroleum Research, NO-7465 Trondheim, Norway

Alex Hansen†

Department of Physics, Norwegian University of Science and Technology, NO-7491 Trondheim, Norway

Bikas K. Chakrabarti‡

Theoretical Condensed Matter Physics Division and Centre for Applied Mathematics and Computational Science, Saha Institute of Nuclear Physics, 1/AF Bidhan Nagar, Kolkata 700064, India

(Published 1 March 2010)

The fiber bundle model describes a collection of elastic fibers under load. The fibers fail successively and, for each failure, the load distribution among the surviving fibers changes. Even though very simple, this model captures the essentials of failure processes in a large number of materials and settings. A review of the fiber bundle model is presented with different load redistribution mechanisms from the point of view of statistics and statistical physics rather than materials science, with a focus on concepts such as criticality, universality, and fluctuations. The fiber bundle model is discussed as a tool for understanding phenomena such as creep and fatigue and how it is used to describe the behavior of fiber-reinforced composites as well as modeling, e.g., network failure, traffic jams, and earthquake dynamics.

DOI: 10.1103/RevModPhys.82.499 PACS number(s): 62.20.M−, 64.60.Ht, 02.50.−r, 05.40.−a

CONTENTS

*pradhan.srutarshi@ntnu.no
†alex.hansen@ntnu.no
‡bikask.chakrabarti@saha.ac.in

I. INTRODUCTION

In materials science and engineering, a class of simple models, known as fiber bundle models (FBMs), has proven to be effective in practical applications such as fiber-reinforced composites. In this context, such models have a history that goes back to the 1920s (Peirce, 1926), and they constitute today an elaborate toolbox for studying such materials, rendering computer studies orders of magnitude more efficient than brute force methods. Since the late 1980s (Sornette, 1989), these models have received increasing attention in the physics community due to their deceptively simple appearance coupled with an extraordinary richness of behaviors. As these models are just at the edge of what is possible analytically and typically are not very challenging from a numerical point of view, so that extremely good statistics on large systems are available, they are perfect as model systems for studying failure phenomena as a part of theoretical physics.

Fracture and material stability have interested humanity for practical reasons ever since we started using tools: our pottery should be able to withstand handling; our huts should be able to withstand normal weather. As science took on the form we know today during the Renaissance, 500 years ago Leonardo da Vinci studied experimentally the strength of wires—fiber bundles—as a function of their length (Lund and Byrne, 2001). Systematic strength studies, but on beams, were also pursued by Galileo Galilei 100 years later; Edme Mariotte (of gas law fame) pressurized vessels until they burst in connection with the construction of a fountain at Versailles. For some reason, mainstream physics moved away from fracture and breakdown problems in the 19th century, and it is only during the last 20 years that fracture problems have been studied within physics proper (see, e.g., Chakrabarti and Benguigui, 1997; Alava *et al.*, 2006). The reason for this is most probably the advent of the computer as a research tool, rendering problems that were beyond the reach of systematic theoretical study now accessible.

If we were to single out the most important contribution from the physics community with respect to fracture phenomena, it must be the focus on *fluctuations* rather than averages. What good is the knowledge of the average behavior of a system when we are faced with a single sample that is liable to break down given the right fluctuation? This review reflects this point of view, and hence fluctuations play an important role throughout it.

Even though we may trace the study of fiber bundles to Leonardo da Vinci, their modern story starts with the work by Peirce (1926) already mentioned. In 1945, Daniels published a seminal review cum research article on fiber bundles, which still today must be regarded as essential reading in the field (Daniels, 1945). In this paper, the fiber bundle model is treated as a problem of statistics and the analysis is performed within this framework rather than being treated within materials science. The fiber bundle is viewed as a collection of elastic objects connected in parallel and clamped to a medium that transmits forces between the fibers. The elongation of a fiber is linearly related to the force it carries, up to a maximum value. When this value is reached, the fiber fails by no longer being able to carry any force. The threshold value is assigned from some initially chosen probability distribution and does not change thereafter. When the fiber fails, the force it carried is redistributed. If the clamps deform under loading, fibers closer to the just-failed fiber will absorb more of the force compared to those further away. If the clamps, on the other hand, are rigid, the force is equally distributed to all the surviving fibers. Daniels discussed this latter case. Typical questions posed and answered in this paper would be the average strength of a bundle of N fibers and also the variance of the average strength of the entire bundle. The present review takes the same point of view, discussing the fiber bundle model as a *statistical model.* Only in Sec. V do we discuss the fiber bundle model in the context of materials science with all the properties of real materials considered. However, we have not attempted to include any discussions of the many experimental studies that have been performed on systems where fiber bundles constitute the appropriate tool. This is beyond the scope of this statistical-physics-based review.

After introducing the fiber bundle model (Sec. II), in Sec. III we present the equal-load-sharing (ELS) model, which was sketched just a few lines back. This seemingly simple model is in fact extremely rich. For example, the load at which catastrophic failure occurs is a second-order critical point with essentially all the features usually seen in systems displaying such behavior. However, in this case, the system is analytically tractable. In fact, we believe that the equal-load-sharing fiber bundle may be an excellent system for teaching second-order phase transitions at the college level. In Sec. III.B, we discuss the burst distribution, i.e., the statistics of simultaneously failing fibers during loading: When a fiber fails and the force it was carrying is redistributed, one or more other fibers may be driven above their failing thresholds. In this equal-load-sharing model, the absolute rigidity of the bar (transmitting forces among the fibers) suppresses the stress fluctuations among the fibers. As such, there is no apparent growth of the (fluctuation-correlation) length scale. Hence, although there are precise recursion relations and their linearized solutions are available near the fixed point (see Sec. III), no straightforward application of the renormalization group techniques (Fisher, 1974) has been made to extract the exponents through length scaling.

In Sec. IV local load sharing (LLS) is discussed. This bit of added realism comes at the added cost that analytical treatment becomes much more difficult. There are, still, a number of analytical results in the literature. One may see intuitively how local load sharing complicates the problem since the relative positions of the fi-

bers now become important. Under global load sharing, every surviving fiber gets the same excess force and, hence, where they are does not matter. There are essentially three local load-sharing models in the literature. The first one dictates that the nearest surviving neighbors of the failing fiber absorb its load. Then there are "softer models" where the redistribution follows a power law in the distance to the failing fiber. Last, there is the model where the clamps holding the fibers are elastic themselves, and this leads to nonequal redistribution of the forces.

Section V contains a review of the use of fiber bundle models in applications such as materials science. We discuss fatigue, thermal failure, viscoelastic effects, and precursors of global failure. We then go on to review the large field of modeling fiber-reinforced composites. Here fiber bundle models constitute the starting point of the analysis, which, by its very nature, is rather complex seen from the viewpoint of statistical physics. Last, we review some applications of fiber bundle models in connection with systems that initially would seem quite far from the concept of a fiber bundle, such as traffic jams.

We end this review with a summary and a few concluding remarks in Sec. VI.

II. FIBER BUNDLE MODELS

Imagine a heavy load hanging from a rigid anchor point (say, at the roof) by a rope or a bundle of fibers. If the load exceeds a threshold value, the bundle fails. How does the failure proceed in the bundle? Unless all the fibers in the bundle have identical breaking thresholds (and that never happens in a real rope), the failure dynamics proceeds in a typical collective load transfer way. One can assume that in this kind of situation the load is equally shared by all the intact fibers in the bundle. However, since the breaking threshold for each of the fibers is different, some fibers fail before others and, consequently, the load per surviving fiber increases as it gets redistributed and shared equally by the rest. This increased load per fiber may induce further breaking of some fibers and the avalanche continues, or it stops if all the surviving fibers can withstand the redistributed load per fiber. This collective or cooperative failure dynamics and the consequent avalanches or bursts are typical for failure in any many-body system. The model captures the essential features of failure during fracture propagation (recorded by acoustic emissions), earthquake avalanches (main and aftershocks), traffic jams (due to dynamic clustering), etc.

The model was first introduced in 1926 by Peirce (1926) in the context of textile engineering. Since then it has been modified a little and investigated, mainly numerically, with various realistic fiber threshold distributions by the engineering community (Daniels, 1945; Coleman, 1957a; Harlow and Phoenix, 1978; Phoenix and Smith, 1983). Starting from the late 1980s, physicists took interest in the avalanche distribution in the model and in its dynamics (Sornette, 1989, 1992; Newman and Gabrielov, 1991; Hemmer and Hansen, 1992; Gomez *et al.*, 1993; Lee, 1994; Andersen *et al.*, 1997; Kloster *et al.*, 1997; Zapperi *et al.*, 1997; Kun *et al.*, 2000; Pradhan *et al.*, 2002). A recursive dynamical equation was set up for the equal-load-sharing version (da Silveira, 1999; Pradhan and Chakrabarti, 2001) and the dynamic critical behavior is now solved exactly (Pradhan *et al.*, 2002; Bhattacharyya *et al.*, 2003; Pradhan and Hemmer, 2007). In addition to the extensive numerical results (Hansen and Hemmer, 1994b; Zhang and Ding, 1994) on the effect of short-range fluctuations (local load-sharing cases), some progress with analytical studies (Harlow, 1985; Harlow and Phoenix, 1991; Gomez *et al.*, 1993; Duxbury and Leath, 1994; Kloster *et al.*, 1997) has also been made.

There are a large number of experimental studies of various materials and phenomena that have been analyzed successfully within the framework of the fiber bundle model. For example, Layton and Sastry (2004) used the fiber bundle model to propose explanations for changes in fibrous collagen and its relation to neuropathy in connection with diabetes. Toffoli and Lehman (2001) proposed a method to monitor the structural integrity of fiber-reinforced ceramic-matrix composites using electrical resistivity measurements. The basic idea here is that, when the fibers in the composite themselves fail rather than just the matrix in which they are embedded, the structure is about to fail. The individual fiber failures are recorded through changes in the electrical conductivity of the material. Acoustic emission, the crackling sounds emitted by materials as they are loaded, provides yet another example where fiber bundle models play an important role [see, e.g., Nechad *et al.* (2005)].

III. EQUAL-LOAD-SHARING MODEL

The simplest and the oldest version of the model is the ELS model, in which the load previously carried by a failed fiber is shared equally by all the remaining intact fibers in the system. As the applied load is shared globally, this model is also known as the global load-sharing (GLS) model or the democratic fiber bundle model. Because of its consequent mean-field nature, some exact results could be extracted for this model and this was demonstrated by Daniels (1945) some 60 years ago. The typical relaxation dynamics of this model has been solved recently, and has established a robust critical behavior (Pradhan *et al.*, 2002; Bhattacharyya *et al.*, 2003; Pradhan and Hemmer, 2007). It may be mentioned at the outset that the ELS or GLS model does not allow for spatial fluctuations (due to the absolute rigidity of the platform in Fig. 1) and hence such models belong to the mean-field category of critical dynamics [see, e.g., Stanley (1987) and Sornette (2000)]. Fluctuations in breaking time or in avalanche statistics (due to randomness in fiber strengths) are of course possible in such models and are discussed in this section.

A bundle can be loaded in two different ways: strain-controlled and force controlled. In the strain-controlled method, at each step the whole bundle is stretched until

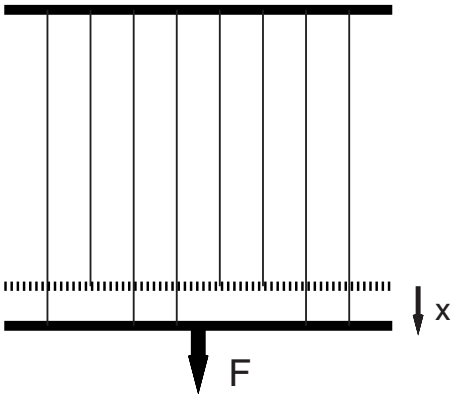

FIG. 1. A fiber bundle model having N parallel fibers. The original position of the rigid platform on which force has been applied is indicated. All the fibers are assumed to have the same elastic constant (normalized to unity here) until they break, while the breaking strengths of these fibers are assumed to be randomly dispersed. As the bundle becomes strained ($x>0$), some weaker fibers (having lower stress or strain capacity) fail, and the number of intact fibers decreases from its starting value N. Consequently, the stress on them (or the strain) increases due to the redistribution or transfer of loads from the failing fibers. Some of these fibers may fail further as they cannot support this extra redistributed load. The process stops if there is no further failure, and the bundle will show nonlinear elastic response (although each fiber has linear elastic behavior until breaking). Otherwise, the bundle fails when the stress concentration on the fibers (due to the dynamic stress redistribution) becomes so high that none of the fibers can withstand that.

the weakest fiber fails. Clearly, when the number of fibers N is very large, strain is increased by an infinitesimal amount at each step until complete breakdown and therefore the process is considered as a *quasistatic* way of loading. On the other hand, in the force-controlled method, the external force (load) on the bundle is increased by the same amount at each step until the breakdown. The basic difference between these two methods is that the first method ensures the failure of a single fiber (the weakest one among the intact fibers) at each loading step, while in the second method sometimes none of the fibers fail and sometimes more than one fails in one loading step.

Let x denote the strain of the fibers in the bundle. Assuming the fibers to be linearly elastic up to their respective failure points (with unit elastic constant), we can represent the stresses on each of the surviving fibers by the same quantity x. The strength (or threshold) of a fiber is usually determined by the stress value x it can bear and beyond which it fails. We therefore denote the strength (threshold) distribution of the fibers in the bundle by $p(x)$ and the corresponding cumulative distribution by $P(x)=\int_0^x p(y)dy$. Two popular examples of threshold distributions are the uniform distribution

$$P(x) = \begin{cases} x/x_r & \text{for } 0 \leq x \leq x_r \\ 1 & \text{for } x > x_r, \end{cases} \tag{1}$$

and the Weibull distribution

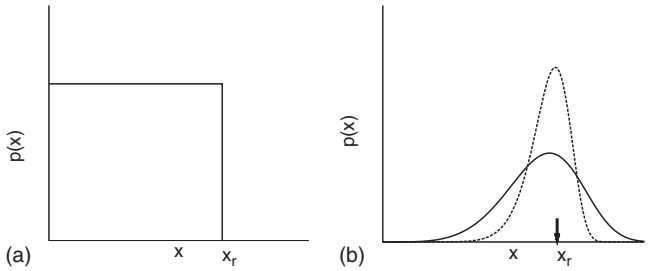

FIG. 2. Threshold distributions: (a) The uniform distribution and (b) the Weibull distribution with $\rho=5$ (solid line) and 10 (dotted line).

$$P(x) = 1 - \exp[-(x/x_r)^\rho]. \tag{2}$$

Here x_r is a reference threshold, and the dimensionless number ρ is the Weibull index (Fig. 2).

In strain-controlled loading, at a strain x, the total force on the bundle is x times the number of intact fibers. The expected or average force at this stage is therefore (Sornette, 1989, 1992; Hemmer and Hansen, 1992)

$$F(x) = Nx[1 - P(x)]. \tag{3}$$

The maximum F_c of $F(x)$ corresponds to the value x_c for which dF/dx vanishes,

$$1 - P(x_c) - x_c p(x_c) = 0. \tag{4}$$

Here the failure process is basically driven by fluctuations and can be analyzed using extreme order statistics (Sornette, 1989, 1992; Hemmer and Hansen, 1992; Kloster *et al.*, 1997).

In the force-controlled method, if force F is applied on a bundle having N fibers, when the system reaches an equilibrium, the strain or effective stress x is (see Fig. 1)

$$x(F) = \frac{F}{N[1 - P(x)]}. \tag{5}$$

Therefore, at equilibrium, Eqs. (3) and (5) are identical. It is possible to construct recursive dynamics (da Silveira, 1998, 1999; Pradhan and Chakrabarti, 2001) of the failure process for a given load and the fixed-point solutions explore the *average behavior* of the system at the equilibrium state.

A. Average behavior

Figure 1 shows a static fiber bundle model in the ELS model where N fibers are connected in parallel to each other (clamped at both ends) and a force is applied at one end. At the first step all fibers that cannot withstand the applied stress break. Then the stress is redistributed on the surviving fibers, which compels further fibers to break. This starts an iterative process that continues until an equilibrium is reached or all fibers fail. The average behavior is manifested when the initial load is macroscopic (very large N).

1. Recursive breaking dynamics

The breaking dynamics can be represented by recursion relations (da Silveira, 1999; Pradhan and Chakrabarti, 2001) in discrete steps. Let N_t be the number of fibers that survive after step t, where t indicates the number of stress redistribution steps. Then one can write (da Silveira, 1999)

$$N_{t+1} = N\left[1 - P\left(\frac{F}{N_t}\right)\right]. \tag{6}$$

Now we introduce $\sigma = F/N$, the applied stress, and $U_t = N_t/N$, the surviving fraction of total fibers. The effective stress after step t becomes $x_t = \sigma/U_t$ and after $t+1$ steps the surviving fraction of total fibers is $U_{t+1} = 1 - P(x_t)$. Therefore we can construct the following recursion relations (Pradhan and Chakrabarti, 2001; Pradhan *et al.*, 2002):

$$x_{t+1} = \frac{\sigma}{1 - P(x_t)}, \quad x_0 = \sigma, \tag{7}$$

and

$$U_{t+1} = 1 - P(\sigma/U_t), \quad U_0 = 1. \tag{8}$$

At equilibrium $U_{t+1} = U_t \equiv U^*$ and $x_{t+1} = x_t \equiv x^*$. These equations [Eqs. (7) and (8)] can be solved at and around the fixed points for the particular strength distribution $p(x)$.

2. Solution of the dynamics: Critical behavior

We now choose the uniform density of fiber strength distribution [Eq. (1)] up to the cutoff $x_r = 1$. Then the cumulative distribution becomes $P(\sigma/U_t) = \sigma/U_t$. Therefore from Eqs. (7) and (8) we can construct a pair of recursion relations,

$$x_{t+1} = \frac{\sigma}{1 - x_t} \tag{9}$$

and

$$U_{t+1} = 1 - \frac{\sigma}{U_t}. \tag{10}$$

These nonlinear recursion equations are somewhat characteristic of the dynamics of fiber bundle models and such dynamics can be obtained in many different ways. For example, the failed fraction $1 - U_{t+1}$ at step $t+1$ is given by the fraction $F/NU_t = \sigma/U_t$ of the load shared by the intact fibers at step t, and for the uniform distribution of thresholds [Fig. 2(a)], one readily gets Eq. (10).

At the fixed point the above relations take the quadratic forms

$$x^{*2} - x^* + \sigma = 0 \tag{11}$$

and

$$U^{*2} - U^* + \sigma = 0, \tag{12}$$

with the solutions

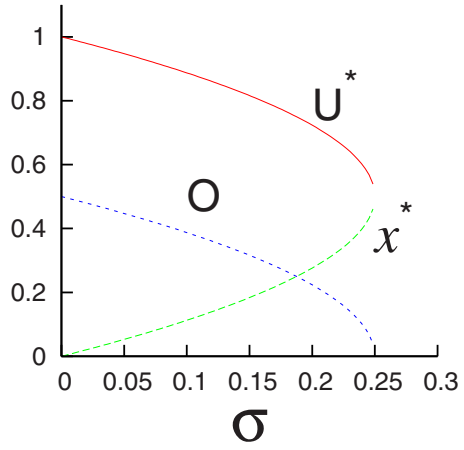

FIG. 3. (Color online) Variation of effective stress (x^*), fraction of unbroken fibers (U^*), and the order parameter (O) with the applied stress σ for a bundle with uniform distribution [Eq. (1)] of fiber strengths.

$$x^*(\sigma) = \tfrac{1}{2} \pm (\sigma_c - \sigma)^{1/2} \tag{13}$$

and

$$U^*(\sigma) = \tfrac{1}{2} \pm (\sigma_c - \sigma)^{1/2}. \tag{14}$$

Here $\sigma_c = \frac{1}{4}$ is the critical value of applied stress beyond which the bundle fails completely. Clearly, for the effective stress [Eq. (13)] solution, that with a $(-)$ sign is the stable fixed point and that with a $(+)$ sign is the unstable fixed point, whereas for a fraction of unbroken fibers [Eq. (14)], it is just the opposite. Now the difference $U^*(\sigma) - U^*(\sigma_c)$ behaves like an order parameter signaling partial failure of the bundle when it is nonzero (positive), although unlike conventional phase transitions it does not have a real-valued existence for $\sigma > \sigma_c$. Here

$$O \equiv U^*(\sigma) - U^*(\sigma_c) = (\sigma_c - \sigma)^{\alpha}, \quad \alpha = \tfrac{1}{2}. \tag{15}$$

Figure 3 shows the variation of x^*, U^*, and O with the externally applied stress value σ. One can also obtain the breakdown susceptibility χ, defined as the change of $U^*(\sigma)$ due to an infinitesimal increment of the applied stress σ:

$$\chi = \left|\frac{dU^*(\sigma)}{d\sigma}\right| = \frac{1}{2}(\sigma_c - \sigma)^{-\beta}, \quad \beta = \frac{1}{2}. \tag{16}$$

Such a divergence in χ has already been reported (Zapperi *et al.*, 1997, 1999a; da Silveira, 1999; Moreno *et al.*, 2000).

To study the dynamics away from criticality ($\sigma \to \sigma_c$ from below), the recursion relation [Eq. (10)] can be replaced by a differential equation

$$-\frac{dU}{dt} = \frac{U^2 - U + \sigma}{U}. \tag{17}$$

Close to the fixed point, $U_t(\sigma) = U^*(\sigma) + \Delta U$ (where $\Delta U \to 0$) and this gives

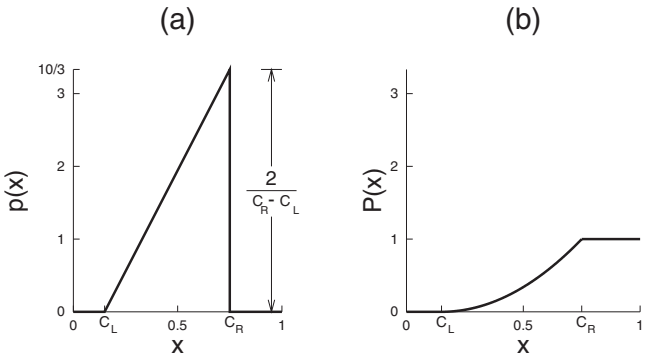

FIG. 4. Increasing threshold distributions: (a) The density function $p(x)$ and (b) the cumulative distribution $P(x)$ of random fiber strengths x distributed with linearly increasing density in the interval $[C_L, C_R]$. In the particular instance shown $C_L=0.15$ and $C_R=0.75$.

$$\Delta U = U_t(\sigma) - U^*(\sigma) \approx \exp(-t/\tau), \tag{18}$$

where $\tau=\frac{1}{2}[\frac{1}{2}(\sigma_c-\sigma)^{-1/2}+1]$. Therefore near the critical point,

$$\tau \propto (\sigma_c - \sigma)^{-\theta}, \quad \theta = \tfrac{1}{2}. \tag{19}$$

At the critical point ($\sigma=\sigma_c$), a dynamic critical behavior has been observed in the relaxation of the failure process to the fixed point. From the recursion relation [Eq. (10)] it can be easily verified that the fraction $U_t(\sigma_c)$ follows a simple power-law decay:

$$U_t = \frac{1}{2}\left(1 + \frac{1}{t+1}\right), \tag{20}$$

starting from $U_0=1$. For large t ($t\to\infty$), this reduces to $U_t-1/2\propto t^{-\eta}$, $\eta=1$, indicating critical slowing down, which is a robust characterization of the critical state.

3. Universality class of the model

The critical properties obtained above are for the uniform threshold distribution, and the natural question is how general the results are. To check the universality of the ELS model, two other types of fiber strength distributions can be easily considered (Bhattacharyya *et al.*, 2003): a linearly increasing and a linearly decreasing density distribution.

For linearly increasing density of fiber strengths in the interval $[C_L, C_R]$, the normalized density function and the cumulative distribution are given by (see Fig. 4)

$$p(x) = \begin{cases} 0, & 0 \leqslant x < C_L \\ \dfrac{2(x-C_L)}{(C_R-C_L)^2}, & C_L \leqslant x \leqslant C_R \\ 0, & C_R < x \end{cases} \tag{21}$$

and

$$P(x) = \begin{cases} 0, & 0 \leqslant x < C_L \\ \left(\dfrac{x-C_L}{C_R-C_L}\right)^2, & C_L \leqslant x \leqslant C_R \\ 1, & C_R < x. \end{cases} \tag{22}$$

Now we introduce the transformed quantities:

$$\Gamma_0 = \frac{\sigma}{C_R - C_L}, \quad \Gamma_L = \frac{C_L}{C_R - C_L}, \quad \Gamma_t = \frac{x_t}{C_R - C_L}. \tag{23}$$

For an initial stress $C_L \leqslant \sigma \leqslant C_R$ (or $\Gamma_L \leqslant \Gamma_0 \leqslant \Gamma_L+1$) along with the cumulative distribution given by Eq. (22), the recursion relations (7) and (8) appear as

$$\Gamma_{t+1} = \frac{\Gamma_0}{1-(\Gamma_t - \Gamma_L)^2} \tag{24}$$

and

$$U_{t+1} = 1 - \left(\frac{\Gamma_0}{U_t} - \Gamma_L\right)^2, \quad U_0 = 1. \tag{25}$$

The fixed-point equations (11) and (12) now assume cubic form:

$$(\Gamma^*)^3 - 2\Gamma_L(\Gamma^*)^2 + (\Gamma_L^2 - 1)\Gamma^* + \Gamma_0 = 0, \tag{26}$$

where $\Gamma^*=x^*/(\sigma_R-\sigma_L)$, and

$$(U^*)^3 + (\Gamma_L^2 - 1)(U^*)^2 - (2\Gamma_L\Gamma_0)U^* + \Gamma_0^2 = 0. \tag{27}$$

Consequently each of the recursions (24) and (25) has three fixed points—only one in each case is found to be stable. For the redistributed stress the fixed points are

$$\Gamma_1^* = \frac{2}{3}\Gamma_L + 2K_0 \cos\frac{\Phi}{3}, \tag{28}$$

$$\Gamma_2^* = \frac{2}{3}\Gamma_L - K_0 \cos\frac{\Phi}{3} + \sqrt{3}K_0 \sin\frac{\Phi}{3}, \tag{29}$$

$$\Gamma_3^* = \frac{2}{3}\Gamma_L - K_0 \cos\frac{\Phi}{3} - \sqrt{3}K_0 \sin\frac{\Phi}{3}, \tag{30}$$

where

$$K_0 = \tfrac{1}{3}\sqrt{3+\Gamma_L^2} \tag{31}$$

and

$$\cos\Phi = \frac{\Gamma_L(9-\Gamma_L^2) - 27\Gamma_0/2}{(3+\Gamma_L^2)^{3/2}}. \tag{32}$$

Similarly, for the surviving fraction of fibers the fixed points are

$$U_1^* = \frac{1-\Gamma_L^2}{3} + 2J_0 \cos\frac{\Theta}{3}, \tag{33}$$

$$U_2^* = \frac{1-\Gamma_L^2}{3} - J_0 \cos\frac{\Theta}{3} + \sqrt{3}J_0 \sin\frac{\Theta}{3}, \tag{34}$$

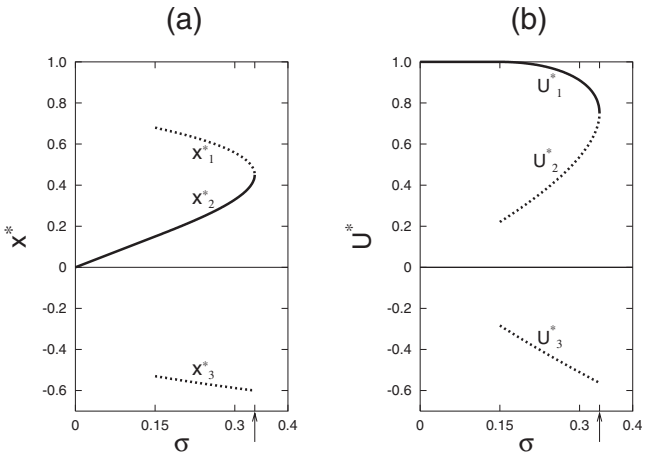

FIG. 5. The fixed points of (a) the redistributed stress and (b) the surviving fraction of fibers for the distribution of fiber strengths shown in Fig. 4. In each part the curve for the stable fixed points is shown by a bold solid line and those for the unstable fixed points are shown by bold broken lines. We have $C_L=0.15$ and $C_R=0.75$, so that $\sigma_c=0.3375$; the position of the critical point is marked by an arrowhead. For $\sigma \leqslant C_L$ the fixed points are trivial: since there are no broken fibers $x^*=\sigma$ and $U^*=U_0=1$.

$$U_3^* = \frac{1-\Gamma_L^2}{3} - J_0 \cos\frac{\Theta}{3} - \sqrt{3} J_0 \sin\frac{\Theta}{3}, \tag{35}$$

where

$$J_0 = \tfrac{1}{3}\sqrt{(\Gamma_L^2-1)^2 + 6\Gamma_L\Gamma_0} \tag{36}$$

and

$$\cos\Theta = \frac{(1-\Gamma_L^2)[(\Gamma_L^2-1)^2 + 9\Gamma_L\Gamma_0] - 27\Gamma_0^2/2}{[(\Gamma_L^2-1)^2 + 6\Gamma_L\Gamma_0]^{3/2}}. \tag{37}$$

Of these fixed points Γ_2^* and U_1^* are stable whereas Γ_1^*, Γ_3^* and U_2^*, U_3^* are unstable (Fig. 5).

The discriminants of the cubic equations (26) and (27) become zero at a critical value σ_c (or Γ_c) of the initial applied stress,

$$\Gamma_c = \frac{\sigma_c}{\sigma_R - \sigma_L} = \tfrac{2}{27}[\Gamma_L(9-\Gamma_L^2) + (3+\Gamma_L^2)^{3/2}], \tag{38}$$

and then each of the quantities Γ and U has one stable and one unstable fixed point. The critical point has the trivial lower bound $\sigma_c \geqslant C_L$. The expression of Γ_c in Eq. (38) shows that it approaches the lower bound as $\Gamma_L \to \infty$, which happens for finite values of C_L and C_R when $(C_R - C_L) \to 0$. It follows that the upper bound for the critical point is also trivial: $\sigma_c \leqslant C_R$. At the critical point we get from Eqs. (32) and (37),

$$\cos\Phi_{\text{crit}} = \cos\Theta_{\text{crit}} = -1 \tag{39}$$

or

$$\Phi_{\text{crit}} = \Theta_{\text{crit}} = \pi. \tag{40}$$

The stable fixed points Γ_2^* and U_1^* are positive real valued when $\Gamma_0 \leqslant \Gamma_c$; thus the fiber bundle always reaches a state of mechanical equilibrium after partial failure under an initial applied stress $\sigma_0 \leqslant \sigma_c$. For $\sigma > \sigma_c$ (or $\Gamma_0 > \Gamma_c$), Γ_2^* and U_1^* are no longer real valued and the entire fiber bundle eventually breaks down. The transition from the phase of partial failure to the phase of total failure takes place when σ just exceeds σ_c and the order parameter for this phase transition is defined as in Eq. (15):

$$O \equiv U_1^* - U_{1\text{-crit}}^*. \tag{41}$$

Close to the critical point but below it, we can write, from Eqs. (37) and (40), that

$$\pi - \Theta \simeq \sin\Theta \simeq \frac{3\sqrt{3}\Gamma_c(3+\Gamma_L^2)^{3/4}(\Gamma_c-\Gamma_0)^{1/2}}{[(\Gamma_L^2-1)^2 + 6\Gamma_L\Gamma_c]^{3/2}} \tag{42}$$

and the expressions for the fixed points in Eqs. (33) and (34) reduce to the forms

$$U_1^* \simeq U_{1\text{-crit}}^* + \frac{\Gamma_c(3+\Gamma_L^2)^{3/4}}{(\Gamma_L^2-1)^2 + 6\Gamma_L\Gamma_c}(\Gamma_c-\Gamma_0)^{1/2} \tag{43}$$

and

$$U_2^* \simeq U_{2\text{-crit}}^* - \frac{\Gamma_c(3+\Gamma_L^2)^{3/4}}{(\Gamma_L^2-1)^2 + 6\Gamma_L\Gamma_c}(\Gamma_c-\Gamma_0)^{1/2}, \tag{44}$$

where

$$U_{1\text{-crit}}^* = U_{2\text{-crit}}^* = \frac{1-\Gamma_L^2}{3} + \frac{1}{3}\sqrt{(\Gamma_L^2-1)^2 + 6\Gamma_L\Gamma_c} \tag{45}$$

is the stable fixed-point value of the surviving fraction of fibers under the critical initial stress σ_c. Therefore, following the definition of the order parameter in Eq. (41) we get from the above equation,

$$O = \frac{\Gamma_c(3+\Gamma_L^2)^{3/4}}{(\Gamma_L^2-1)^2 + 6\Gamma_L\Gamma_c}(\Gamma_c-\Gamma_0)^{1/2}, \quad \Gamma_0 \to \Gamma_c - . \tag{46}$$

When the transformed variable Γ_0 is replaced by the original σ, Eq. (46) shows that the order parameter goes to zero continuously following the same power law as in Eq. (15) for the previous case when σ approaches its critical value from below.

Similarly the susceptibility diverges by the same power law as in Eq. (16) on approaching the critical point from below,

$$\chi = \left|\frac{dU_1^*}{d\sigma}\right| \propto (\Gamma_c-\Gamma_0)^{-1/2}, \quad \Gamma_0 \to \Gamma_c - . \tag{47}$$

The critical dynamics of the fiber bundle is given by the asymptotic closed-form solution of the recursion [Eq. (25)] for $\Gamma_0 = \Gamma_c$:

$$U_t - U_{1\text{-crit}}^* \sim \left[\frac{(U_{1\text{-crit}}^*)^4}{3(\Gamma_c)^2 - 2\Gamma_L\Gamma_c U_{1\text{-crit}}^*}\right]\frac{1}{t}, \quad t \to \infty, \tag{48}$$

where Γ_c and $U_{1\text{-crit}}^*$ are given in Eqs. (38) and (45), respectively. This shows that the asymptotic relaxation of the surviving fraction of fibers to its stable fixed point

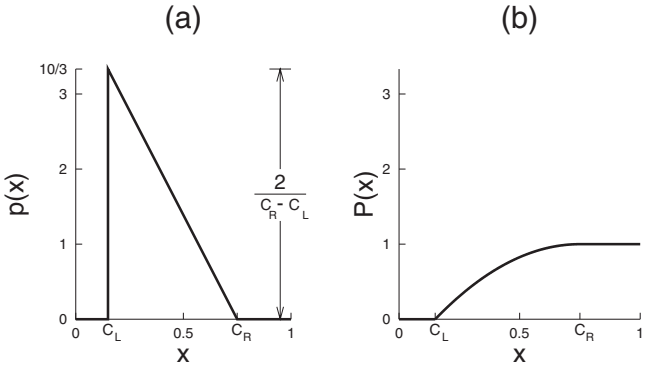

FIG. 6. Decreasing threshold distribution: (a) The density function $p(x)$ and (b) the cumulative distribution $P(x)$ of fiber strengths x distributed with linearly decreasing density in the interval $[C_L, C_R]$. Similar to the cases shown in Fig. 4 we have $C_L=0.15$ and $C_R=0.75$ in this example also.

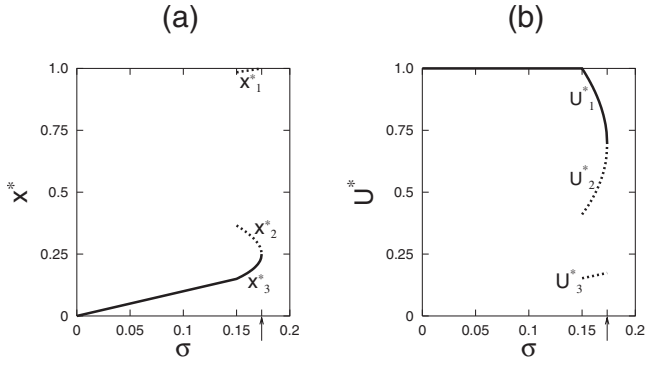

FIG. 7. The fixed points of (a) the redistributed stress and (b) the surviving fraction of fibers for the distribution of fiber strengths shown in Fig. 6. The curve for the stable fixed points is shown by a bold solid line and those for the unstable fixed points are shown by bold broken lines. In this example too we have $C_L=0.15$ and $C_R=0.75$; here $\sigma_c=0.173\,611$, marked by an arrowhead. The critical point is located lower than that in Fig. 5 due to an abundance of fibers of lower strengths compared to the previous case.

under the critical initial stress has the same (inverse of step number) form as found in the case of uniform density of fiber strengths [Eq. (20)].

We now consider a fiber bundle with a linearly decreasing density of fiber strengths in the interval $[C_L, C_R]$. The normalized density function and cumulative distribution (see Fig. 6) are

$$p(x) = \begin{cases} 0, & 0 \le x < C_L \\ \dfrac{2(C_R - x)}{(C_R - C_L)^2}, & C_L \le x \le C_R \\ 0, & C_R < x \end{cases} \tag{49}$$

and

$$P(x) = \begin{cases} 0, & 0 \le x < C_L \\ 1 - \left(\dfrac{C_R - x}{C_R - C_L}\right)^2, & C_L \le x \le C_R \\ 1, & C_R < x. \end{cases} \tag{50}$$

With the transformed quantities defined in Eq. (23) the recurrences [Eqs. (7) and (8)] for $C_L \le \sigma \le C_R$ appear as

$$\Gamma_{t+1} = \frac{\Gamma_0}{(1 + \Gamma_L - \Gamma_t)^2} \tag{51}$$

and

$$U_{t+1} = \left(1 + \Gamma_L - \frac{\Gamma_0}{U_t}\right)^2, \quad U_0 = 1. \tag{52}$$

The fixed-point equations are again cubic:

$$(\Gamma^*)^3 - 2(1+\Gamma_L)(\Gamma^*)^2 + (1+\Gamma_L)^2\Gamma^* - \Gamma_0 = 0, \tag{53}$$

$$(U^*)^3 - (1+\Gamma_L)^2(U^*)^2 + 2(1+\Gamma_L)\Gamma_0 U^* - \Gamma_0^2 = 0, \tag{54}$$

and they have the following solutions:

$$\Gamma_1^* = \frac{2}{3}(1+\Gamma_L) + 2K_0' \cos\frac{\Phi'}{3}, \tag{55}$$

$$\Gamma_2^* = \frac{2}{3}(1+\Gamma_L) - K_0' \cos\frac{\Phi'}{3} + \sqrt{3}K' \sin\frac{\Phi'}{3}, \tag{56}$$

$$\Gamma_3^* = \frac{2}{3}(1+\Gamma_L) - K_0' \cos\frac{\Phi'}{3} - \sqrt{3}K' \sin\frac{\Phi'}{3}, \tag{57}$$

where

$$K_0' = \frac{1+\Gamma_L}{3}, \tag{58}$$

$$\cos\Phi' = \frac{27\Gamma_0}{2(1+\Gamma_L)^3} - 1, \tag{59}$$

and

$$U_1^* = \frac{(1+\Gamma_L)^2}{3} + 2J_0' \cos\frac{\Theta'}{3}, \tag{60}$$

$$U_2^* = \frac{(1+\Gamma_L)^2}{3} - J_0' \cos\frac{\Theta'}{3} + \sqrt{3}J_0' \sin\frac{\Theta'}{3}, \tag{61}$$

$$U_3^* = \frac{(1+\Gamma_L)^2}{3} - J_0' \cos\frac{\Theta'}{3} - \sqrt{3}J_0' \sin\frac{\Theta'}{3}, \tag{62}$$

where

$$J_0' = \tfrac{1}{3}\sqrt{(1+\Gamma_L)^4 - 6(1+\Gamma_L)\Gamma_0}, \tag{63}$$

$$\cos\Theta' = \frac{(1+\Gamma_L)^3[(1+\Gamma_L)^3 - 9\Gamma_0] + 27\Gamma^2/2}{[(1+\Gamma_L)^4 - 6(1+\Gamma_L)\Gamma_0]^{3/2}}. \tag{64}$$

Here Γ_3^* and U_1^* are stable fixed points while the rest are unstable (Fig. 7).

The discriminants of Eqs. (53) and (54) show that the critical applied stress in this case, σ_c' (or Γ_c'), is given by

$$\Gamma_c' = \frac{\sigma_c'}{C_R - C_L} = \frac{4}{27}(1+\Gamma_L)^3 \tag{65}$$

or

$$\sigma_c' = \frac{4C_R^3}{27(C_R - C_L)^2}. \tag{66}$$

In order to satisfy the condition $\sigma_c' \geqslant C_L$, it follows from Eq. (66) that $C_R \geqslant 3C_L$, which imposes an upper bound $\sigma_c' \leqslant C_R/3$.

As before, for $\Gamma_0 \leqslant \Gamma_c'$ the stable fixed points are real valued, which indicates that only partial failure of the fiber bundle takes place before a state of mechanical equilibrium is reached; for $\Gamma_0 > \Gamma_c'$ the fixed points are not real and a phase of total failure exists. The order parameter O of the transition is given by the definition in Eq. (41).

For $\Gamma_0 = \Gamma_c'$ we get the following properties from Eqs. (59)–(61) and (64):

$$U^*_{1\text{-crit}} = U^*_{2\text{-crit}} = \tfrac{4}{9}(1+\Gamma_L)^2, \tag{67}$$

$$\cos\Theta'_{\text{crit}} = -1 \quad \text{or} \quad \Theta'_{\text{crit}} = \pi, \tag{68}$$

and

$$\cos\Phi'_{\text{crit}} = 1 \quad \text{or} \quad \Phi'_{\text{crit}} = 0. \tag{69}$$

Comparing Eqs. (69) and (68) with Eq. (40) we see that the critical values of Θ and Θ' are the same whereas those of Φ and Φ' differ by π radians.

Near the critical point, but below it, we get from Eqs. (60) and (61)

$$U_1^* \simeq U^*_{1\text{-crit}} + \tfrac{4}{3}(1+\Gamma_L)^{1/2}(\Gamma_c' - \Gamma_0)^{1/2} \tag{70}$$

and

$$U_2^* \simeq U^*_{2\text{-crit}} - \tfrac{4}{3}(1+\Gamma_L)^{1/2}(\Gamma_c' - \Gamma_0)^{1/2}. \tag{71}$$

Therefore, by the definition of the order parameter in Eq. (41) and that of the susceptibility in Eq. (47), we get in this case $O \propto (\Gamma_c' - \Gamma_0)^{1/2}$ and $\chi \propto (\Gamma_c' - \Gamma_0)^{-1/2}$, $\Gamma_0 \to \Gamma_c' -$. These power laws have the same exponents as the corresponding ones in the previous cases and differ from those only in the critical point and the critical amplitude.

At the critical point the asymptotic relaxation of the surviving fraction of fibers to its stable fixed point [obtained as an asymptotic solution to Eq. (52)] is again found to be a power-law decay similar to Eqs. (20) and (48):

$$U_t - U^*_{1\text{-crit}} \sim \frac{4}{3}\frac{U^*_{1\text{-crit}}}{t}, \quad t \to \infty$$

$$\sim \frac{16}{27}(1+\Gamma_L)^2\frac{1}{t}. \tag{72}$$

The two density functions [Eqs. (21) and (49)] can be transformed from one to the other by a reflection on the line $x = (C_L + C_R)/2$ [compare Figs. 4(a) and 6(a)]. But the fixed-point equations and their solutions do not have this symmetry. This is because the density function $p(x)$ does not appear directly in the recursion relations for the dynamics. It is the cumulative distribution $P(x)$ which appears in the recursion relations. Equations (22) and (50) show that the cumulative distributions of these two cases are not mutually symmetric about any value of the threshold stress x [compare Figs. 4(b) and 6(b)]. However, a certain relation exists between the critical values of the applied stress for a special case of these two models: if $C_L = 0$, we get from Eqs. (38) and (65) that $\sigma_c/C_R = \sqrt{4/27}$ and $\sigma_c'/C_R = 4/27$, respectively; therefore we have $\sigma_c'/C_R = (\sigma_c/C_R)^2$.

The critical behavior of the models discussed here shows that the power laws found here are independent of the form of the cumulative distribution P. The three threshold distributions studied here have a common feature: the function $x^*[1 - P(x^*)]$ has a maximum which corresponds to the critical value of the initial applied stress. All threshold distributions having this property are therefore expected to lead to the same universality class as the three studied here. If the threshold distribution does not have this property, we may not observe a phase transition at all. For example, consider a fiber bundle model with $P(x) = 1 - 1/x$, $x \geqslant 1$. Here $x^*[1 - P(x^*)] = 1$ and the evolution of the fiber bundle is given by the recursion relation $U_{t+1} = U_t/\sigma$, which implies that there is no dynamics at all for $\sigma = 1$ and an exponential decay to complete failure, $U_t = (\sigma)^{-t}$, for $\sigma > 1$. There are no critical phenomena and therefore no phase transition. However, this general conclusion may not be true for finite-sized bundles (McCartney and Smith, 1983).

Thus the ELS fiber bundles (for different fiber threshold distributions) show a phase transition with a well-defined order parameter, which shows similar power-law variation in the way the critical point is approached. For all cases discussed here, the susceptibility and relaxation time diverge following similar power laws and the failure processes show similar critical slowing at the critical point. This strongly suggests that the critical behavior is universal, which we now prove through general arguments (Hemmer *et al.*, 2006).

When an iteration is close to the fixed point, we have for the deviation

$$\Delta U_{t+1} = P\left(\frac{\sigma}{U^*}\right) - P\left(\frac{\sigma}{U^* + \Delta U_t}\right) = \Delta U_t \frac{\sigma}{U^{*2}} p(\sigma/U^*) \tag{73}$$

to lowest order in ΔU_t. This guarantees an exponential relaxation to the fixed point, $\Delta U_t \propto e^{-t/\tau}$, with parameter

$$\tau = \left[\ln\left(\frac{U^{*2}}{\sigma p(\sigma/U^*)}\right)\right]^{-1}. \tag{74}$$

Criticality is determined by the extremum condition (4), which by the relation (8) takes the form

$$U_c^2 = \sigma p(\sigma/U_c).$$

Thus $\tau = \infty$ at criticality. To study the relaxation at criticality we must expand Eq. (73) to second order in ΔU_t

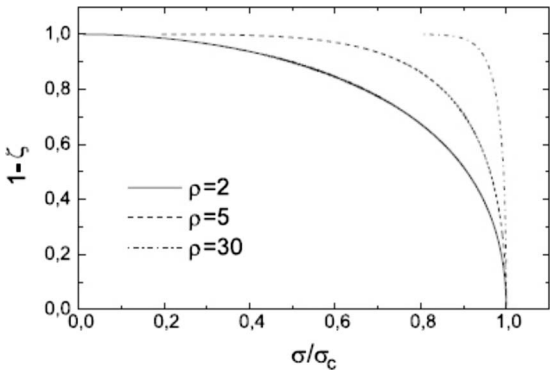

FIG. 8. Branching ratio as a function of applied stress for three different ρ (Weibull index). From Moreno *et al.*, 2000.

since to first order we simply get the useless equation $\Delta U_{t+1}=\Delta U_t$. To second order we obtain

$$\Delta U_{t+1}=\Delta U_t - C\Delta U_t^2,$$

with a positive constant C. This is satisfied by

$$\Delta U_t=\frac{1}{Ct}+O(t^{-2}).$$

Hence, in general, the dominating critical behavior for the approach to the fixed point is a power law with $\eta=1$. The values $\alpha=\beta=\theta=\frac{1}{2}$ can be shown to be consequences of the parabolic maximum of the load curve at criticality. Thus all threshold distributions for which the macroscopic strength function has a single parabolic maximum are in this universality class.

It is clear that at the critical stress value σ_c ELS fiber bundles show a phase transition from a partially to a completely broken state. What is the order of this phase transition? Zapperi *et al.* (1997, 1999a, 1999b) considered the fraction of unbroken fibers as the order parameter and as it has a discontinuity at the critical stress value, they suggested, after a mean-field analysis, that it can be seen as a first-order phase transition similar to spinodal instability (Monette, 1994). The additional reason for identifying the transition at $\sigma=\sigma_c$ as a first-order spinodal point had been (Kun *et al.*, 2000) that, in the presence of short-range interactions (as in LLS, see Sec. IV), the transition becomes discontinuous and first-order-like. It is indeed hard to identify continuously changing order parameter there. We, however, believe the transition in ELS to be second order. Chronologically, a little later, a new parameter was identified (Moreno *et al.*, 2000): the branching ratio (ζ), which is defined as the probability of triggering further breaking given an individual failure. The branching ratio continuously approaches (Fig. 8) the value 1 at the critical stress (σ_c) starting from zero (for very small σ). It also shows a power-law variation: $1-\zeta \propto (\sigma_c-\sigma)^\beta$, with $\beta=1/2$. Therefore $1-\zeta$ acts as the order parameter, showing a continuous transition at the critical point, signaling a second-order phase transition. As mentioned, Pradhan and Chakrabarti (2001) and Pradhan *et al.* (2002) considered the difference between the fraction of unbroken fibers at any σ and at σ_c as the order parameter (O); it shows a similar continuous variation with the applied stress: $O \propto (\sigma_c-\sigma)^\beta$, with $\beta=1/2$. Apart from this, the susceptibility and relaxation time diverge at the critical point following power laws having universal exponent values (Pradhan *et al.*, 2002; Bhattacharyya *et al.*, 2003). One may therefore conclude that at the critical point the ELS fiber bundles show a second-order phase transition with robust critical behavior as discussed here.

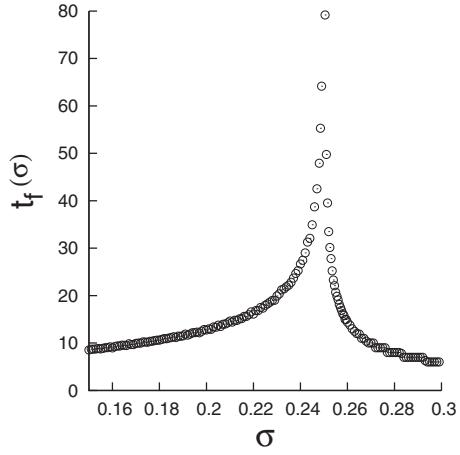

FIG. 9. Number of relaxation steps $t_f(\sigma)$ for a fiber bundle with a uniform threshold distribution [Eq. (1)]. Here $\sigma_c=0.25$. The figure is based on 1000 samples, each with $N=10^6$ fibers.

Finally, we compare the ELS fiber bundle model studied here with the mean-field Ising model. Though the order parameter exponent (equal to $\frac{1}{2}$) of this model is identical to that of the mean-field Ising model, the two models are not in the same universality class. The susceptibilities in these models diverge with critical exponents $\frac{1}{2}$ and 1, respectively, on approaching the critical point. The dynamical critical exponents are not the same either: in this fiber bundle model the surviving fraction of fibers under the critical applied stress decays toward its stable fixed point as t^{-1}, whereas the magnetization of the mean-field Ising model at the critical temperature decays to zero as $t^{-1/2}$.

4. Relaxation behavior and critical amplitude ratio

When an external load F is applied to a fiber bundle, the iterative failure process continues until all fibers fail or an equilibrium situation with a nonzero bundle strength is reached. Since the number of fibers is finite, the number of steps t_f in this sequential process is *finite*. Following Pradhan and Hemmer (2007), we now determine how t_f depends on the applied stress σ.

The state of the bundle can be characterized as *precritical* or *postcritical* depending on the stress value relative to the critical stress $\sigma_c=F_c/N$ above which the bundle collapses completely. The function $t_f(\sigma)$ that we now focus on exhibits critical divergence when the critical point is approached from either side. As an example, we show in Fig. 9 the $t_f(\sigma)$ obtained by simulation for a uniform threshold distribution.

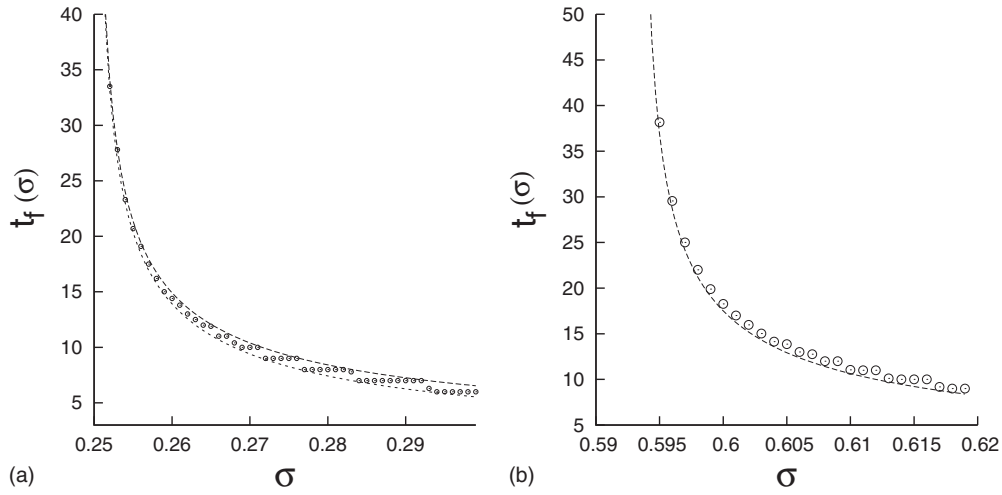

FIG. 10. Simulation results with postcritical stress for (a) the uniform threshold distribution [Eq. (1)] and (b) the Weibull distribution [Eq. (2)] with index 5. The graphs are based on 10 000 samples with $N=10^6$ fibers in each bundle. Open circles represent simulation data and dashed lines are the theoretical estimates, Eqs. (82) and (83) in (a) and Eq. (92) in (b).

We study the stepwise failure process in the bundle when a fixed external load $F=N\sigma$ is applied. Let N_t be the number of intact fibers at step number t, with $N_0=N$. We want to determine how N_t decreases until the degradation process stops. When N is a large number, we recall the basic recursion [Eq. (8)] to formulate the breaking dynamics,

$$U_{t+1}=1-P(\sigma/U_t), \tag{75}$$

where $U_t=N_t/N$ is considered as a continuous variable.

a. Postcritical relaxation

We study first the postcritical situation $\sigma>\sigma_c$, with positive values of $\epsilon=\sigma-\sigma_c$, and start with the simplest one, uniform threshold distribution (1) with the critical point at $x_c=1/2$, $\sigma_c=1/4$. Then the basic recursion relation (75) takes the form

$$U_{t+1}=1-\frac{\sigma}{U_t}=1-\frac{\frac{1}{4}+\epsilon}{U_t}. \tag{76}$$

This nonlinear iteration can be transformed into a linear relation. We first introduce $U_t=\frac{1}{2}-y_t\sqrt{\epsilon}$ into Eq. (76), with the result

$$\frac{y_{t+1}-y_t}{1+y_ty_{t+1}}=2\sqrt{\epsilon}. \tag{77}$$

Then we set $y_t=\tan v_t$, which gives

$$2\sqrt{\epsilon}=\frac{\tan v_{t+1}-\tan v_t}{1+\tan v_{t+1}\tan v_t}=\tan(v_{t+1}-v_t). \tag{78}$$

Hence we get $v_{t+1}-v_t=\tan^{-1}(2\sqrt{\epsilon})$, with the solution

$$v_t=v_0+t\tan^{-1}(2\sqrt{\epsilon}). \tag{79}$$

In the original variable the solution reads

$$U_t=\frac{1}{2}-\sqrt{\epsilon}\tan\left[\tan^{-1}\left(\frac{\frac{1}{2}-U_0}{\sqrt{\epsilon}}\right)+t\tan^{-1}(2\sqrt{\epsilon})\right] \tag{80}$$

$$=\frac{1}{2}-\sqrt{\epsilon}\tan[-\tan^{-1}(1/2\sqrt{\epsilon})+t\tan^{-1}(2\sqrt{\epsilon})], \tag{81}$$

where $U_0=1$ has been used.

Equation (76) shows that when U_t obtains a value in the interval $(0,\sigma)$, the next iteration gives complete bundle failure. Taking $U_t=\sigma$ as the penultimate value gives a lower bound t_f^l for the number of iterations, while using $U_t=0$ in Eq. (81) gives an upper bound t_f^u. Adding unity for the final iteration, Eq. (81) gives the bounds

$$t_f^u(\sigma)=1+\frac{2\tan^{-1}(1/2\sqrt{\epsilon})}{\tan^{-1}(2\sqrt{\epsilon})} \tag{82}$$

and

$$t_f^l(\sigma)=1+\frac{\tan^{-1}\left[\left(\frac{1}{4}-\epsilon\right)\Big/\sqrt{\epsilon}\right]+\tan^{-1}(1/2\sqrt{\epsilon})}{\tan^{-1}(2\sqrt{\epsilon})}. \tag{83}$$

Figure 10(a) shows that these bounds nicely embrace the simulation results.

Note that both the upper and lower bounds behave as $\epsilon^{-1/2}$ for small ϵ. A rough approximation near the critical point is

$$t_f(\sigma)\approx\kappa_+(\sigma-\sigma_c)^{-1/2}, \tag{84}$$

with $\kappa_+=\pi/2$.

Due to the inherent simplicity, uniform distribution is somewhat easy to analyze. Therefore we now discuss how to handle other distributions. We start with a

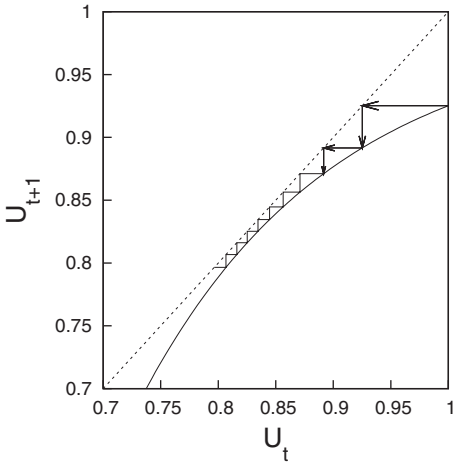

FIG. 11. The iteration function $f(U)$ for the Weibull distribution [Eq. (2)] with index 5. Here $\sigma=0.6$, slightly greater than the critical value $\sigma_c=0.593\,399\,4$.

Weibull distribution [Eq. (2)] with index 5. The critical parameters for this case are $x_c=5^{-1/5}=0.724\,78$ and $\sigma_c=(5e)^{-1/5}=0.593\,399\,4$.

The interesting values of the external stress are close to σ_c because for large supercritical stresses the bundle breaks down almost immediately. For σ slightly above σ_c the iteration function

$$U_{t+1}=f(U_t)=1-P(\sigma/U_t)=e^{-(\sigma/U_t)^5} \tag{85}$$

takes the form shown in Fig. 11.

The iteration function is almost tangent to the reflection line $U_{t+1}=U_t$ and a long channel of width proportional to ϵ appears. The dominating number of iterations occurs within this channel (see Fig. 11). The channel wall formed by the iteration function is almost parabolic and is well approximated by a second-order expression,

$$U_{t+1}=U_c+(U_t-U_c)+a(U_t-U_c)^2+b(\sigma_c-\sigma). \tag{86}$$

Here $U_c=e^{-1/5}$ is the fixed point, $U_{t+1}=U_t$, of the iteration at $\sigma=\sigma_c$. With $u=(U-U_c)/b$ and $\epsilon=\sigma-\sigma_c$ Eq. (86) takes the form

$$u_{t+1}-u_t=-Au_t^2-\epsilon, \tag{87}$$

with $A=ab$. In the channel u changes very slowly, so we may treat the difference equation as a differential equation,

$$\frac{du}{dt}=-Au^2-\epsilon, \tag{88}$$

with the solution

$$t\sqrt{A\epsilon}=-\tan^{-1}(u\sqrt{A/\epsilon})+\text{const}. \tag{89}$$

Thus

$$t_e-t_s=(A\epsilon)^{-1/2}[\tan^{-1}(u_s\sqrt{A/\epsilon})-\tan^{-1}(u_e\sqrt{A/\epsilon})] \tag{90}$$

is the number of iterations in the channel, starting with u_s, ending with u_e. This treatment is general and can be applied to any threshold distribution near criticality. Although the vast majority of the iterations occur in the channel, there are a few iterations at the entrance and exit of the channel that may require attention in special cases. The situation is similar to type-I intermittency in dynamical systems, but in our case the channel is traversed only once.

For the Weibull distribution the expansion [Eq. (86)] has the precise form

$$U_t=e^{-(\sigma/U)^5}\simeq e^{-1/5}+(U-U_c)-\frac{5}{2}e^{1/5}(U-U_c)^2-5^{1/5}(\sigma-\sigma_c), \tag{91}$$

where $U_c=e^{-1/5}$, $a=\frac{5}{2}e^{1/5}$, $b=5^{1/5}$, and $A=\frac{5}{2}(5e)^{1/5}$. For completeness we must also consider the number of iterations needed to reach the entrance to the channel. It is not meaningful to use the quadratic approximation [Eq. (91)] where it is not monotonically increasing, i.e., for $U>U_m=U_c+1/(2a)=\frac{6}{5}e^{-1/5}\simeq 0.98$. Thus we take $U_s=U_m$ as the entrance to the channel and add one extra iteration to arrive from $U_0=1$ to the channel entrance. (Numerical evidence for this extra step: for $\sigma=\sigma_c$ the iteration [Eq. (85)] starts as follows: $U_0=1.00$, $U_1=0.93$, $U_2=0.90$, while using the quadratic function with $U_0=U_m=0.98$ as the initial value, we get after one step $U_1=0.90$, approximately the same value that the exact iteration reaches after two steps.) With $U_e=0$ we obtain from Eq. (90), in the Weibull case, the estimate

$$t_f=1+(A\epsilon)^{-1/2}[\tan^{-1}(e^{-1/5}\sqrt{A/\epsilon}/5b)+\tan^{-1}(e^{-1/5}\sqrt{A/\epsilon}/b)], \tag{92}$$

with $A=\frac{5}{2}(5e)^{1/5}$ and $b=5^{1/5}$.

Near the critical point Eq. (92) has the asymptotic form

$$t_f\approx\pi(A\epsilon)^{-1/2}=\kappa_+(\sigma-\sigma_c)^{-1/2}, \tag{93}$$

with $\kappa_+=\pi(2/5)^{1/2}(5e)^{-1/10}$. The critical index is the same as for the uniform threshold distribution. The theoretical estimates give an excellent representation of the simulation data [see Fig. 10(b)].

b. Precritical relaxation

We now assume the external stress to be precritical, $\sigma<\sigma_c$, and introduce the positive parameter $\varepsilon=\sigma_c-\sigma$ to characterize the deviation from the critical point. Starting with uniform threshold distribution and introducing $U_t=\frac{1}{2}+\sqrt{\varepsilon}/z_t$ and $\sigma=\frac{1}{4}-\varepsilon$ into Eq. (76), one gets

$$2\sqrt{\varepsilon}=\frac{z_{t+1}-z_t}{1-z_{t+1}z_t}. \tag{94}$$

In this case we set $z_t=\tanh w_t$, which gives

$$2\sqrt{\varepsilon}=\frac{\tanh w_{t+1}-\tanh w_t}{1-\tanh w_{t+1}\tanh w_t}=\tanh(w_{t+1}-w_t). \tag{95}$$

Thus $w_{t+1}-w_t=\tanh^{-1}(2\sqrt{\varepsilon})$, i.e.,

$$w_t=w_0+t\tanh^{-1}(2\sqrt{\varepsilon}). \tag{96}$$

Starting with $U_0=1$, we obtain $z_0=2\sqrt{\varepsilon}$ and hence

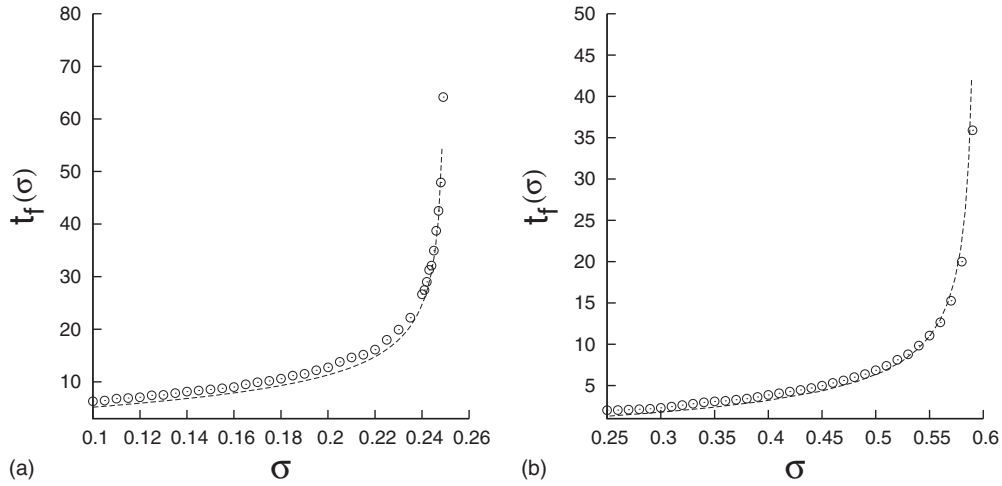

FIG. 12. Simulation results with precritical stress for (a) the uniform threshold distribution [Eq. (1)] and (b) the Weibull distribution [Eq. (2)] with index 5. The graphs are based on 10 000 samples with $N=10^6$ fibers in each bundle. Open circles represent simulation data and the dotted lines are the theoretical estimates, Eq. (101) in (a) and Eqs. (111) and (112) in (b).

$$w_t = (1+t)\tanh^{-1}(2\sqrt{\varepsilon}). \tag{97}$$

This corresponds to

$$U_t = \frac{1}{2} + \frac{\sqrt{\varepsilon}}{\tanh[(1+t)\tanh^{-1}(2\sqrt{\varepsilon})]} \tag{98}$$

in the original variable.

Apparently U_t reaches a fixed point $U^*=\frac{1}{2}+\sqrt{\varepsilon}$ after an infinite number of iterations. However, for a bundle with a finite number of fibers, only a finite number of steps is needed for the iteration to arrive at a fixed point N^*, which is (Pradhan *et al.*, 2002; Pradhan and Hemmer, 2007)

$$N^* = \frac{N}{2}(1-\sqrt{1-4\sigma}) + \frac{1}{2}[1+(1-4\sigma)^{-1/2}]. \tag{99}$$

As a consequence, we can use

$$U_t = \frac{N^*}{N} = \frac{1}{2} + \sqrt{\varepsilon} + \frac{1}{4N}(2+\varepsilon^{-1/2}) \tag{100}$$

as the final value in Eq. (98). Consequently, we obtain the following estimate for the number of iterations to reach this value:

$$t_f(\sigma) = -1 + \frac{\coth^{-1}\{1+(1+2\sqrt{\varepsilon})/4N\varepsilon\}}{\tanh^{-1}(2\sqrt{\varepsilon})}. \tag{101}$$

Figure 12(a) shows that the simulation data are well approximated by the analytic formula (101).

For very large N, Eq. (101) is approximated by

$$t_f = \frac{\ln(N)}{4}\varepsilon^{-1/2} = \kappa_-(\sigma_c-\sigma)^{-1/2}, \tag{102}$$

with $\kappa_-=\ln(N)/4$. The critical behavior is again characterized by a square root divergence.

Again we use the Weibull distribution [Eq. (2)] as an example of a threshold distribution. In principle, the iteration

$$U_{t+1} = 1 - P(\sigma/U_t) \tag{103}$$

will reach a fixed point U^* after infinitely many steps. The deviation from the fixed point U_t-U^* will decrease exponentially near the fixed point,

$$U_t - U^* \propto e^{-t/\tau}, \tag{104}$$

with

$$\tau = 1/\ln[U^{*2}\sigma^{-1}/p(\sigma/U^*)]. \tag{105}$$

For the Weibull threshold distribution with index=5,

$$p(\sigma/U^*) = 5(\sigma/U^*)^4\exp[-(\sigma/U^*)^5] = 5\sigma^4/U^{*3} \tag{106}$$

and thus

$$\tau = 1/\ln(U^{*5}/5\sigma^5). \tag{107}$$

If we allow ourselves to use the exponential formula [Eq. (104)] all the way from $U_0=1$, we obtain

$$U_t - U^* = (1-U^*)e^{-t/\tau}. \tag{108}$$

For a finite number N of fibers the iteration will stop after a finite number of steps. It is a reasonable supposition to assume that the iteration stops when N_t-N^* is of the order 1. This corresponds to taking the left-hand side of Eq. (108) equal to $1/N$. The corresponding number of iterations is then given by

$$t_f = \tau\ln[N(1-U^*)] \tag{109}$$

in general and

$$t_f = \frac{\ln[N(1-U^*)]}{\ln(U^{*5}/5\sigma^5)} \tag{110}$$

in the Weibull case. Solving the Weibull iteration $U^*=\exp[-(\sigma/U^*)^5]$ with respect to σ and inserting into Eq. (110), we obtain

$$t_f = -\frac{\ln[N(1-U^*)]}{\ln[5(-\ln U^*)]}, \tag{111}$$

$$\sigma = U^*(-\ln U^*)^{1/5}. \tag{112}$$

These two equations represent the function $t(\sigma)$ in parameter form, with U^* running from $U_c = e^{-1/5}$ to $U^* = 1$.

For $U^* = U_c = e^{-1/5}$ Eq. (111) shows that t_f is infinite, as it should be. To investigate the critical neighborhood we set $U^* = U_c(1+\Delta U)$, with ΔU small, to obtain to lowest order

$$t_f = \frac{\ln(N)}{5\Delta U}, \tag{113}$$

$$\sigma_c - \sigma = \tfrac{5}{2}\sigma(\Delta U)^2. \tag{114}$$

The combination of Eqs. (113) and (114) gives, once more, the square root divergence

$$t_f(\sigma) \simeq \kappa_-(\sigma_c\sigma)^{-1/2}, \tag{115}$$

now with the magnitude

$$\kappa_- = 10^{-1/2}(5e)^{-1/10}\ln(N). \tag{116}$$

Simulation results for the precritical Weibull distribution are shown in Fig. 12(b), which shows good agreement with the analytical solutions (111) and (112).

For a general threshold distribution the divergence and its amplitude are easily deduced by expanding both the load curve $\sigma = x[1-P(x)]$ and the characteristic time τ around the critical threshold x_c. To lowest contributing order in $x_c - x$ we find

$$\sigma = \sigma_c - \tfrac{1}{2}[2p(x_c) + x_c p'(x_c)] + (x_c - x)^2 \tag{117}$$

and

$$\tau = \frac{x_c p(x_c)}{2p(x_c) + x_c^2 p'(x_c)}(x_c - x). \tag{118}$$

Inserting for $x_c - x$ from the equation above and using Eq. (110), we find

$$t_f = \kappa_-(\sigma_c - \sigma)^{-1/2}, \tag{119}$$

with

$$\kappa_- = x_c p(x_c)[4p(x_c) + 2x_c p'(x_c)]^{-1/2}\ln(N). \tag{120}$$

To show how the magnitude of the amplitude κ_- depends on the form of the threshold distribution, we consider a Weibull distribution

$$P(x) = 1 - e^{(x/a)^\rho} \tag{121}$$

with varying coefficient ρ and constant average strength. With $a = \Gamma(1+1/\rho)$ the average strength $\langle x\rangle$ equals unity, and the width takes the value

$$w = (\langle x^2\rangle - \langle x\rangle^2)^{1/2} = [\Gamma(1+2/\rho)/\Gamma^2(1+1/\rho) - 1]^{1/2}. \tag{122}$$

Here Γ is the Gamma function. Using the power-series expansion $\Gamma(1+z) = 1 - 0.577z + 0.989z^2 + \cdots$, we see how the width decreases with increasing ρ,

$$w \simeq \frac{1.52}{\rho}. \tag{123}$$

For the Weibull distribution [Eq. (121)] we use Eq. (120) to calculate the amplitude κ_-, with the result

$$\kappa_- = [\Gamma(1+1/\rho)/2\rho]^{1/2}(\rho e)^{-1/2\rho}\ln(N) \simeq (2\rho)^{-1/2}\ln(N), \tag{124}$$

the last expression for large ρ. A comparison between Eqs. (123) and (124) shows that for narrow distributions

$$\kappa_- \propto \sqrt{w}. \tag{125}$$

That narrow distributions give small amplitudes could be expected: many fibers with strengths of almost the same magnitude will tend to break simultaneously; hence the relaxation process goes more quickly.

c. Universality of critical amplitude ratio

As a function of the initial stress σ the number of relaxation steps $t_f(\sigma)$ shows a divergence $|\sigma - \sigma_c|^{-1/2}$ at the critical point on both the precritical and postcritical sides. This is a generic result, valid for a general probability distribution of the individual fiber strength thresholds. On the postcritical side $t_f(\sigma)$ is independent of the system size N for large N. On the precritical side there is, however, a weak (logarithmic) N dependence, as witnessed by Eqs. (46), (47), and (55). Note that the critical amplitude ratio takes the same value $\kappa_-/\kappa_+ = \ln(N)/2\pi$ for the uniform and Weibull distributions. This shows the universal nature of the critical amplitude ratio, independent of the threshold distribution. Note the difference from normal critical phenomena (Aharony, 1976) due to the appearance of $\ln(N)$ in the amplitude ratio here.

5. Nonlinear stress-strain behavior

The fiber bundle model correctly captures the nonlinear elastic behavior in the ELS mode (Sornette, 1989; Bernardes, 1994; Pradhan *et al.*, 2002). In the case of strain-controlled loading, using the theory of extreme order statistics, it has been shown (Sornette, 1989) that ELS bundles show nonlinear stress-strain behavior after an initial linear part up to which no fiber fails. Similar nonlinear behavior is seen in the force-controlled loading case as well. Moreover, from the recursive failure dynamics, the amount of stress drop at the breaking point can be calculated exactly (Pradhan *et al.*, 2002). To demonstrate the scenario we consider an ELS bundle with uniform fiber strength distribution, having a low cutoff C_L, such that for stresses below the low cutoff, none of the fibers fail. Hence, until failure of any of the fibers, the bundle shows linear elastic behavior. As soon as the fibers start to fail, the stress-strain relationship becomes nonlinear. This nonlinearity can be easily calculated in the ELS model using Eq. (8) for the failure dynamics of the model.

Fibers here are assumed to be elastic, each having unit force constant, with their breaking strengths (thresholds) distributed uniformly within the interval $[C_L, 1]$,

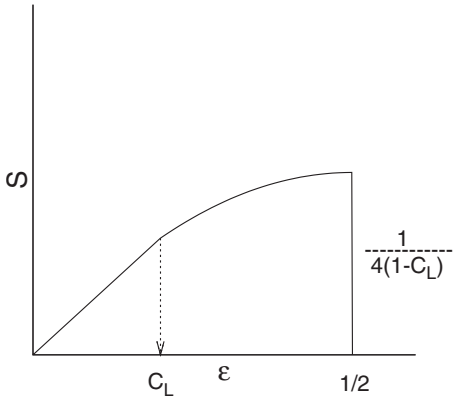

FIG. 13. The stress-strain curve for an ELS bundle having uniform fiber strength distribution with a low cutoff $C_L=0.2$.

$$p(x)=\begin{cases}0, & 0\leqslant x\leqslant C_L\\ \dfrac{1}{1-C_L}, & C_L<x\leqslant 1.\end{cases} \tag{126}$$

For an applied stress $\sigma\leqslant C_L$ none of the fibers break, though they are elongated by an amount $\varepsilon=x=\sigma$. The dynamics of breaking starts when applied stress σ becomes greater than C_L. For $\sigma>C_L$, the basic recursion relation [Eq. (8)] takes the form

$$U_{t+1}=\frac{1}{1-C_L}\left(1-\frac{\sigma}{U_t}\right), \tag{127}$$

which has stable fixed points,

$$U^*(\sigma)=\frac{1}{2(1-C_L)}\left[1+\left(1-\frac{\sigma}{\sigma_c}\right)^{1/2}\right]. \tag{128}$$

The model now has a critical point $\sigma_c=1/4(1-C_L)$ beyond which the bundle fails completely. At each fixed point, there will be an equilibrium elongation $\varepsilon(\sigma)$, and a corresponding stress $S=U^*\varepsilon(\sigma)$ develops in the system (bundle). From Eq. (127), one gets (for $\sigma>C_L$)

$$U^*(\sigma)=\frac{1-x^*}{1-C_L},\quad x^*=\frac{\sigma}{U^*}. \tag{129}$$

Also, from the force balance condition, at each fixed point $\varepsilon(\sigma)=x^*$. Therefore, the stress-strain relation for the ELS model finally becomes

$$S=\begin{cases}\varepsilon, & 0\leqslant\sigma\leqslant C_L\\ \varepsilon(1-\varepsilon)/(1-C_L), & C_L\leqslant\sigma\leqslant\sigma_c\\ 0, & \sigma>\sigma_c.\end{cases} \tag{130}$$

The stress-strain relation in an ELS bundle is shown in Fig. 13, where the initial linear region has unit slope (the force constant of each fiber). This Hooke's region for the stress S continues up to the strain value $\varepsilon=C_L$, until which not one of the fibers breaks. After this, nonlinearity appears due to the failure of a few of the fibers and the consequent decrease of $U^*(\sigma)$. It finally drops to zero discontinuously by an amount $x_c^*U^*(\sigma_c)=1/4(1-C_L)$ at the breaking point $\sigma=\sigma_c$ or $\varepsilon=x_c^*=1/2$ for the bundle. It may be noted that in this model the internal stress x_c^* is universally equal to 1/2, independent of C_L at the failure point $\sigma=\sigma_c$.

6. Effect of a low cutoff: Instant failure situation

A low cutoff in the fiber threshold distribution excludes the presence of very weak fibers in a bundle. The weaker fibers mainly reduce the strength of a bundle. But in practice we always try to build stronger and stronger materials (ropes, cables, etc.) from the fibrous elements. Therefore this situation (exclusion of weaker fibers) is very realistic. Here we discuss the effect (Pradhan and Hansen, 2005) of a low cutoff on the failure properties of ELS bundles.

We follow the weakest-fiber-breaking approach (Daniels, 1945; Hemmer and Hansen, 1992): the applied load is tuned in such a way that only the weakest fiber (among the intact fibers) will fail after each step of loading. We first find the extreme condition when the whole bundle fails instantly after the first fiber ruptures. As the strength thresholds of N fibers are uniformly distributed between C_L and 1 [Eq. (126)], the weakest fiber fails at a stress C_L (for large N). After this single fiber failure, the load will be redistributed within intact fibers resulting in a global stress $x_f=NC_L/(N-1)$. Now, the number of intact fibers having strength threshold below x_f is

$$NP(x_f)=N\int_{C_L}^{x_f}p(y)dy=\frac{N(x_f-C_L)}{(1-C_L)}. \tag{131}$$

Stress redistribution can break at least another fiber if $NP(x_f)\geqslant 1$ and this "second" failure will trigger another failure, and so on. Thus the successive breaking of fibers cannot be stopped until the complete collapse of the bundle. Clearly, there cannot be any fixed point (critical point) for such an "instant failure" situation. Setting the value of x_f we get

$$\frac{N\left(\dfrac{NC_L}{N-1}-C_L\right)}{(1-C_L)}\geqslant 1, \tag{132}$$

which gives

$$C_L\geqslant (N-1)/(2N-1). \tag{133}$$

In the large-N limit the above condition can be written as $C_L\geqslant 1/2$. Therefore, the condition to get a fixed point in the failure process is $C_L<1/2$.

We can also calculate how many steps are required to attain the final catastrophic failure for $C_L<1/2$. We assume that we have to increase the external load n times before the final failure. At each step of such load increment only one fiber fails. Then after n steps the following condition should be fulfilled to have a catastrophic failure:

$$N\int_{x_i}^{x_i[1+1/(N-n)]}p(y)dy\geqslant 1, \tag{134}$$

where

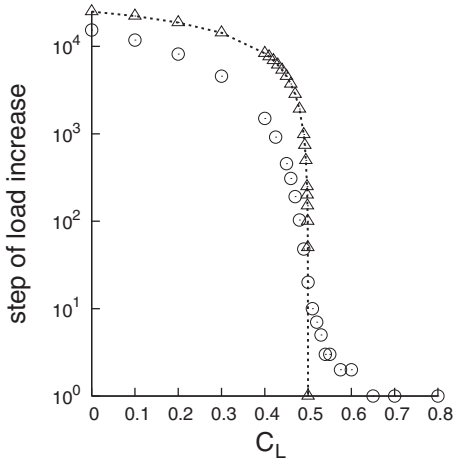

FIG. 14. The number of steps of load increase (until final failure) plotted against C_L for an ELS model having 50 000 fibers. The dotted line represents the analytic form [Eq. (136)], the triangles are the simulated data for a strictly uniform strength distribution, and the circles represent the data (averages are taken for 5000 samples) for a uniform on average distribution.

$$x_i = C_L + \frac{n(1-C_L)}{N}. \tag{135}$$

The solution gives

$$n = \frac{N}{2}\left(1 - \frac{C_L}{1-C_L}\right). \tag{136}$$

The above equation suggests that at $C_L = 1/2$, $n=0$. But in reality we have to set the external load once to break the weakest fiber of the bundle. Therefore, $n=1$ for $C_L \geqslant 1/2$ (Fig. 14). To check the validity of the above calculation we take "strictly uniform" and uniform on average distributions of fiber strength. In our strictly uniform distribution the strength of the kth fiber (among N fibers) is $C_L + (1-C_L)k/N$. We can see in Fig. 14 that the "strictly uniform distribution" exactly obeys the analytic formula (136) but the uniform on average distribution, shows slight disagreement, which comes from the fluctuation in the distribution function for a finite system size. This fluctuation will disappear in the limit $N \to \infty$ where we expect perfect agreement.

B. Fluctuations

If the contributions to breakdown phenomena in materials science by statistical physics were to be expressed in one word, that word would have to be fluctuations. In the context of fiber bundles, this concept refers to the effects of the fibers each having properties that are statistically distributed around some mean, which cannot be reproduced by substituting the fiber bundle by an equivalent one where each fiber is identical to all the others.

Intuitively, it is not difficult to accept that fluctuations must play an important role in the breakdown properties of fiber bundles or in fracture and breakdown phenomena in general. A plane ride in turbulent weather compared to one in smooth weather is a reminder of this.

Closely connected to the question of fluctuations is that of phase transitions and criticality (Stanley, 1987). Leaving the fiber bundles for a moment, consider a fluid whose temperature is slowly raised. At a well-defined temperature determined by the surrounding pressure, the fluid starts to boil. Each gas bubble that rises to the surface is due a fluctuation being larger than a well-defined size for which the bubble grows rather than shrinks away. At a particular pressure the character of the boiling changes. There is no longer any size that determines whether a nascent bubble grows or shrinks. There are bubbles of all sizes. At this particular point, the system is critical and undergoes a second-order phase transition. The boiling process at other pressures signals a first-order transition.

A brittle material under stress develops microcracks. These appear where the material is weak or where the local stress field is high. As the stress increases, more and more microcracks accumulate until either one or a few microcracks become unstable and grow to macroscopic dimensions causing failure. The spatial fluctuations of the local material properties cause the appearance of microcracks. Their subsequent growth accentuates these initial fluctuations but in a highly complex manner due to interactions between the growing cracks. There are similarities between this scenario and a first-order transition (Zapperi *et al.*, 1997). On the other hand, stable mode-I crack growth as studied experimentally by Schmittbuhl and Måløy (1997) and Måløy and Schmittbuhl (2001) indicates that the advancing crack front shows a dynamics compatible with being at a critical point.

We now turn to the global load-sharing fiber bundle model in light of the preceding remarks.

1. Burst distribution for continuous load increase

When a fiber ruptures somewhere, the stress on the intact fibers increases. This may in turn trigger further fiber failures, which can produce bursts (avalanches) that lead either to a stable situation or to breakdown of the whole bundle. A burst is usually defined as the amount or number (Δ) of simultaneous fiber failures during loading. One may study the distribution $D(\Delta)$ of the bursts appearing during the entire failure process until the complete breakdown of the bundle.

The property of the fiber bundle model of interest in the present context is the fluctuation-driven *burst distribution.* In order to define this property, we again consider a finite bundle containing N elastic fibers whose strength thresholds are picked randomly from a probability density $p(x)$. Let x_k be the ordered sequence of failure thresholds: $x_1 \leqslant x_2 \leqslant \cdots \leqslant x_N$. Then the external load or force F on the bundle [Eq. (3)] at the point where the kth fiber is about to fail can be written as

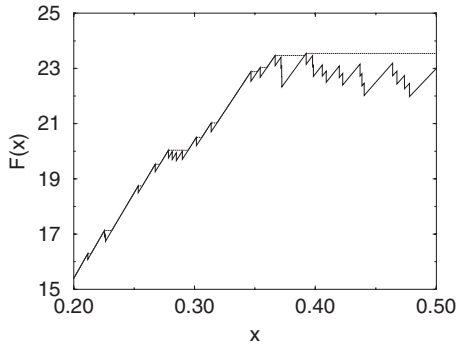

FIG. 15. The solid curve indicates the total force $F(x)$ as a function of x. However, when our control parameter is F rather than x, the system will follow the dotted line [Eq. (138)]. The bursts are the horizontal parts of $F_{ph}(x)$. Here $N=100$.

$$F_k = (N+1-k)x_k, \tag{137}$$

where the elastic constant of the fibers is set equal to unity as before. Note that the sequence of external loads F_k is not monotonically increasing. This may be readily seen from Eq. (137); the total load is the product of a monotonically increasing *fluctuating* quantity x_k and a monotonically *decreasing* quantity $(N+1-k)$. Suppose now that our control parameter is the total load F and that $k-1$ fibers have broken. In order to be in this situation, $F>F_k>F_j$ for all $j<k$. The latter inequality ensures that the situation we are studying is not unstable. We increase F until it reaches F_k at which fiber k breaks. If now $F_{k+1}\leqslant F_k$, then fiber $k+1$ will also break without the external load F being further increased. The same may be true for F_{k+2} and so on until the $(k+\Delta-1)$th bond breaks. Thus, $F_{k+j}\leqslant F_k$ for $j<\Delta$. If now $F_{k+\Delta}>F_k$, the burst of breaking bonds then stops at this point, and we have experienced a burst event of size Δ.

The total force F expressed as a function of elongation x is shown in Fig. 15. When the control parameter is elongation x, the solid curve is followed. However, when the force F is the control parameter, the broken lines given by

$$F_{ph} = \text{LMF } F(x), \tag{138}$$

where LFM designates the least monotonic function.

a. Generic case

Hemmer and Hansen (1992) showed that the average number of burst events of size Δ per fiber $D(\Delta)/N$ follows a power law of the form

$$D(\Delta)/N = C\Delta^{-\xi} \tag{139}$$

in the limit $N\to\infty$. Here

$$\xi = \frac{5}{2} \tag{140}$$

is the *universal* burst exponent. The value (140) is, under very mild assumptions, independent of the threshold distribution $P(x)$: the probability density needs to have a quadratic maximum somewhere in the interval $x_{\min}<x<x_{\max}$. We demonstrate this in Fig. 16. The prefactor C in Eq. (139) is given by

$$C = \frac{x_c p(x_c)^2}{\sqrt{2\pi}[x_c p'(x_c) + 2p(x_c)]}, \tag{141}$$

where x_c is the solution of

$$x_c p(x_c) = 1 - P(x_c) \tag{142}$$

and is the value of x for which the characteristic has a maximum. Equations (139)–(142) were derived by Hemmer and Hansen (1992) using combinatorial arguments. However, we will take an alternative route in the following, based on a mapping between the global load-sharing model and a Brownian process (Sornette, 1992; Hansen and Hemmer (1994a). Before we explain this mapping we quote, for later comparison, the results of the Hemmer-Hansen analysis (Hemmer and Hansen, 1992):

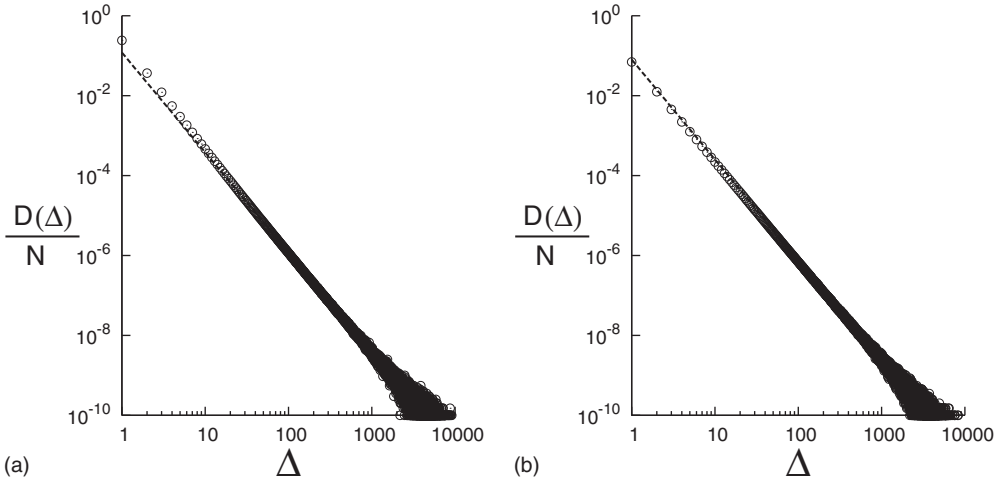

FIG. 16. The burst distribution $D(\Delta)/N$ for (a) the uniform distribution and (b) the Weibull distribution with index 5. The dotted lines represent the power law with exponent $\xi=5/2$. Both are based on 20 000 samples of bundles each with $N=10^6$ fibers.

the probability $\Phi(\Delta,x)$ that a burst event at elongation x will have the size Δ is

$$\Phi(\Delta,x) = \frac{\Delta^{\Delta-1}}{\Delta!}\frac{m(x)}{1-m(x)}\{[1-m(x)]e^{m(x)-1}\}^{\Delta}, \tag{143}$$

where

$$m(x) = 1 - \frac{xp(x)}{1-P(x)}. \tag{144}$$

Note in particular that by Eq. (142) $m(x_c)=0$. We now assume that we do not load the fiber bundle until complete collapse, i.e., until $x=x_c$, but stop at a value $x_s < x_c$. We may then ask for $D(\Delta,x_s)/N$, the expected number of burst events of size Δ during the breakdown process that occurs between $x=0$ and $x=x_s$. This is given by

$$\begin{aligned}\frac{D(\Delta,x_s)}{N} &= \int_0^{x_s} p(x)dx\ \Phi(\Delta,x) \\ &= \frac{\Delta^{-3/2}}{\sqrt{2\pi}}\int_0^{x_s} dx\ p(x)\frac{m(x)}{1-m(x)} \\ &\quad\times\{[1-m(x)]e^{m(x)}\}^{\Delta},\end{aligned} \tag{145}$$

where on the right-hand side the Stirling approximation $\Delta! \approx \sqrt{2\pi}\Delta^{\Delta+1/2}e^{-\Delta}$ for large Δ has been used. The integrand in Eq. (145) is strongly peaked near $x=x_c$. We therefore expand it to second order in $y=x_c-x$ to find

$$\begin{aligned}\frac{D(\Delta,x_s)}{N} &= \frac{\Delta^{-3/2}}{\sqrt{2\pi}}p(x_c)m'(x_c) \\ &\quad\times\int_{x_c-x_s}^{\infty} dy\ ye^{-m'(x_c)^2y^2\Delta/2},\end{aligned} \tag{146}$$

where we have extended the upper integration limit to ∞. We may use this integral to get

$$\frac{D(\Delta,x_s)}{N} = C\Delta^{-5/2}e^{-m'(x_c)^2\Delta(x_c-x_s)^2/2}, \tag{147}$$

where C is defined by Eq. (141).

We may write Eq. (147) in scaling form,

$$\frac{D(\Delta,x_s)}{N} = \Delta^{-\xi}G(\Delta,x_s) = \Delta^{-\xi}G(\Delta^{\mu}(x_c-x_s)), \tag{148}$$

where

$$G(y) = Ce^{-m'(x_c)^2y^2/2}. \tag{149}$$

In particular, $G(y)$ tends to the constant C for $y\to 0$. Two universal critical exponents appear, $\xi=5/2$ [Eq. (140)] and

$$\mu = \frac{1}{2}. \tag{150}$$

It is, thus, in the above sense that the fracture process of the fiber bundle approaches a critical point at total breakdown: the distribution of burst events follows a power law with an upper cutoff that diverges as the bundle approaches total failure.

Sornette (1992) and later on Hansen and Hemmer (1994a), derived the burst distribution [Eq. (139)] from the assumption that F_k may be directly interpreted as a biased random walk. The precise nature of this random walk is elucidated below. It is a peculiar asymmetric walk with variable step length. In the limit $N\to\infty$ and continuous time variable $k/N\to t$ and $\Delta k/N\to\delta t>0$, this random walk may be mapped onto a continuous Brownian process. Such Brownian processes have been studied by Phoenix and Taylor (1973), Daniels and Skyrme (1985), and Daniels (1989) in connection with the distribution of the strength S of fiber bundles. In the following we derive Eq. (145) by means of a biased random-walk model with variable step length. We find this an interesting example of universality in statistical physics: the asymptotic behavior of one model is found by using a different model with the same asymptotic behavior as the first one, but which is simpler to solve before the continuum limit is taken.

Under increasing load the variation of the force per fiber $f=F/N$ will consist of a systematic nonfluctuating part, given by the average load-elongation characteristics, with a small fluctuation of order $1/\sqrt{N}$ superimposed.

The precise value of the force fluctuation depends on whether one studies the force $f(x)$ at given elongation or the force f_k at which fiber number k breaks. We calculate the variance of f, σ_f^2, for both quantities, starting with the constant-k ensemble.

The force per fiber when the kth fiber is about to break is, since $F_k=(N+1-k)x_k$,

$$f_k = [1-P(\bar{x}_k)]x_k, \tag{151}$$

where x_k is the elongation when the kth fiber breaks, and we have defined $\bar{x}_k$ by

$$P(\bar{x}_k) = \frac{k}{N+1}. \tag{152}$$

For large N, $\bar{x}_k$ is essentially the average value of x_k. For a fixed k the variance of f_k is by Eq. (151) given by the variance of x_k,

$$\sigma_f^2(k) = [1-P(x_k)]^2\sigma_{x_k}^2, \tag{153}$$

and therefore the probability $\varphi(x)dx$ that the kth threshold in the ordered threshold sequence lies in the interval $(x,x+dx)$. This probability is given by

$$\varphi(x)dx = \frac{N!}{(k-1)!(N-k)!}P(x)^{k-1}[1-P(x)]^{N-k}p(x)dx. \tag{154}$$

For large k and N, and using Eq. (152), this is close to the Gaussian distribution,

$$\varphi(x)dx = \left(\frac{Np(\bar{x}_k)^2}{2\pi P(\bar{x}_k)[1-P(\bar{x}_k)]}\right)^{1/2} \times e^{-Np(\bar{x}_k)^2(x-\bar{x}_k)^2/2P(\bar{x}_k)[1-P(\bar{x}_k)]}dx. \quad (155)$$

This gives the variance of x_k and thus of f_k,

$$\sigma_f^2(k) = \frac{P(\bar{x}_k)[1-P(\bar{x}_k)]^3}{Np(\bar{x}_k)^2}. \quad (156)$$

We now compare with the force fluctuation at constant elongation. The force per fiber is the following function of elongation x:

$$f(x) = N^{-1}\sum_{i=1}^{N} x\Theta(t_i - x), \quad (157)$$

where t_i is the breakdown threshold for the ith fiber and $\Theta(t)$ is the Heaviside function. This gives immediately the average force

$$\langle f\rangle_x = x[1-P(x)], \quad (158)$$

i.e., the characteristics, as well as the variance

$$\sigma_f^2(x) = \frac{x^2P(x)[1-P(x)]}{N}. \quad (159)$$

Although the two types of force fluctuation have different variances, in both cases $\sigma \propto 1/\sqrt{N}$.

The nonmonoticities of the force f within the fluctuation zone produce bursts. Since the fluctuations are so small for large N, one can treat the burst events *locally.*

We now consider the force sequence F_k as a stochastic process. Since we seek the *asymptotic* burst distribution, we are interested in the behavior after many steps of the process. It is convenient, however, to start with the one-step process.

We determine the probability distribution of the force increase $\Delta F = F_{k+1} - F_k$ between two consecutive bursts, the first one taking place at elongation x_k with $F_k = (N-k+1)x_k$. Since $\Delta F = (N-k)(x_{k+1}-x_k) - x_k$, we have

$$\Delta F \geqslant -x_k. \quad (160)$$

The probability of finding the $(k+1)$th threshold in $(x_{k+1}, x_{k+1}+dx_{k+1})$ for given x_k,

$$(N-k-1)\frac{[1-P(x_{k+1})]^{N-k-2}}{[1-P(x_k)]}p(x_{k+1})dx_{k+1}, \quad (161)$$

gives directly using the connection $x_{k+1} = x_k + [\Delta F(x_k) + x_k]/(N-k)$ the probability density $\rho(\Delta F; x_k)$ of ΔF,

$$\rho(\Delta F; x_k) = \frac{N-k-1}{N-k}\frac{\left[1-P\left(x_k + \frac{\Delta F + x_k}{N-k}\right)\right]^{N-k-2}}{[1-P(x_k)]^{N-k-1}} \times p\left(x_k + \frac{\Delta F + x_k}{N-k}\right). \quad (162)$$

For large $N-k$ this simplifies to

$$\rho(\Delta F; x_k) = \begin{cases} \dfrac{p(x_k)}{1-P(x_k)\exp\left(-\dfrac{(\Delta F + x_k)p(x_k)}{1-P(x_k)}\right)} & \text{for } \Delta F \geqslant -x_k \\ 0 & \text{for } \Delta F < -x_k. \end{cases} \quad (163)$$

This one-dimensional random walk is asymmetric in more than one way. First, it has nonzero bias,

$$\langle \Delta F\rangle(x_k) = \frac{1-P(x_k) - x_k p(x_k)}{p(x_k)}. \quad (164)$$

In addition, the probability distribution around this average is very asymmetric.

The variance is easily determined:

$$\sigma_{\Delta F}^2(x_k) = \left(\frac{1-P(x_k)}{p(x_k)}\right)^2. \quad (165)$$

The Brownian motion limit of a one-dimensional random walk is completely determined by the first and second moments of the single-step probability distribution. The results just obtained enable us therefore to select an "ordinary" biased random walk with constant step length a, which has the same Brownian motion limit as the burst process.

We imagine having a one-dimensional random walk along the z axis with a constant bias. Each step is of length a. Let the probability to take a step in the negative z direction be q and let p be the probability to take a step in the positive z direction. The walk is biased when p is different from q. The probability distribution of the position z_1 after one step has the average

$$\langle z_1\rangle = a(p-q) \quad (166)$$

and variance

$$\sigma_1^2 = 4pqa^2. \quad (167)$$

Elimination of a yields

$$\frac{p-q}{2\sqrt{pq}} = \frac{\langle z_1\rangle}{\sigma_1}. \quad (168)$$

Since $p+q=1$, the bias parameters are determined.

After k steps a Gaussian distribution

$$\frac{e^{-[z_k - z_0 - ka(p-q)]^2/8pqa^2k}}{\sqrt{8\pi pqa^2k}} \quad (169)$$

is approached when k increases.

The two processes will have the same asymptotic behavior when we make the identification

$$\frac{p-q}{2\sqrt{pq}} = \frac{\langle \Delta F\rangle}{\sigma_F} = 1 - \frac{x_k p(x_k)}{1-P(x_k)} = m(x_k), \quad (170)$$

where $m(x)$ is defined by Eq. (144). When the bias is small, both p and q are close to $1/2$, and we have to lowest order

$$p = \frac{1}{2}[1 + m(x)],$$
$$q = \frac{1}{2}[1 - m(x)]. \tag{171}$$

We have now made the promised mapping between the fiber bundle problem and a random walk with a constant bias. A constant bias may be used since bursts can be treated locally.

The next step is to calculate the burst distribution for such a biased random walk. Since this biased random walk by construction has the same asymptotic behavior in the limit $N \to \infty$ as the original fiber bundle problem, the two burst distributions will asymptotically be the same.

In terms of the biased random walk, a burst event of size Δ at "time" k may be defined as follows: (i) $z_{k+i} < z_k$ for $0 < i < \Delta$ and $z_{k+\Delta} \geqslant z_k$. (ii) Furthermore, to ensure that we are not counting burst events *inside* other burst events, the condition $z_k > z_j$ for $k > j$ is necessary.

The first condition is in fact a special case of the "gambler's ruin" problem (Feller, 1966). A gambler plays a series of independent games against a bank with infinite resources. In each game, the gambler either loses or wins one euro, and the probability that the bank wins is $p = (1+B)/2$, while the probability that the gambler wins is $q = (1-B)/2$. If the gambler starts out with a capital of z euros, the probability that she is ruined after precisely Δ games is

$$\pi(z,\Delta) = \frac{z}{\Delta}\binom{\Delta}{\frac{\Delta}{2} - \frac{z}{2}} p^{(\Delta - z)/2} q^{(\Delta + z)/2}. \tag{172}$$

The probability that condition (i) is fulfilled for a biased random walk burst of size Δ is then

$$\frac{1}{2}\pi(z = 1,\Delta) = \frac{\Delta^{-3/2}}{\sqrt{2\pi}}\sqrt{\frac{1-B}{1+B}}(1 - B^2)^{\Delta/2}, \tag{173}$$

where we have assumed that $\Delta \gg 1$.

The probability that a biased random walker returns at least once to the origin is (Feller, 1966) $1 - |p - q| = 1 - B$. The probability condition (ii), namely, that $z_j > z_k$ for all $j < k$ is fulfilled, is then simply $1 - (1 - B) = B$ and we have that the probability for having a burst of size Δ happening at "time" k is

$$\Phi_{\mathrm{RW}}(\Delta,B) = \frac{1}{2}B\pi(z = 1,\Delta) = \frac{\Delta^{-3/2}}{\sqrt{2\pi}}Be^{-B^2\Delta/2}, \tag{174}$$

where we also assumed that $B \ll 1$.

Returning to the fiber bundle model, the bias $B = m(x)$. When x is close to x_c, we have $B = m'(x_c)y$, where $y = (x_c - x)$. Thus, the probability to have a burst of size Δ between y and $y + dy$ is

$$\Phi_{\mathrm{RW}}(\Delta,m'(x_c)y)p(x_c)dy = \frac{\Delta^{-3/2}}{\sqrt{2\pi}}p(x_c)m'(x_c)e^{-m'(x_c)y^2\Delta/2}. \tag{175}$$

Thus, the cumulative burst distribution up the elongation x_s is

$$\int_{x_c - x_s}^{\infty} \Phi_{\mathrm{RW}}(\Delta,m'(x_c)y)p(x_c)dy. \tag{176}$$

Comparing this expression to Eq. (146), we see that they are identical. This completes the derivation of the asymptotic burst distribution via the mapping between the random-walk problem and the burst process.

b. Special cases

The burst distribution given in Eq. (145) is valid when the threshold distribution has a parabolic maximum inside the interval of the thresholds. We now consider threshold distributions that do not reach their maximum at the boundaries of the interval (Kloster *et al.*, 1997). Model examples of such threshold distributions are

$$P(x) = \begin{cases} 0 & \text{for } x \leqslant x_0 \\ 1 - [1 + (x - x_0)/x_r]^{-\alpha_0} & \text{for } x > x_0. \end{cases} \tag{177}$$

Here α_0 and x_0 are positive parameters and x_r is a reference quantity, which we for simplicity set equal to unity in the following. These distributions are all characterized by diverging moments. When $\alpha_0 \leqslant 1$, even the first moment—the mean—as well as all other moments diverge. This class of threshold distributions is rich enough to exhibit several qualitatively different burst distributions.

The corresponding macroscopic bundle strength per fiber is

$$\frac{\langle F \rangle(x)}{N} = \begin{cases} x & \text{for } x \leqslant x_0 \\ \dfrac{x}{(1 + x - x_0)^{\alpha_0}} & \text{for } x > x_0. \end{cases} \tag{178}$$

In Fig. 17 the corresponding macroscopic force curves $\langle F \rangle(x)$ are sketched. We note that when $\alpha_0 \to 1$, the plateau in Eq. (178) becomes infinitely wide.

The distribution of burst sizes is given by Eq. (145). In the present case the function $m(x)$ takes the form

$$m(x) = \frac{xp(x)}{1 - P(x)} = \frac{\alpha_0 x}{1 + x - x_0}. \tag{179}$$

A simple special case is $x_0 = 1$, corresponding to

$$p(x) = \alpha_0 x^{-\alpha_0 - 1} \quad \text{for } x \geqslant 1$$

since then the function (179) is independent of f,

$$m(x) = \alpha_0.$$

This gives

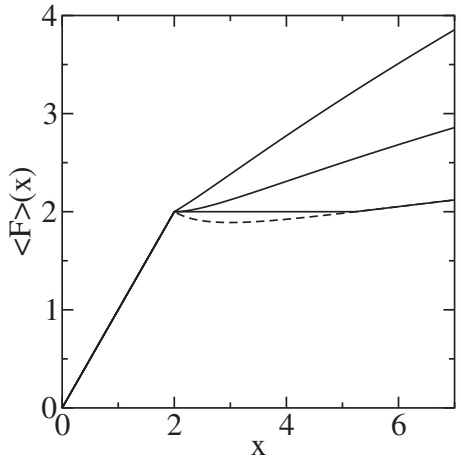

FIG. 17. The macroscopic bundle strength $\langle F\rangle(x)$ for the distribution [Eq. (177)], with $x_0=2x_r$, and for $\alpha_0=1/3$ (upper curve), 1/2 (middle curve), and 2/3 (lower curve). The broken part of the $\alpha_0=2/3$ curve is unstable and the macroscopic bundle strength will follow the solid line.

$$\frac{D(\Delta)}{N}=\frac{1-\alpha_0}{\alpha_0}\frac{\Delta^{\Delta-1}}{\Delta!}[\alpha_0 e^{-\alpha_0}]^{\Delta}$$
$$\simeq\frac{1-\alpha_0}{\alpha_0\sqrt{2\pi}}\Delta^{-3/2}[\alpha_0 e^{1-\alpha_0}]^{\Delta}. \quad (180)$$

In other cases it is advantageous to change the integration variable in Eq. (145) from x to m:

$$\frac{D(\Delta)}{N}=\frac{\Delta^{\Delta-1}}{e^{\Delta}\Delta!}\frac{1}{\alpha_0^{\alpha_0-1}(1-x_0)^{\alpha_0}}\int_{\alpha_0 x_0}^{\alpha_0}(\alpha_0-m)^{\alpha_0-1}$$
$$\times(1-m)m^{-1}(me^{1-m})^{\Delta}\,dm. \quad (181)$$

The asymptotics for large Δ, beyond the $\Delta^{-3/2}$ dependence of the prefactor, is determined by the Δ-dependent factor in the integrand. The maximum of me^{1-m} is unity, obtained for $m=1$, and the asymptotics depends crucially on whether $m=1$ falls either outside the range of integration or inside (including the border). If the maximum falls inside the range of integration the $D(\Delta)\propto\Delta^{-5/2}$ dependence remains. A special case of this is $\alpha_0=1$, for which the maximum of the integrand is located at the integration limit and the macroscopic force has a "quadratic" maximum at infinity. Another special case is $\alpha_0 x_0=1$ (and $\alpha_0<1$), for which again the standard asymptotics $\Delta^{-5/2}$ is valid. In this instance the macroscopic force has a quadratic *minimum* at $x=x_0$ (see Fig. 17 for $\alpha_0=1/2$), and critical behavior arises just as well from a minimum as from a maximum.

In the remaining cases, in which $m=1$ is not within the range of integration in Eq. (181), the burst distribution is always a power law with an exponential cutoff,

$$\frac{D(\Delta)}{N}\simeq\Delta^{-\xi}A^{\Delta}. \quad (182)$$

Here ξ and A depend on the parameter values x_0 and α_0, however. This is easy to understand. Since

TABLE I. Asymptotic behavior of the burst distribution for strong threshold distributions in the ELS model.

Parameters	Asymptotics
$0\leqslant x_0<1,\ \alpha_0<1$	$\Delta^{-3/2-\alpha_0}(\alpha e^{1-\alpha_0})^{\Delta}$
$0\leqslant x_0<1,\ \alpha_0=1$	$\Delta^{-5/2}$
$x_0=1,\ \alpha_0<1$	$\Delta^{-3/2}(\alpha_0 e^{1-\alpha_0})^{\Delta}$
$1<x_0<\alpha_0^{-1}$	$\Delta^{-5/2}(\alpha_0 x_0 e^{1-\alpha_0 x_0})^{\Delta}$
$1<x_0=\alpha_0^{-1}$	$\Delta^{-5/2}$
$1<\alpha_0^{-1}<x_0$	$\Delta^{-5/2}e^{-\Delta/\Delta_0}$

$$\frac{dm(x)}{dx}=\frac{\alpha_0(1-x_0)}{(1+x-x_0)^2}, \quad (183)$$

we see that $m(x)$ is a monotonically decreasing function for $x_0>1$, so that the maximum of me^{1-m} is obtained at the lower limit $x=x_0$, where $m=\alpha_0 x_0$. The asymptotics

$$D(\Delta)\propto\Delta^{-5/2}(\alpha_0 x_0 e^{1-\alpha_0 x_0})^{\Delta} \quad (184)$$

follows.

This is true merely for $\alpha_0 x_0<1$, however. For $\alpha_0 x_0>1$ the macroscopic force $\langle F\rangle(x)$ *decreases* near $x=x_0$ so that a macroscopic burst takes place at a force x_0 per fiber, and stabilization is obtained at a larger elongation x_1 (Fig. 17). The subsequent bursts have an asymptotic

$$D(\Delta)\propto\Delta^{-5/2}[a(f_1)e^{1-m(x_1)}]^{\Delta}, \quad (185)$$

determined by the neighborhood of $x=x_1$. For $t_0<1$, the maximum of me^{1-m} is obtained at $x=\infty$, leading to the asymptotic

$$D(\Delta)\propto\Delta^{-3/2-\alpha_0}(\alpha_0 e^{1-\alpha_0})^{\Delta}, \quad (186)$$

reflecting the power-law behavior of the integrand at infinity.

The results are summarized in Table I. Note that the $x_0=1$ result [Eq. (180)] cannot be obtained by setting $x_0=1$ in Eq. (184) since in Eq. (181) the order of the limits $\Delta\to\infty$ and $x_0\to1$ is crucial.

c. Crossover behavior

When all the bursts are recorded for the entire failure process, we have seen that the burst distribution $D(\Delta)$ follows the asymptotic power law $D\propto\Delta^{-5/2}$. If we just sample bursts that occur near the breakdown point, a different behavior is seen. As an illustration we consider the uniform threshold distribution and compare the complete burst distribution with what one gets when one samples merely burst from breaking fibers in the threshold interval $(0.9x_c,x_c)$. Figure 18 shows that in the latter case a different power law is seen.

This observation may be of practical importance, as it gives a criterion for the imminence of catastrophic failure (Pradhan, Hansen, and Hemmer, 2005). This proposal has so far not been tested experimentally. However, it is interesting to note the observation by Kawamura of a crossover behavior in the magnitude dis-

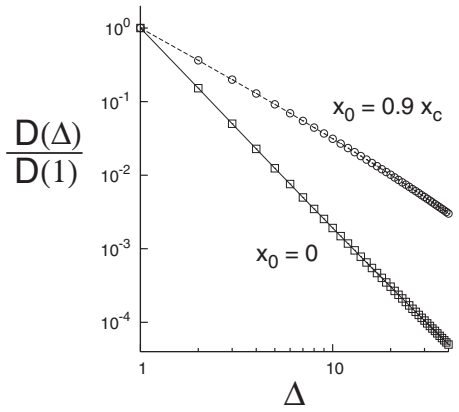

FIG. 18. The distribution of bursts for thresholds uniformly distributed in an interval (x_0,x_c), with $x_0=0$ and $0.9x_c$. Based on 50 000 samples, each containing $N=10^6$ fibers. The exponents of the distributions are $\xi=5/2$ and $3/2$, respectively.

tribution before large earthquakes appears (Kawamura, 2006). We return to this result in Sec. V.C and Fig. 61.

We introduce the following notation in Eq. (145):

$$\frac{D(\Delta)}{N} = \frac{\Delta^{\Delta-1}e^{-\Delta}}{\Delta!}\int_0^{x_c} p(x)r(x)[1-r(x)]^{\Delta-1} \times \exp[\Delta r(x)]dx, \tag{187}$$

where

$$r(x) = 1 - \frac{xp(x)}{Q(x)} = \frac{1}{Q(x)}\frac{d}{dx}[xQ(x)] \tag{188}$$

and $Q(x)=\int_x^\infty p(x)dx$. We note that $r(x)$ vanishes at the point x_c. If we have a situation in which the weakest fiber has its threshold x_0 just a little below the critical value x_c, the contribution to the integral in the expression (187) for the burst distribution will come from a small neighborhood of x_c. Since $r(x)$ vanishes at x_c, it is small here, and we may in this narrow interval approximate the Δ-dependent factors in Eq. (187) as follows:

$$\begin{aligned}(1-r)^\Delta e^{\Delta r} &= \exp\{\Delta[\ln(1-r)+r]\} \\ &= \exp\{-\Delta[r^2/2 + O(r^3)]\} \\ &\approx \exp[-\Delta r(x)^2/2].\end{aligned} \tag{189}$$

We also have

$$r(x) \approx r'(x_c)(x-x_c). \tag{190}$$

Inserting everything into Eq. (187), we obtain to dominating order

$$\begin{aligned}\frac{D(\Delta)}{N} &= \frac{\Delta^{\Delta-1}e^{-\Delta}}{\Delta!}\int_{x_0}^{x_c} p(x_c)r'(x_c)(x-x_c) \\ &\quad \times e^{-\Delta r'(x_c)^2(x-x_c)^2/2}\,dx \\ &= \frac{\Delta^{\Delta-2}e^{-\Delta}p(x_c)}{|r'(x_c)|\Delta!}[e^{-\Delta r'(x_c)^2(x-x_c)^2/2}]_{x_0}^{x_c} \\ &= \frac{\Delta^{\Delta-2}e^{-\Delta}}{\Delta!}\frac{p(x_c)}{|r'(x_c)|}[1-e^{-\Delta/\Delta_c}],\end{aligned} \tag{191}$$

with

$$\Delta_c = \frac{2}{r'(x_c)^2(x_c-x_0)^2}. \tag{192}$$

By use of the Stirling approximation $\Delta! \simeq \Delta^\Delta e^{-\Delta}\sqrt{2\pi\Delta}$, the burst distribution [Eq. (191)] may be written as

$$\frac{D(\Delta)}{N} = C\Delta^{-5/2}(1-e^{-\Delta/\Delta_c}), \tag{193}$$

with a nonzero constant

$$C = (2\pi)^{-1/2}p(x_c)/|r'(x_c)|. \tag{194}$$

We can see from Eq. (193) that there is a crossover at a burst length around Δ_c,

$$\frac{D(\Delta)}{N} \propto \begin{cases}\Delta^{-3/2} & \text{for } \Delta \ll \Delta_c \\ \Delta^{-5/2} & \text{for } \Delta \gg \Delta_c.\end{cases} \tag{195}$$

We have thus shown the existence of a crossover from the generic asymptotic behavior $D \propto \Delta^{-5/2}$ to the power law $D \propto \Delta^{-3/2}$ near criticality, i.e., near global breakdown. The crossover is a universal phenomenon, independent of the threshold distribution $p(x)$.

The simulation results we have shown so far are based on *averaging* over a large number of samples. For applications it is important that the crossover signal can also be seen in a single sample. We show in Fig. 19 that equally clear crossover behavior is seen in a *single* fiber bundle when N is large enough. Also, as a practical tool one must sample finite intervals (x_i, x_f) during the fracture process. The crossover will be observed when the interval is close to the failure point (Pradhan, Hansen, and Hemmer, 2005) and Pradhan *et al.* (2006).

The ELS fiber bundle model is a simple model in that it is analytically tractable. A step up in complexity from the ELS fiber bundle model is the random fuse model (Herrmann and Roux, 1990). While resisting most ana-

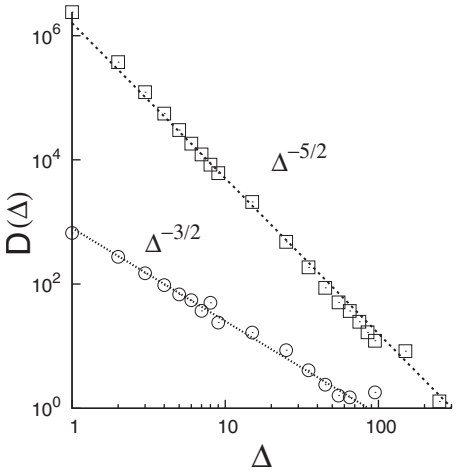

FIG. 19. The distribution of bursts for the uniform threshold distribution for a single fiber bundle with $N=10^7$ fibers. Results with $x_0=0$, i.e., when all bursts are recorded, are shown as squares and data for bursts near the critical point $(x_0=0.9x_c)$ are shown as circles.

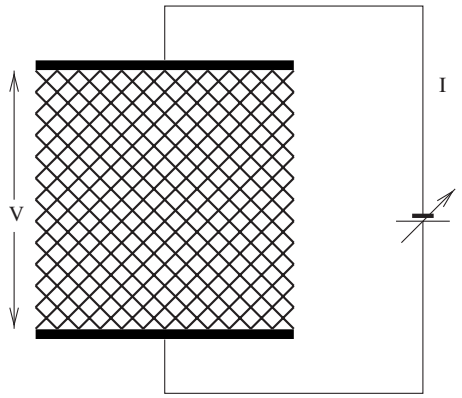

FIG. 20. A fuse model of size 100×100. Each bond is a fuse with a burn-out threshold t drawn from a probability distribution $p(t)$.

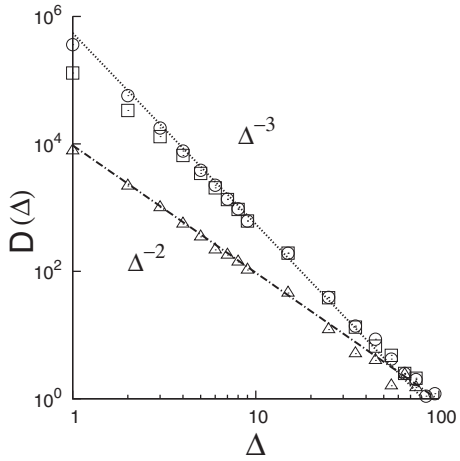

FIG. 21. The burst distribution based on 300 sample random fuse lattices of size 100×100. The threshold t is uniformly distributed on the unit interval. On average, catastrophic failure sets in after 2097 fuses have blown. The circles denote the burst distribution measured throughout the entire breakdown process. The squares denote the burst distribution based on bursts appearing after the first 1000 fuses have blown. The triangles denote the burst distribution after 2090 fuses have blown. The two straight lines indicate power laws with exponents $\xi=3$ and 2, respectively.

lytical treatments, this model retains *computational* tractability. The fuse model consists of a lattice in which each bond is a fuse, i.e., an Ohmic resistor as long as the electric current it carries is below a threshold value. If the threshold is exceeded, the fuse burns out irreversibly. The threshold t of each bond is drawn from an uncorrelated distribution $p(t)$. The lattice is placed between electrical bus bars and an increasing current is passed through it. The lattice is a two-dimensional square placed at 45° with regard to the bus bars, and the Kirchhoff equations are solved numerically at each node, assuming that all fuses have the same resistance. We show the model in Fig. 20. The ELS fiber bundle model may be interpreted as a mean-field version of the random fuse model (Zapperi *et al.*, 1997). Hence, the random fuse model may be used as a testing ground for results (see Table II) found with the ELS fiber bundle model to explore their robustness when other effects not present in the fiber bundle model enter.

To test the crossover phenomenon in a more complex situation than for the ELS fiber bundle model, we consider the random fuse model (Pradhan, Hansen, and Hemmer, 2006). When one records all the bursts in the random fuse model, the distribution follows a power law $D(\Delta)\propto\Delta^{-\xi}$ with $\xi\approx3$, which is consistent with the value reported in recent studies. We show the histogram in Fig. 21. With a system size of 100×100, 2097 fuses blow on the average before catastrophic failure sets in. When the burst distribution is measured only after the first 2090 fuses have blown, a different power law is found, this time with $\xi=2$. After 1000 blown fuses, on the other hand, ξ remains the same as for the histogram recording the entire failure process (Fig. 21).

In Fig. 22 we show the power dissipation E in the network as a function of the number of blown fuses and as a function of the total current. The dissipation is given as the product of the voltage drop across the network V times the total current that flows through it. The breakdown process starts by following the lower curve and follows the upper curve returning to the origin. It is interesting to note the linearity of the unstable branch of this curve. In Fig. 23 we record the avalanche distribution for power dissipation $D_d(\Delta)$.

Recording, as before, the avalanche distribution throughout the entire process as well as recording only close to the point at which the system catastrophically fails, we obtain two power laws, with exponents $\xi=2.7$ and 1.9, respectively. It is interesting to note that in this case there is not a difference of unity between the two exponents. The power dissipation in the fuse model corresponds to the stored elastic energy in a network of elastic elements. Hence, the power dissipation avalanche histogram in the mechanical system would correspond to

TABLE II. Exponents for order parameter (O), breakdown susceptibility (χ), relaxation time (τ), avalanche size distribution $D(\Delta)$, and energy burst distribution $g(E)$ in the ELS model.

Exponent for	Value	Comment
Order parameter (α)	1/2	
Breakdown susceptibility (β)	1/2	
Relaxation time (θ)	1/2	Amplitude ratio $=\ln N/2\pi$
Avalanche size distribution (ξ)	3	Discrete load increase
	5/2	Continuous load increase
Energy burst distribution (ξ_e)	5/2	In the asymptotic limit; for the low energy limit, distribution is nonuniversal

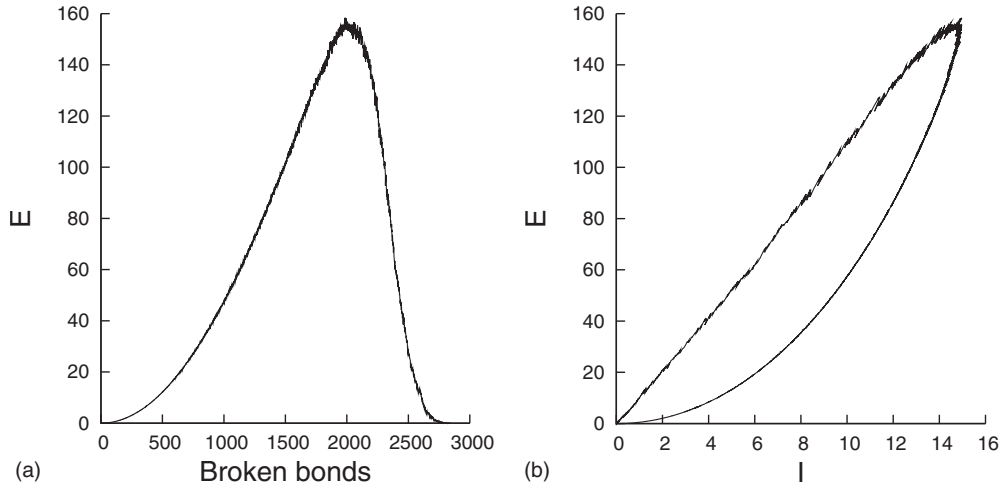

FIG. 22. Power dissipation E as a function of the number of broken bonds (upper) and as a function of the total current I flowing in the fuse model (lower).

the released energy. Such a mechanical system could serve as a simple model for earthquakes.

Divakaran and Dutta (2007a) studied the critical behavior of a bundle of fibers under global load-sharing scheme with threshold strength chosen randomly from a distribution which is uniform but discontinuous. The form of the distribution is

$$p(x) = \begin{cases} \dfrac{1}{1-(x_2-x_1)}, & 0 < x \leqslant x_1 \\ 0, & x_1 < x < x_2 \\ \dfrac{1}{1-(x_2-x_1)}, & x_2 \leqslant x \leqslant 1, \end{cases} \tag{196}$$

where $x_2 - x_1$ is the gap in the threshold distribution as shown in Fig. 24. Here a fraction f of the fibers belongs to the weaker section ($0 < x \leqslant x_1$) and the remaining belong to the stronger section ($x_2 \leqslant x \leqslant 1$). The condition of uniformity of the distribution demands

$$x_1 = \frac{f}{1-f}(1-x_2), \tag{197}$$

so that fixing x_1 and f immediately settles the value of x_2.

To study the dynamics of this model, the recursive equation approach was again used. The redistributed stress must cross x_2 for the complete failure of the bundle to take place. When the external load is such that the redistributed stress at an instant t, i.e., $x(t)$, is greater than x_2, the fixed-point solution has the form

$$U^* = \frac{1}{2[1-(x_2-x_1)]}\left(1+\sqrt{1-\frac{\sigma}{\sigma_c}}\right), \tag{198}$$

so that the critical stress σ_c is

$$\sigma_c = \frac{1}{4[1-(x_2-x_1)]} \tag{199}$$

and the redistributed stress at the critical point is found to be 1/2 as in the uniform distribution (Pradhan, Hansen, and Hemmer, 2005). This immediately restricts

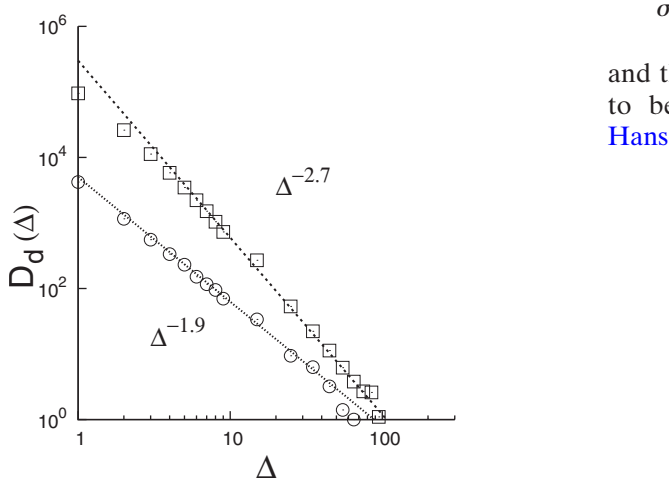

FIG. 23. The power dissipation avalanche histogram $D_d(\Delta)$ for the fuse model. The slopes of the two straight lines are −2.7 and −1.9, respectively. The circles show the histogram of avalanches recorded after 1000 fuses have blown, whereas the squares show the histogram recorded after 2090 fuses have blown. This is close to catastrophic failure.

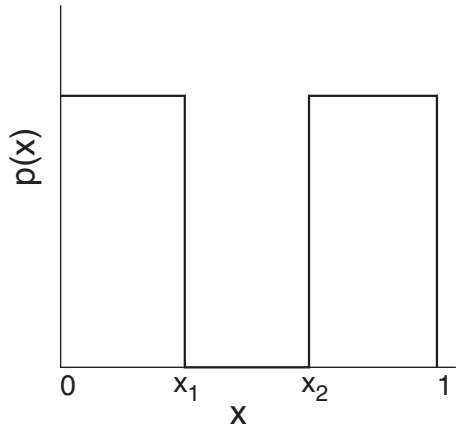

FIG. 24. Mixed uniform distribution.

the value of x_2 to be less than $1/2$ and therefore $x_2=0.5$ is defined as the critical distribution in this model. On the other hand, the uniformity condition [Eq. (197)] sets another restriction, namely, $x_1<f$. Interestingly, the critical stress is a function of the gap x_2-x_1 and reduces to one-fourth when the gap goes to zero. The exponents related to the order parameter and susceptibility stick to their mean-field values. However, the existence of a forbidden region shows a prominent signature in the avalanche size distribution of the mixed model. The expression for the total avalanche size distribution $D(\Delta)$ in this model includes two terms, one due to the contribution from thresholds between 0 and x_1 and the other from the stronger section of fibers. Hence, the total avalanche size $D(\Delta)$ is $D(\Delta)/N=D_1(\Delta)+D_2(\Delta)$, where

$$D_1(\Delta)=\frac{\Delta^{\Delta-1}}{\Delta!}\frac{1}{1-x_2+x_1}\int_0^{x_1}dx\left(\frac{1-x_2+x_1-2x}{x}\right)\times\left[\frac{x}{1-x_2+x_1-x}\exp\left(-\frac{x}{1-x_2+x_1-x}\right)\right]^{\Delta} \tag{200}$$

and

$$D_2(\Delta)=\frac{\Delta^{\Delta-1}}{\Delta!}\frac{1}{1-x_2+x_1}\int_{x_2}^{0.5}dx\left(\frac{1-2x}{x}\right)\times\left[\frac{x}{1-x}\exp\left(-\frac{x}{1-x}\right)\right]^{\Delta}. \tag{201}$$

The leading behavior of $D_1(\Delta)$ is given by (Divakaran and Dutta, 2007a)

$$D_1(\Delta)=\Delta^{-5/2}e^{(1-x_m)\Delta}x_m^{\Delta}, \tag{202}$$

where

$$x_m=\frac{x_1}{1-x_2}, \tag{203}$$

which clearly indicates a rapid fall of the contribution of weaker fibers. On the other hand, $D_2(\Delta)$ resembles the imminent failure behavior studied by Pradhan, Hansen, and Hemmer (2005), where the avalanche size exponent shows a crossover from $5/2$ to $3/2$ as $x_2\to0.5$. For the mixed model, the total avalanche size distribution $D(\Delta)$ shows a nonuniversal behavior for small Δ values, though eventually there is a crossover to the universal mean-field value. The most fascinating observation is the following: though the gap in the distribution is always present, nonuniversality is prominent only in the limit $x_2\to0.5$. Divakaran and Dutta showed that this nonuniversal behavior stems from the avalanche of fibers in the weak section and only in the vicinity of the critical distribution, the contribution of $D_1(\Delta)$ overcomes $D_2(\Delta)$. Otherwise, the faster fall of $D_1(\Delta)$ and large value of $D_2(\Delta)$ together force the avalanche size exponent to be $5/2$. It should be noted that the nonuniversal behavior is most prominent at a critical distribution where the avalanche size exponent crosses over to $3/2$ in the asymptotic limit. The typical behavior of $D(\Delta)$

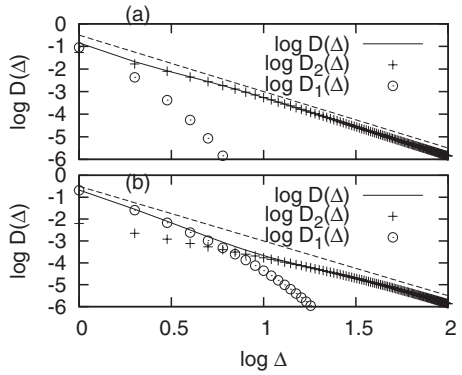

FIG. 25. Total avalanche size distribution $D(\Delta)$, $D_1(\Delta)$, and $D_2(\Delta)$ obtained by numerical integration of Eqs. (200) and (201). (a) corresponds to $x_1=0.08, x_2=0.28$, and $f=0.1$ and (b) corresponds to $x_1=0.25$, $x_2=0.42$, and $f=0.3$. As $x_2\to0.5$, the nonuniversal region increases in the small Δ region, whereas $\Delta\propto\Delta^{-5/2}$ for large Δ. The dotted line has a slope of $-5/2$. From Divakaran and Dutta, 2007a.

is shown in Fig. 25 for two different distributions, highlighting the increase in nonuniversal region as x_2 approaches 0.5. However, for many discontinuities in the threshold distributions, avalanche size distribution shows a nonuniversal, non-power-law behavior (Divakaran and Dutta, 2008) for small-size avalanches, although the large avalanches still exhibit similar crossover behavior as we discuss here.

Divakaran and Dutta also looked at the model where fibers from two different Weibull distributions are mixed (Divakaran and Dutta, 2007b). Though an interesting variation of the critical stress with the mixing parameter was obtained using a probabilistic method introduced by Moreno *et al.* (2000), there is no deviation in the avalanche size exponent. Hidalgo, Kovacs, *et al.* (2008) recently studied the infinite-gap limit of the discontinuity model. They considered a fraction α_{inf} of the fibers having infinite threshold strength mixed with fibers having threshold chosen from a distribution $p(x)$. They observed a critical fraction α_c such that for $\alpha_{\text{inf}}>\alpha_c$, the avalanche size exponent switches from the well-known mean-field exponent $\xi=5/2$ to a lower value $\xi=9/4$. It was also shown that such a behavior is observed for those distributions where the macroscopic constitutive behavior has a maximum and a point of inflection. They also claimed that below a critical gap the model of Hidalgo, Kovacs, *et al.* (2008) of reduces to the discontinuity model of Divakaran and Dutta. Kun and Nagy (2008) studied the global load-sharing fiber bundle model in a wedge-shaped geometry. That is, the fibers are connected to two rigid blocks placed at an angle with respect to each other. The fibers are loaded by rotating the blocks with respect to each other, resulting in a linear loading gradient on them. In the limit of a threshold distribution tending toward zero width, the fibers break in an orderly fashion according to the load and, hence position in the wedge. As the width is increased, a process zone—i.e., a zone where some fibers fail whereas others stay intact—develops. When the threshold distri-

bution is wide enough, the process zone spans the entire bundle. In this limit a burst size exponent $\xi=5/2$ is recovered. However, with a narrower distribution, so that a well-defined process zone smaller than the size of the bundle develops, the burst exponent $\xi=2.0$ is found.

2. Burst distribution for discrete load increase

When the bundle is stretched continuously from zero, fluctuation plays a crucial role and the generic result is a power law (Hemmer and Hansen, 1992) $D(\Delta)\propto\Delta^{-\xi}$, for large Δ, with $\xi=5/2$. However, experiments may be performed in a different manner, where the load is increased in finite steps of size δ. The value of the exponent then increases (Pradhan *et al.*, 2002; Hemmer and Pradhan, 2007) to 3: $D(\Delta)\propto\Delta^{-3}$. The basic reason for the difference in the power laws is that an increase in steps of the external load reduces the fluctuations in the force. The derivation (see Sec. III.B.1) of the asymptotic size distribution $D(\Delta)\propto\Delta^{-5/2}$ of avalanches, corresponding to stretching by infinitesimal steps, shows the importance of force fluctuations (Hemmer and Hansen, 1992). An effective reduction of the fluctuations requires that the size δ of the load increase is large enough so that a considerable number of fibers break in each step.

Here is an analytic derivation, following Hemmer and Pradhan (2007), showing how to calculate the burst distribution in such a situation. For the uniform distribution of thresholds [Eq. (1)], the load curve is parabolic,

$$\langle F\rangle = Nx(1-x), \tag{204}$$

so that the expected critical load equals $F_c=N/4$. With a sufficiently large δ we may use the macroscopic load equation [Eq. (204)] to determine the number of fibers broken in each step. The load values are $m\delta$, with m taking the values $m=0,1,2,\ldots,N/4\delta$ for the uniform threshold distribution. By Eq. (204) the threshold value corresponding to the load $m\delta$ is

$$x_m = \frac{1}{2}(1-\sqrt{1-4m\delta/N}). \tag{205}$$

The expected number of fibers broken when the load is increased from $m\delta$ to $(m+1)\delta$ is close to

$$\Delta = N dx_m/dm = \delta/\sqrt{1-4m\delta/N}. \tag{206}$$

Here the minimum number of Δ is δ, obtained in the first load increase. The integral over all m from 0 to $N/4\delta$ yields a total number $N/2$ of broken fibers, as expected, since the remaining one-half of the fibers burst in one final avalanche.

The number of avalanches of size between Δ and $\Delta+d\Delta$, $D(\Delta)d\Delta$, is given by the corresponding interval of the counting variable m: $D(\Delta)d\Delta=dm$. Since

$$\frac{d\Delta}{dm} = \frac{2\delta^2}{N}(1-4m\delta/N)^{-3/2} = \frac{2}{N\delta}\Delta^3, \tag{207}$$

we obtain the following distribution (Pradhan *et al.*, 2002; Hemmer and Pradhan, 2007) of avalanche sizes:

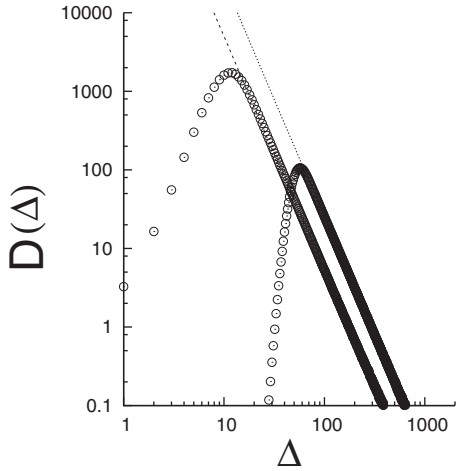

FIG. 26. Avalanche size distribution for the uniform threshold distribution [Eq. (1)] when the load is increased in steps of $\delta=10$ and 50 (upper curve). The dotted lines show the theoretical asymptotics [Eq. (208)] for $\delta=10$ and 50. Based on 10 000 samples with $N=10^6$ fibers in the bundle.

$$D(\Delta) = \frac{dm}{d\Delta} = \frac{1}{2}N\delta\Delta^{-3} \quad (\Delta \geqslant \delta). \tag{208}$$

For consistency, one may estimate the total number of bursts by integrating $D(\Delta)$ from $\Delta=\delta$ to ∞, with the result $N/4\delta$, as expected.

Figure 26 shows that the theoretical power law [Eq. (208)] fits the simulation results perfectly for sufficiently large Δ. The simulation records also a few bursts of magnitude less than δ because there is a nonzero probability to have bundles with considerably fewer fibers than the average in a threshold interval. However, these events will be of no importance for the asymptotic power law in the size distribution.

In order to see whether the asymptotic exponent value $\xi=3$ is general, simulations for another threshold distribution have been performed, the Weibull distribution [Eq. (2)] with index 5, which confirms similar asymptotic behavior (Fig. 27).

For a general threshold distribution $P(x)$ a load interval δ and a threshold interval are connected via the load equation $\langle F\rangle=Nx[1-P(x)]$. Since $d\langle F\rangle/dx=N[1-P(x)-xp(x)]$, an increase δ in the load corresponds to an interval

$$dx = \frac{\delta}{N[1-P(x)-xp(x)]} \tag{209}$$

of fiber thresholds. The expected number of fibers broken by this load increase is therefore

$$\Delta = Np(x)dx = \frac{p(x)}{1-P(x)-xp(x)}\delta. \tag{210}$$

Note that this number diverges at the critical point, i.e., at the maximum of the load curve, as expected.

Following the similar method, as in the case of uniform distribution, we can determine (Hemmer and Pradhan, 2007) the asymptotic distribution for large Δ:

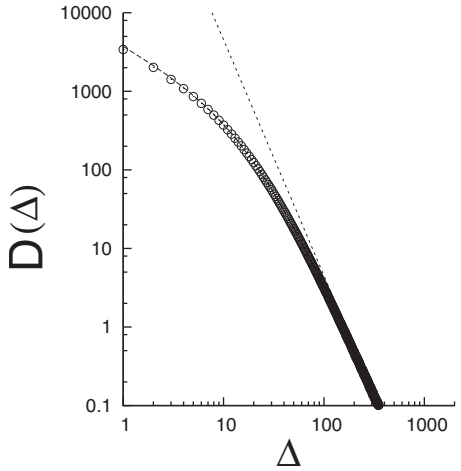

FIG. 27. Avalanche size distribution for the Weibull distribution [Eq. (2)] with index 5. Open circles represent simulation data, dashed lines are analytic expressions [Eq. (213)], and the dotted line is the asymptotic power law with exponent −3. The load is increased in steps of $\delta=20$. Based on 10 000 samples of bundles with $N=10^6$ fibers.

$$D(\Delta) \simeq C\Delta^{-3}, \tag{211}$$

with a nonzero constant

$$C = N\delta\frac{p(x_c)^2}{2p(x_c)+x_c p'(x_c)}, \tag{212}$$

where we have used that at criticality $1-P(x_c)=x_c p(x_c)$. Thus the asymptotic exponent value $\xi=3$ is universal.

For the Weibull distribution considered in Fig. 27 we obtain

$$D(\Delta) = N\delta\Delta^{-3}\frac{25x^9e^{-x^5}}{4+5x^5} \quad \text{and} \quad \Delta = \frac{5\delta x^4}{1-5x^5}. \tag{213}$$

This burst distribution must be given in parameter form; x cannot be eliminated explicitly. The critical point is at $x=5^{-1/5}$ and the asymptotics is given by Eq. (211), with $C=N\delta(625e)^{-1/5}$.

If we let the load increase δ shrink to zero, we must recover the asymptotic $D(\Delta)\propto\Delta^{-5/2}$ power law valid for continuous load increase. Thus, as a function of δ, there must be a crossover from one behavior to the other. It is to be expected that for $\delta\ll 1$ the $D(\Delta)\propto\Delta^{-5/2}$ asymptotics is seen and when $\delta\gg 1$ the $D(\Delta)\propto\Delta^{-3}$ asymptotics is seen.

3. Energy bursts in fiber bundle model

So far we have discussed in detail the statistical distribution of the *size* of avalanches in fiber bundles (Hemmer and Hansen, 1992; Pradhan, Hansen, and Hemmer, 2005; Hemmer *et al.*, 2006; Raischel *et al.*, 2006). Sometimes the avalanches cause a sudden internal stress redistribution in the material and are accompanied by a rapid release of mechanical energy. A useful experimental technique to monitor the energy release is to measure the acoustic emissions (AEs), the elastically radiated waves produced in the bursts (Fazzini, 1991; Diodati *et al.*, 1991; Scott, 1991; Petri *et al.*, 1994; Garcimartín *et al.*, 1997; Guarino *et al.*, 1998). Experimental observations suggest that AE signals follow power-law distributions. What is the origin of such power laws? Can we explain it through the general scheme of fluctuation-guided breaking dynamics that has been demonstrated well in the ELS fiber bundle model?

We now determine the statistics of the energies released (Pradhan and Hemmer, 2008) in fiber bundle avalanches. As the fibers obey Hooke's law, the energy stored in a single fiber at elongation x equals $\frac{1}{2}x^2$, where for simplicity we have set the elasticity constant equal to unity. The individual thresholds x_i are assumed to be independent random variables with the same cumulative distribution function $P(x)$ and a corresponding density function $p(x)$.

a. Energy statistics

We characterize a burst by the number Δ of fibers that fail and by the lowest threshold value x among the Δ failed fibers. The threshold value $x_{\max}$ of the strongest fiber in the burst can be estimated to be

$$x_{\max} \simeq x + \frac{\Delta}{Np(x)} \tag{214}$$

since the expected number of fibers with thresholds in an interval δx is given by the threshold distribution function as $Np(x)\delta x$. The last term in Eq. (214) is of the order $1/N$, so for a very large bundle the differences in threshold values among the failed fibers in one burst are negligible. Hence the energy released in a burst of size Δ that starts with a fiber with threshold x is given by

$$E = \frac{1}{2}\Delta x^2. \tag{215}$$

Following Hemmer and Hansen (1992) the expected number of bursts of size Δ, starting at a fiber with a threshold value in the interval $(x,x+dx)$, is

$$f(\Delta,x)dx = N\frac{\Delta^{\Delta-1}}{n!}\frac{1-P(x)-xp(x)}{x}X(x)^\Delta e^{-\Delta X(x)}\,dx, \tag{216}$$

where

$$X(x) = \frac{xp(x)}{1-P(x)}. \tag{217}$$

The expected number of bursts with energies less than E is therefore

$$G(E) = \sum_\Delta \int_0^{\sqrt{2E/\Delta}} f(\Delta,x)dx, \tag{218}$$

with a corresponding energy density

$$g(E) = \frac{dG}{dE} = \sum_\Delta (2E\Delta)^{-1/2} f(\Delta,\sqrt{2E/\Delta}). \tag{219}$$

Explicitly,

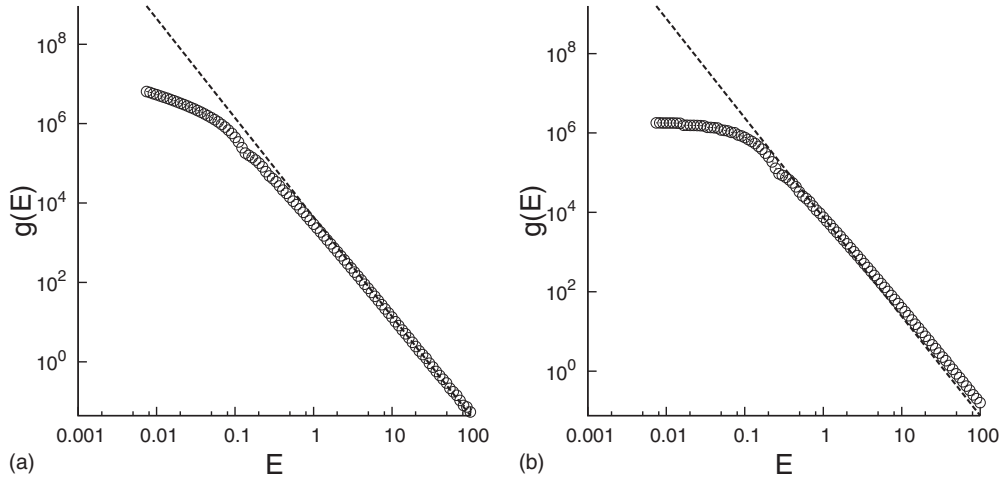

FIG. 28. Simulation results for $g(E)$ characterizing energy bursts in fiber bundles with (a) the uniform threshold distribution [Eq. (1)] and (b) the Weibull distribution [Eq. (2)] of index 2. The graphs are based on 1000 samples with $N=10^6$ fibers in each bundle. Open circles represent simulation data and dashed lines are the theoretical results [Eqs. (226) and (227)] for the asymptotics.

$$g(E) = N\sum_{\Delta} g_{\Delta}(E), \tag{220}$$

with

$$g_{\Delta}(E) = \frac{\Delta^{\Delta-1}}{2E\Delta!}[1 - P(s) - sp(s)] \times\left[\frac{sp(s)}{1-P(s)}\exp\left(-\frac{sp(s)}{1-P(s)}\right)\right]^{\Delta}. \tag{221}$$

Here $s\equiv\sqrt{2E/\Delta}$. With a critical threshold value x_c, it follows from Eq. (215) that a burst energy E can be obtained only if Δ is sufficiently large, $\Delta \geqslant 2E/x_c^2$. Thus the sum over n starts with $\Delta = 1+[2E/x_c^2]$, where $[a]$ denotes the integer part of a.

b. High-energy asymptotics

Bursts with high energies correspond to bursts in which many fibers rupture. In this range we use Stirling's approximation for the factorial $\Delta!$, replace $1+[2E/x_c^2]$ by $2E/x_c^2$, and replace the summation over Δ by an integration. Thus

$$g(E) \simeq \frac{N}{2E^{3/2}\pi^{1/2}}\int_{2E/x_c^2}^{\infty}\frac{e^{\Delta}}{\Delta^{3/2}}[1 - P(s) - sp(s)] \times\left[\frac{sp(s)}{1-P(s)}\exp\left(-\frac{sp(s)}{1-P(s)}\right)\right]^{\Delta} d\Delta. \tag{222}$$

By changing integration variable from Δ to s we obtain

$$g(E) \simeq \frac{N}{2E^{3/2}\pi^{1/2}}\int_0^{x_c}[1 - P(s) - sp(s)] \times\left[\frac{sp(s)}{1-P(s)}\exp\left(1-\frac{sp(s)}{1-P(s)}\right)\right]^{\Delta} ds = \frac{N}{2E^{3/2}\pi^{1/2}}\int_0^{x_c}[1 - P(s) - sp(s)]e^{-Eh(s)}\, ds, \tag{223}$$

with

$$h(s) \equiv \left(-\frac{1-P(s)-sp(s)}{1-P(s)} + \ln\frac{1-P(s)}{sp(s)}\right)\frac{2}{s^2}. \tag{224}$$

For large E the integral [Eq. (223)] is dominated by the integration range near the minimum of $h(s)$. At the upper limit $s=x_c$ we have $h(x_c)=0$ since $1-P(x_c) = x_c p(x_c)$. This is also a minimum of $h(s)$, having quadratic form

$$h(s) \simeq \left(\frac{2p(x_c)+x_c p'(x_c)}{x_c^2 p(x_c)}\right)^2 (x_c - s)^2. \tag{225}$$

Inserting these expressions into Eq. (223) and integrating, we obtain the following asymptotic expression:

$$g(E) \simeq N\frac{C}{E^{5/2}} \sim E^{-\xi_e}, \tag{226}$$

where

$$C = \frac{x_c^4 p(x_c)^2}{4\pi^{1/2}[2p(x_c)+x_c p'(x_c)]}. \tag{227}$$

In Fig. 28 we compare the theoretical formula with simulations for the uniform distribution [Eq. (1)], which corresponds to $x_c=\frac{1}{2}$ and $C=2^{-7}\pi^{-1/2}$, and for the Weibull distribution [Eq. (2)] with index $\rho=2$, which corresponds to $x_c=2^{-1/2}$ and $C=2^{-5}(2\pi e)^{-1/2}$.

The corresponding asymptotics [Eq. (226)] are also shown in Fig. 28. For both threshold distributions the

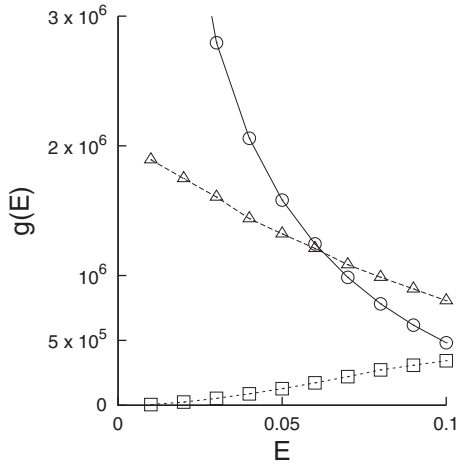

FIG. 29. Simulation results for the burst distribution $g(E)$, in the low-energy regime, for the uniform threshold distribution (circles), the Weibull distribution with $\rho=2$ (triangles), and Weibull distribution with $\rho=5$ (squares). The graphs are based on 1000 samples with $N=10^6$ fibers in each bundle.

agreement between the theoretical asymptotics and the simulation results is satisfactory. The exponent $-5/2$ in the energy burst distribution is clearly universal. Note that the asymptotic distribution of the burst magnitudes Δ is governed by the same exponent (Hemmer and Hansen, 1992).

c. Low-energy behavior

The low-energy behavior of the burst distribution is by no means universal: $g(E)$ may diverge, vanish, or stay constant as $E\to 0$, depending on the nature of the threshold distribution. In Fig. 29 we show simulation results for the low-energy part of $g(E)$ for the uniform distribution and the Weibull distributions of index 2 and 5.

We see that $g(E)$ approaches a finite limit in the Weibull $\rho=2$ case, approaches zero for Weibull $\rho=5$, and apparently diverges in the uniform case. All this is easily understood since bursts with low energy predominantly correspond to single fiber bursts ($\Delta=1$, i.e., $E=x^2/2$) and to fibers with low threshold values. The number of bursts with energy less than E therefore corresponds to the number of bursts with $x<\sqrt{2E}$, which is close to $NP(\sqrt{2E})$. This gives

$$g(E) \simeq N\frac{p(\sqrt{2E})}{\sqrt{2E}} \quad \text{when } E\to 0. \tag{228}$$

For the uniform distribution $g(E)$ should therefore diverge as $(2E)^{-1/2}$ for $E\to 0$. The simulation results in Fig. 29 are consistent with this divergence. For the Weibull distribution of index 2, on the other hand Eq. (228) gives $g(E)\to 2N$ when $E\to 0$, a value in agreement with simulation results in the figure. Note that for a Weibull distribution of index ρ, the low-energy behavior is $g(E)\propto E^{(\rho-2)/2}$. Thus the Weibull with $\rho=2$ is a borderline case between divergence and vanishing of the low-energy density. The same lowest-order results can be obtained from the general expression (220) which can also provide more detailed low-energy expansions.

For high energies the energy density obeys a power law with exponent $-5/2$. This asymptotic behavior is universal, independent of the threshold distribution. A similar power-law dependence is found in some experimental observations on acoustic emission studies (Petri *et al.*, 1994; Garcimartín *et al.*, 1997) of loaded composite materials. In contrast, the low-energy behavior of $g(E)$ depends crucially on the distribution of the breakdown thresholds in the bundle. $g(E)$ may diverge, vanish, or stay constant for $E\to 0$.

IV. LOCAL LOAD-SHARING MODEL

So far we have studied fiber bundles where the force once carried by a failing fiber is spread equally among all the surviving fibers. This may often be a very good approximation. However, intuitively it is natural that fibers closer to a failing fiber experience more of an effect than fibers further away—an effect reminiscent of stress enhancement around cracks. In this section we discuss three classes of model where there are local effects in how the forces carried by failed fibers are distributed. We start with the most extreme, where the forces are totally absorbed by the nearest surviving fibers. We then move on to models where the stress is distributed according to a power law in the distance from the failing fiber, and lastly to a model where we assume the *clamps* the fibers are attached to are soft and therefore deform due to the loading of the fibers—as can be seen in pulling on the hairs on one's arm.

A. Stress alleviation by nearest neighbors

The extreme form for local load redistribution is that all extra stresses caused by a fiber failure are taken up by the nearest-neighbor surviving fibers (Harlow and Phoenix, 1981, 1991; Phoenix and Smith, 1983; Harlow, 1985; Kuo and Phoenix, 1987; Duxbury and Leath, 1994). The simplest geometry is one dimensional, so that the N fibers are ordered linearly, with or without periodic boundary conditions. In this case precisely *two* fibers, one on each side, take up and divide equally the extra stress (see Fig. 30). When the strength thresholds take only two values, the bundle strength distribution has been found analytically (Harlow, 1985; Harlow and Phoenix, 1991; Duxbury and Leath, 1994).

At a total force F on the bundle the force on a fiber surrounded by n_l previously failed fibers on the left-hand side, and n_r on the right-hand side is then

$$\frac{F}{N}\left[1+\frac{1}{2}(n_l+n_r)\right]=f(2+n_l+n_r). \tag{229}$$

Here

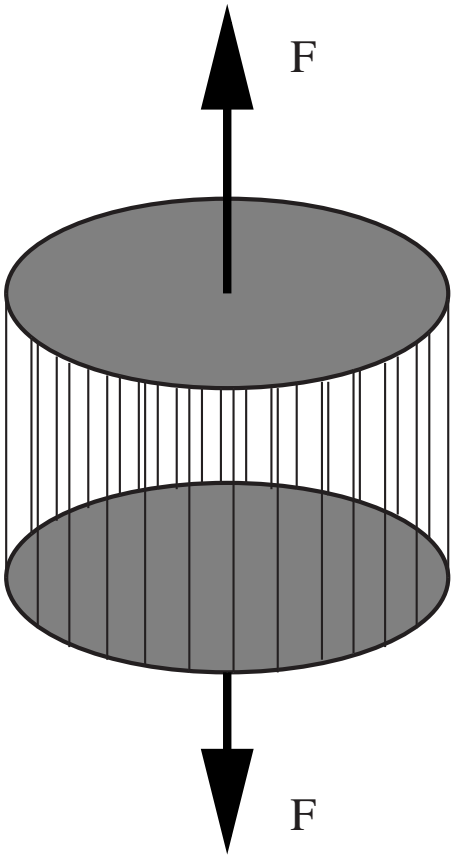

FIG. 30. A fiber bundle with periodic boundary conditions. The externally applied force F is the control parameter.

$$f = \frac{F}{2N} \tag{230}$$

is one-half the force per fiber and is a convenient variable to use as the driving *force parameter.*

Zhang and Ding (1994) and Hansen and Hemmer (1994b) studied numerically the burst distribution in the local load-sharing model. In Fig. 31 we show simulation results similar to those first appearing in Hansen and Hemmer (1994b) using threshold strengths randomly distributed on the unit interval. Again a power-law distribution seems to appear. However, the burst exponent ξ seems much larger than in the global load-sharing model [Eq. (140)],

$$\xi \simeq 5. \tag{231}$$

Thus the relative frequency of long (nonfatal) bursts is considerably reduced.

It was concluded from the numerics that systems with local load sharing are not in the universality class of fiber bundles with global load redistribution.

Kloster *et al.* (1997) set out to analytically calculate the burst distribution in the local load-sharing model, finding the surprising result that there is no power-law distribution of bursts at all; it is exponential. They did not find the burst distribution for general threshold distribution. Rather, they limited their study to the uniform threshold distribution in the force parameter f, given by

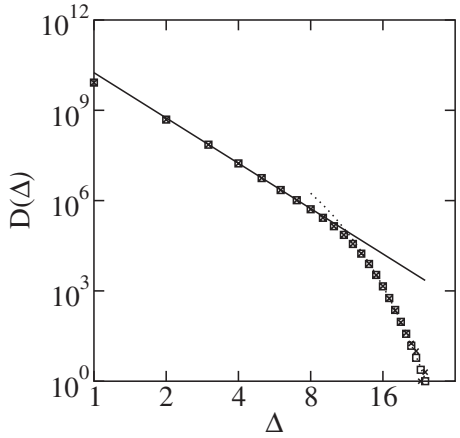

FIG. 31. Burst distribution in local model as found numerically for 4 000 000 samples with $N=20\,000$ fibers (crosses) and calculated from Eq. (233) (boxes). The straight line shows the power law Δ^{-5} and the broken curve the function $\exp(-\Delta/\Delta_0)$ with $\Delta_0=1.1$. Note the small value of Δ_0.

$$P(f) = \begin{cases} f & \text{for } 0 \leqslant f < 1 \\ 1 & \text{for } f \geqslant 1. \end{cases} \tag{232}$$

Bursts in the local and global models have different characters. In the local model a burst develops with one failure acting as the seed. If many neighboring fibers have failed, the load on the fibers on each side is high; and if they burst the load on the new neighbors will be even higher, etc. In this way a weak region in the bundle may be responsible for the failure of the whole bundle. For a large number N of fibers the probability of a weak region somewhere is higher. This hints in a qualitative way that the maximum load the bundle is able to carry does not increase proportionally to N but more slowly than linearly.

The result of a calculation based on combinatorics (Kloster *et al.*, 1997) was the burst distribution

$$D(\Delta) = \int_0^{1/(\Delta+2)} \sum_{n=1}^{N} \sum_{L_1=\Delta}^{M(f)} \sum_{L_2=0}^{M(f)-L_1} \frac{P_f(n,L_1;f)}{S(L_1;f)} p(L_1,\Delta;f) \times P_f(N-n-1,L_2;f)[1-(L_1+L_2+2)f]df, \tag{233}$$

where $S(l;f)$ is the probability that selected regions of l consecutive fibers have all failed whereas the two fibers at both boundaries are still intact at force parameter y and $p(l,a;f)df$ is the probability that a force increase from f to $f+df$ leads to a burst of length l and magnitude a. $P_f(n,L;f)$ is the probability at force parameter f that among the first n fibers there is no fatal burst and that the last L fibers of these have all failed.

The load distribution rule [Eq. (229)] implies that a burst of size Δ necessarily leads to a complete breakdown of the whole bundle if the external force is too high, i.e., if x exceeds a critical value $x_{\max}$. Since here a fiber can at most take a load of unity, we have

$$f_{\max} = \frac{1}{\Delta + 2}. \tag{234}$$

We now attempt to find a simple estimate for the maximal force per fiber that the fiber bundle can tolerate. In order to do that we assume that the fatal burst occurs in a region where no fibers have previously failed so that the burst has the same magnitude and length. We know that a single burst of length $\Delta = f^{-1} - 2$ is fatal [Eq. (234)], so our criterion is simply

$$D(f^{-1} - 2) = 1. \tag{235}$$

If we take into account that the two fibers adjacent to the burst should hold, and ignore the rest of the bundle, the gap distribution would be

$$N^{-1}D(\Delta) \approx \int_0^{1/(\Delta+2)} [1 - (2 + \Delta)f]^2 p(\Delta,\Delta;f)df$$

$$= \frac{2p(\Delta,\Delta)}{\Delta(\Delta + 1)(\Delta + 2)^{\Delta+1}}. \tag{236}$$

With the abbreviation

$$R_\Delta = \frac{p(\Delta,\Delta)}{(\Delta - 1)!},$$

we have

$$D(\Delta)/N \approx \frac{2(\Delta + 2)!}{\Delta^2(\Delta + 1)^2(\Delta + 2)^{\Delta+2}} R_\Delta$$

$$\simeq \frac{\sqrt{8\pi(\Delta + 2)}}{\Delta^2(\Delta + 1)^2} e^{-\Delta-2} R_\Delta, \tag{237}$$

using Stirling's formula.

Taking logarithms we have

$$\ln D(\Delta) - \ln N = -(\Delta + 2)\left[1 + \frac{\ln R_\Delta}{\Delta + 2} + O\left(\frac{\ln \Delta}{\Delta}\right)\right]$$

$$\simeq -(\Delta + 2), \tag{238}$$

using that

$$\lim_{n\to\infty} R_n^{1/n} = 1 \tag{239}$$

for R_Δ when Δ is large.

The failure criterion (235)] then takes the form

$$\ln N \simeq \frac{1}{f}. \tag{240}$$

Since $f = F/2N$ we have the following estimate for the maximum force F that the fiber bundle can tolerate before complete failure:

$$F \simeq \frac{2N}{\ln N}. \tag{241}$$

Due to the assumption that the fatal burst occurs in a region with no previously failed fibers, the numerical prefactor is an overestimate. The size dependence

$$F \propto \frac{N}{\ln N} \tag{242}$$

shows that the maximum load the fiber bundle can carry does not increase proportionally to the number of fibers but more slowly. This is to be expected since the probability of finding somewhere a stretch of weak fibers that start a fatal burst increases when the number of fibers increases.

The $N/\ln N$ dependence agrees with a previous estimate by Zhang and Ding (1995, 1996) for a uniform threshold distribution. The bimodal distribution used by Harlow and Phoenix (1991) and Duxbury and Leath (1994) also shows this behavior.

The burst distribution [Eq. (238)] is exponential. The probability of a single burst zipping through the fiber bundle grows with the system size N. This contrasts strongly with the global load-sharing model whose strength (the maximum force it can sustain) grows linearly with N and whose burst distribution follows a universal power law. If the latter behavior is reminiscent of a second-order transition with a critical point, the local load-sharing model behaves more as if moving toward a first-order phase transition.

We now discuss the effect of a low cutoff (in fiber strength distribution) on the failure properties of the LLS model. As in the case of the ELS model (see Sec. III.A), we consider a uniform fiber threshold distribution having a low cutoff C_L [Eq. (126)]. We present a probabilistic argument to determine the upper limit of C_L beyond which the whole bundle fails at once. Following the weakest-fiber-breaking approach the first fiber fails at an applied stress C_L (for large N). As we are using periodic boundary conditions, the n_c nearest neighbors (n_c is the coordination number) bear the terminal stress of the failing fiber and their stress value rises to $x_f = C_L(1 + 1/n_c)$. Now, the number of nearest neighbors (intact) having a strength threshold below x_f is $(\mathrm{NN})_{\mathrm{fail}} = n_c P(x_f)$ [see Eq. (131)]. Putting the value of $P(x_f)$ and x_f we finally get

$$(\mathrm{NN})_{\mathrm{fail}} = \frac{C_L}{1 - C_L}. \tag{243}$$

If $(\mathrm{NN})_{\mathrm{fail}} \geqslant 1$, then at least another fiber fails and this is likely to trigger a cascade of failure events resulting in complete collapse of the bundle. Therefore, to avoid the instant failure situation we must have $(\mathrm{NN})_{\mathrm{fail}} < 1$, from which we get the upper bound of C_L: $C_L < \frac{1}{2}$. As the above condition does not depend on the coordination number n, at any dimension the whole bundle is likely to collapse at once for $C_L \geqslant 1/2$. It should be mentioned that the LLS model should behave almost like the ELS model at the limit of infinite dimensions and therefore the identical bound (of C_L) in both cases is not surprising. A numerical study (Pradhan and Hansen, 2005) confirmed (Fig. 32) the above analytic argument in one dimension. When the average step value goes below 1.5, then one-step failure is the dominating mode. One can find the extreme limit of C_L when all the nearest neigh-

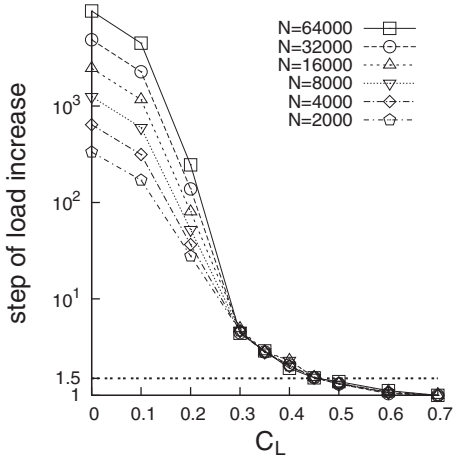

FIG. 32. Numerical estimate of the upper bound of C_L in the LLS model: for $C_L \geq 0.5$ the average step values go below 1.5, i.e., the bundle fails at one step in most of the realizations.

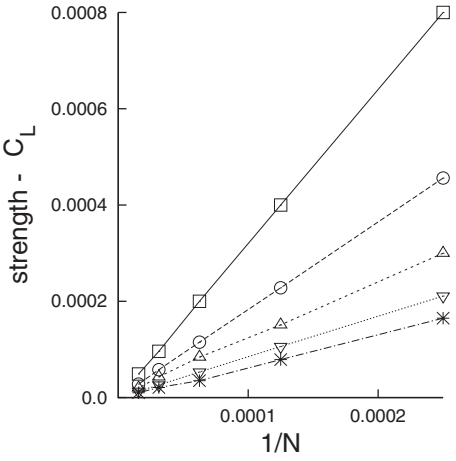

FIG. 33. The strength $-C_L$ is plotted against $1/N$ for different C_L values: 0.3 (square), 0.35 (circle), 0.4 (up triangle), 0.45 (down triangle), and 0.5 (star). All the straight lines approach 0 as $N \to \infty$.

bors fail after the weakest fiber breaks. Then the LLS bundle collapses instantly for sure. Setting $(\mathrm{NN})_{\mathrm{fail}}=n_c$ one gets the condition $C_L \geq n_c/(1+n_c)$, where the stress level of all the nearest neighbors crosses the upper cutoff 1 of the strength distribution. Clearly such failure is very rapid (like a chain reaction) and does not depend on the shape of the strength distributions, except for the upper cutoff. Also, as n_c increases (ELS limit), C_L for instant failure assumes the trivial value 1. Similar sudden failure in FBM has been discussed by Moreno, Gómez, and Pacheco (2001) in the context of a "one-sided load transfer" model.

The local load-sharing scheme introduces stress enhancement around the failed fiber, which accelerates damage evolution. Therefore, a few isolated cracks can drive the system toward complete failure through growth and coalescence. The LLS model shows zero strength (for fiber threshold distributions starting from zero value) at the limit $N \to \infty$, following a logarithmic dependence on the system size (N) (Smith, 1980; Gomez *et al.*, 1993; Pradhan and Chakrabarti, 2003a). Now for threshold distributions having a low cutoff (C_L), the ultimate strength of the bundle cannot be less than C_L. For such a uniform distribution [Eq. (126)], numerical simulations showed (Fig. 33) that as C_L increases the quantity (strength $-C_L$) approaches zero following straight lines with $1/N$, but the slope gradually decreases, which suggests that the system size dependence of the strength gradually becomes weaker.

Hansen and Hemmer (1994a) introduced and studied a model interpolating between the global load-sharing fiber bundle and a variant of a local load-sharing model. Kim (2004) and Pradhan, Chakrabarti, and Hansen (2005) followed up this work. In the model studied by Pradhan, Chakrabarti, and Hansen (2005) a fraction g of the load a failing fiber carries would be distributed among its surviving neighbors and a fraction $1-g$ among all surviving fibers. Hence, for $g=1$ the model would be purely local load sharing, whereas for $g=0$ it would be purely global load sharing. We show in Fig. 34 space-time diagrams of the one-dimensional version of the model for different values of g. For increasing values of g, there is increasing localization.

Both Kim (2004) and Pradhan, Chakrabarti, and Hansen (2005) found a phase transition when interpolating between the global load-sharing model and the local load-sharing model discussed earlier. In the one-dimensional model shown in Fig. 34, the critical value of g is $g_c=0.79\pm0.01$ for a flat threshold distribution (Pradhan, Chakrabarti, and Hansen, 2005).

B. Intermediate load-sharing models

A crucial mechanism in brittle fracture is the stress enhancement that occurs at crack tips. The stress field has a $1/\sqrt{r}$ singularity, where r is the distance to the crack tip, in this region. It is the interplay between fracture growth due to this singularity and weak spots in the

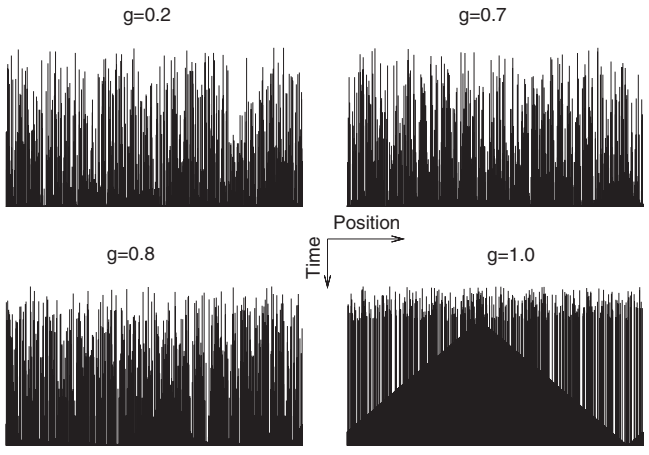

FIG. 34. Space-time diagram of breaking sequences of the interpolating fiber bundle model of Pradhan, Chakrabarti, and Hansen (2005). Black lines represent broken fibers and white regions are unbroken parts of the bundle. As the interpolation parameter g is increased, there is increasing localization of the failing fibers.

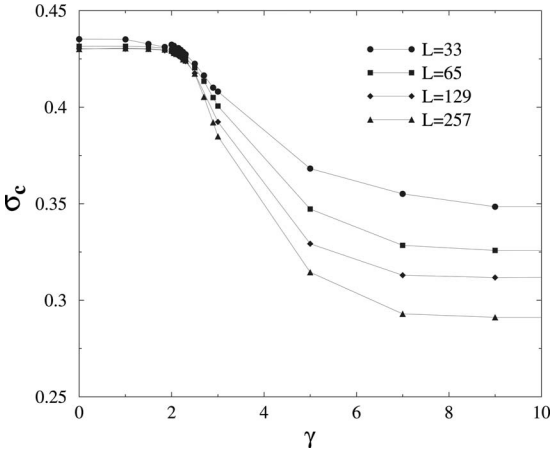

FIG. 35. Strength at failure σ_c as a function of γ in the variable range fiber bundle of Hidalgo, Moreno, *et al.* (2002) .

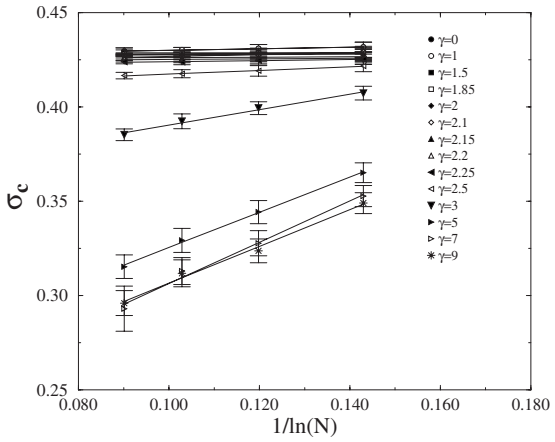

FIG. 36. Strength at failure σ_c as a function of the number of fibers N for different range exponents γ in the variable range fiber bundle of Hidalgo, Moreno, *et al.* (2002) .

material that drive the development of the fracture process (Herrmann and Roux, 1990). Clearly, there is a cutoff in the stress field as $r \to 0$. This may be caused by nonlinearities in the material constitutive relations or by microstructure in the material such as the presence of crystallites.

Hidalgo, Moreno, *et al.* (2002) introduced a fiber bundle that contains a power-law dependence on the distance from a failing fiber on the force redistribution in order to model the stress singularity seen around crack tips. The fiber bundle is implemented as a regular two-dimensional grid of parallel fibers clamped between two stiff blocks. Assuming that fiber j has just failed, a force transfer function

$$F(r_{i,j},\gamma) = \frac{Z}{r_{ij}^{\gamma}}, \tag{244}$$

where

$$\frac{1}{Z} = \sum_{i \in I} \frac{1}{r_{ij}^{\gamma}} \tag{245}$$

and I is the set of intact fibers, redistributes the forces. γ is treated as a parameter on the unit interval. There are two limiting cases, $\gamma \to 0$ which recovers the global load-sharing fiber bundle and $\gamma \to \infty$ which recovers the local load-sharing model with nearest-neighbor stress alleviation (Sec. IV.A). The load increase on fiber i is hence given by

$$f_i \to f_i + \sum_{j \in B} f_j F(r_{ij},\gamma), \tag{246}$$

where B is the set of failed fibers up to that point.

This model is too complex for analytical treatment and numerical simulations must be invoked. Around $\gamma = 2.0$ there is a transition in behavior between essentially global load sharing and local load sharing as described in Sec. IV.A: for $\gamma < 2.0$, the maximum sustainable force scales the number of fibers in the bundle at the outset N, whereas for $\gamma > 2.0$, an $N/\ln N$ behavior is observed as in Eq. (242). This is seen in Figs. 35 and 36.

The burst distribution shows a power-law distribution with exponent $\xi = 5/2$, again signaling global load-sharing behavior for smaller values of γ. As γ is increased, deviations from this behavior are seen. This must be interpreted as a crossover toward local load-sharing behavior as described in the previous section (see Fig. 37).

Lastly, the structure of the clusters of failed fibers at breakdown is studied. The global load-sharing model implemented in two dimensions does not yield anything particular. There is a percolation transition in the cluster size distribution when the relative density of failed fibers reaches the percolation threshold, but this has no particular significance in the evolution of the model. Hidalgo, Moreno, *et al.* (2002) found a cluster distribution having two distinct behaviors, depending on whether γ is smaller than or larger than 2. There is no clear power-law behavior (see Fig. 38).

Hidalgo, Zapperi, and Herrmann (2008) studied an anisotropic version of this model. The force transfer function [Eq. (244)] in this work is generalized to

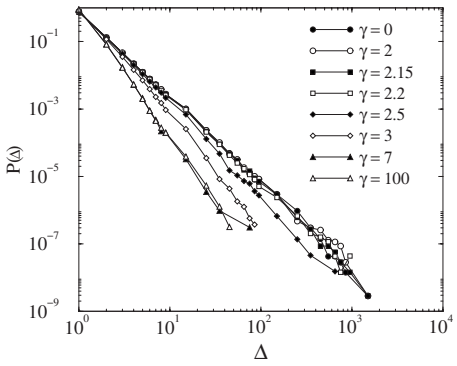

FIG. 37. Burst size distribution for different range exponents γ in the variable range fiber bundle of Hidalgo, Moreno, *et al.* (2002). The data points where $\gamma \leqslant 2.0$ can be fitted to a power law with exponent $\xi = 5/2$. For larger γ, the slope becomes steeper and resembles the behavior seen in the local load-sharing model (see Fig. 31).

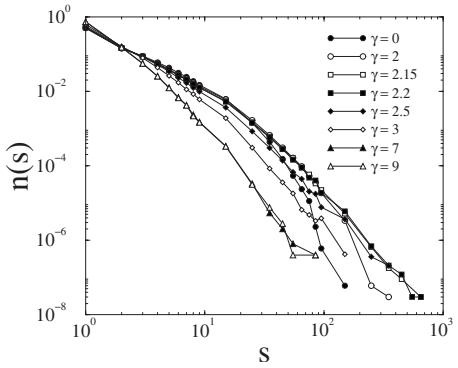

FIG. 38. Size distribution of clusters of broken bonds at collapse in the variable range fiber bundle of Hidalgo, Moreno, *et al.* (2002). There is no evident power-law behavior.

$$F(r_{i,j},\gamma) = \frac{Z}{[\alpha\Delta x_{i,j}^2 + (1-\alpha)\Delta y_{i,j}^2)]^{\gamma/2}}, \tag{247}$$

where α is an anisotropy parameter. The behavior of this model turns out to be quite similar to that found in the isotropic model.

Raischel *et al.* (2006) introduced a low cutoff in the threshold distribution (Pradhan *et al.*, 2002) in the variable-range fiber bundle model of Hidalgo, Moreno, *et al.* (2002). They studied the burst distribution as a function of γ and cutoff in the failure thresholds in terms of deformation ϵ_L. Figure 39 summarizes their findings: for the explored values of γ in the range $2.0 \leqslant \gamma \leqslant 6.0$, a crossover from burst exponent $\xi=5/2$ to $\xi=3/2$ is seen for small ϵ_L, whereas for larger $\gamma \approx 6.0$, the burst distribution may be fitted to a value $\xi=9/2$ for small ϵ_L.

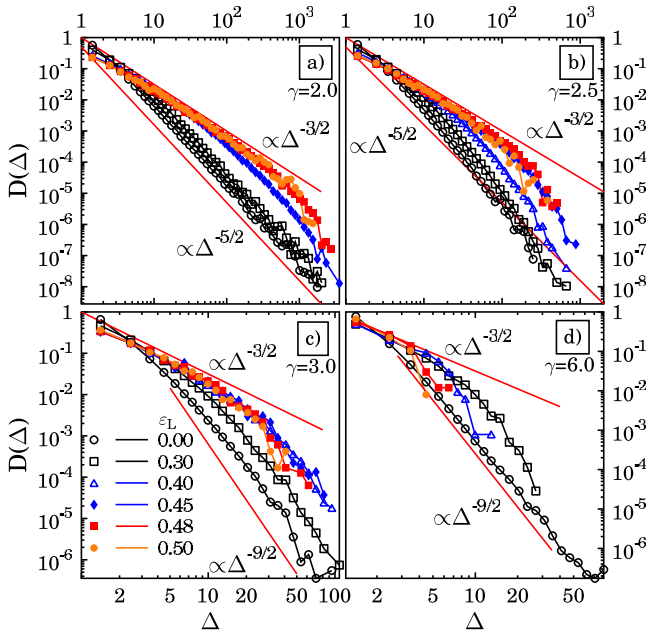

FIG. 39. (Color online) Burst size distributions in the variable-range fiber bundle model for different γ and ϵ_L values: γ=(a) 2.0, (b) 2.5, (c) 3.0, and (d) 6.0. From Raischel *et al.*, 2006.

Newman and Gabrielov (1991) and Newman *et al.* (1994) introduced a fiber bundle model where the fibers are hierarchically organized. The fibers are paired two by two. Each of these pairs is seen as an "order-1" fiber. This pairing is repeated for the order-1 fibers, creating order two fibers and so on. Within each sub-bundle, the fibers are subject to equal load sharing. If the cumulative threshold distribution for the fibers at order zero is $P_0(x)=P(x)$, then the threshold distribution at level 1 is

$$P_1(x) = P_0(x)[2P_0(2x) - P_0(x)], \tag{248}$$

a result which is readily generalized to any level. Even though the starting point here is global load sharing, the approximation introduced by treating the fibers at each level as fibers with given thresholds leads to the introduction of spatial load dependence in the model. To our knowledge, bursts have not been studied within this framework.

C. Elastic medium anchoring

In this section we generalize the fiber bundle problem to include more realistically the elastic response of the surfaces to which the fibers are attached. So far, these have been assumed to be infinitely stiff for the equal-load-sharing model or their response has been modeled as very soft but in a fairly unrealistic way in the local load-sharing models (see Sec. IV.A). We will end up with a description that is somewhat related to the models of the previous section, in particular, the model of Hidalgo, Moreno, *et al.* (2002). Batrouni *et al.* (2002) studied a realistic model for the elastic response of the clamps. The model was presented in the context of the failure of weldings. In this language, the two clamps were seen as elastic media glued together at a common interface.

Without loss of generality, one of the media may be assumed to be infinitely stiff whereas the other is soft. When a force is applied to a given fiber, the soft clamp responds by a deformation falling off inversely with the distance from the loaded fiber. Hence, the problem becomes one of solving the response of the surface with respect to a given loading of the fibers. Fibers exceeding their maximally sustainable load fail, and the forces and deformations must be recalculated. The two clamps can be pulled apart by controlling (fixing) either the applied force or the *displacement.* The displacement is defined as the change in the distance between two points, one in each clamp positioned far from the interface. The line connecting these points is perpendicular to the average position of the interface. In our case, the pulling is accomplished by controlling the displacement. As the displacement is increased slowly, fibers will fail, eventually ripping the two surfaces apart.

We now concretize these ideas in a model. It consists of two-dimensional square $L \times L$ lattices with periodic boundary conditions. The lower one represents the hard stiff surface and the upper one the elastic surface. The nodes of the two lattices are matched (i.e., there is no relative lateral displacement). The fibers are modeled as in the previous sections: elastic up to a threshold value

which has been individually chosen for each fiber from some threshold distribution. The spacing between the fibers is a in both the x and y directions. The force that each fiber is carrying is transferred over an area of size a^2 to the soft clamp: as the two clamps are separated by controlling the displacement of the hard clamp relative to the zero level D, the forces carried by the fibers increase from zero. When the force carried by a fiber reaches its breaking threshold, it breaks irreversibly and the forces redistribute themselves through the deformation of the soft clamp. Hence, the fibers are broken one by one until the two clamps are no longer in mechanical contact. The force f_i carried by the ith fiber is given by

$$f_i = -k(u_i - D), \tag{249}$$

where k is the spring constant and u_i is the deformation of the elastic clamp at site i. All unbroken fibers have $k=1$ while a broken fiber has $k=0$. The quantity $u_i - D$ is, therefore, the length, and since $k=1$, also the force carried by fiber i. The deformation of the soft clamp is described by the coupled system of equations,

$$u_i = \sum_j G_{i,j} f_j, \tag{250}$$

where the elastic Green's function $G_{i,j}$ is given by (Landau and Litshitz, 1958; Johnson, 1985)

$$G_{i,j} = \frac{1-s^2}{\pi e a^2} \int_{-a/2}^{+a/2} \int_{-a/2}^{+a/2} \frac{dx'\, dy'}{|(x-x', y-y')|}. \tag{251}$$

In this equation, s is the Poisson ratio, e is the elastic constant, and $|\vec{i}-\vec{j}|$ is the distance between sites i and j. The indices i and j run over all L^2 sites. The integration over the area a^2 is done to average the force from the fibers over this area. As remarked by Batrouni *et al.* (2002), the Green's function [Eq. (251)] applies for a medium occupying the infinite half space. However, with a judicious choice of elastic constants, it may be used for a finite medium if its range is small compared to L, the size of the system.

By combining Eqs. (249) and (250), one obtains

$$(\mathbf{I} + \mathbf{KG})\vec{f} = \mathbf{K}\vec{D}, \tag{252}$$

where matrix-vector notation is used. $\mathbf{I}$ is the $L^2 \times L^2$ identity matrix and $\mathbf{G}$ is the Green's function represented as an $L^2 \times L^2$ dense matrix. The constant vector $\vec{D}$ is L^2 dimensional. The *diagonal* matrix $\mathbf{K}$ is also $L^2 \times L^2$. Its matrix elements are either 1 for unbroken fibers or 0 for broken ones.

Once Eq. (252) is solved for the force $\vec{f}$, Eq. (250) yields the deformations of the elastic clamp.

Equation (252) is of the familiar form $\mathbf{A}\vec{x} = \vec{b}$. Since the Green's function connects all nodes to all other nodes, the $L^2 \times L^2$ matrix $\mathbf{A}$ is dense, which puts severe limits on the size of the system that may be studied.

The simulation proceeds as follows: one starts with all springs present, each with its stochastic breakdown threshold. The two media are then pulled apart, the forces calculated using the conjugate gradient (CG) algorithm (Batrouni and Hansen, 1988; Press *et al.*, 1992), and the fiber nearest to its threshold is broken, i.e., the matrix element corresponding to it in the matrix $\mathbf{K}$ is zeroed. Then the new forces are calculated, a new fiber is broken, and so on until all fibers have failed.

However, there are two problems that render the simulation of large systems extremely difficult from a numerical point of view. The first is that since $\mathbf{G}$ is $L^2 \times L^2$ *dense* matrix, the number of operations per CG iteration scales like L^4. Even more serious is the fact that as the system evolves and springs are broken, the matrix $\mathbf{I}+k\mathbf{G}$ becomes ill conditioned. To overcome the problematic L^4 scaling of the algorithm, the matrix-vector multiplications are done in Fourier space since the Green's function is diagonal in this space. Symbolically, these multiplications may be written as follows:

$$(\mathbf{I} + \mathbf{K}\mathbf{F}^{-1}\mathbf{F}\mathbf{G})\mathbf{F}^{-1}\mathbf{F}\vec{f} = \mathbf{K}\vec{D}, \tag{253}$$

where $\mathbf{F}$ is the fast Fourier transform (FFT) operator and $\mathbf{F}^{-1}$ is its inverse ($\mathbf{F}^{-1}\mathbf{F}=1$). Since $\mathbf{I}$ and $\mathbf{K}$ are diagonal, operations involving them are performed in real space. With this formulation, the number of operations per iteration in the CG algorithm now scales like $L^2 \ln(L)$ rather than L^4.

To overcome the ill conditioning of the matrix $\mathbf{I}+k\mathbf{G}$ we need to precondition the matrix (Batrouni *et al.*, 1986; Batrouni and Hansen, 1988). This means that instead of solving Eq. (253), one solves the equivalent problem

$$\mathbf{Q}(\mathbf{I} + \mathbf{K}\mathbf{F}^{-1}\mathbf{F}\mathbf{G})\mathbf{F}^{-1}\mathbf{F}\vec{f} = \mathbf{Q}\mathbf{K}\vec{D}, \tag{254}$$

where we simply have multiplied both sides by the arbitrary positive definite preconditioning matrix $\mathbf{Q}$. Clearly, the ideal choice is $\mathbf{Q}_0 = (\mathbf{I}+\mathbf{KG})^{-1}$, which would always solve the problem in one iteration. Since this is not possible in general, we look for a form for $\mathbf{Q}$ which satisfies the following two conditions: (1) as close as possible to $\mathbf{Q}_0$ and (2) fast to calculate. The choice of a good $\mathbf{Q}$ is further complicated by the fact that, as the system evolves and fibers are broken, corresponding matrix elements of $\mathbf{K}$ are set to zero. So, the matrix $\mathbf{I}+\mathbf{KG}$ evolves from the initial form $\mathbf{I}+\mathbf{G}$ to the final one $\mathbf{I}$. Batrouni *et al.* (2002) did not find a fixed $\mathbf{Q}$ that worked throughout the entire breakdown process. They therefore chose the form

$$\mathbf{Q} = \mathbf{I} - (\mathbf{KG}) + (\mathbf{KG})(\mathbf{KG}) - (\mathbf{KG})(\mathbf{KG})(\mathbf{KG}) + \cdots, \tag{255}$$

which is the Taylor series expansion of $\mathbf{Q}_0 = (\mathbf{I}+\mathbf{KG})^{-1}$. For best performance, the number of terms kept in the expansion is left as a parameter since it depends on the physical parameters of the system. It is important to emphasize the following points. (a) As fibers are broken, the preconditioning matrix evolves with the ill-conditioned matrix and therefore remains a good approximation of its inverse throughout the breaking process. (b) All matrix multiplications involving $\mathbf{G}$ are done

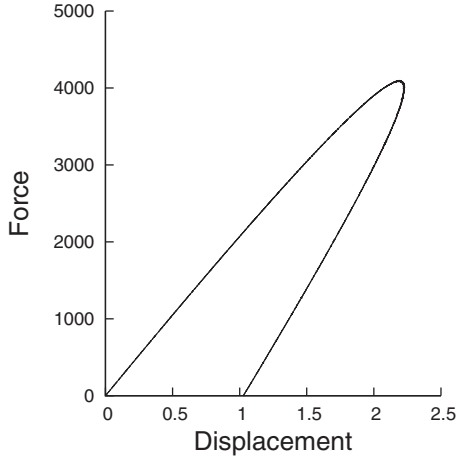

FIG. 40. Force-displacement curve, 128×128 systems with $e=10$.

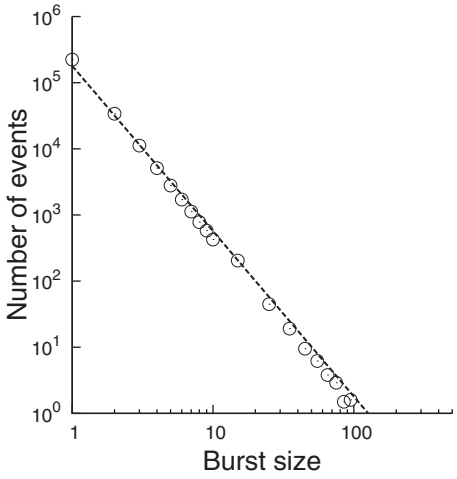

FIG. 42. Burst distribution for 128×128, $e=10$. The slope of the straight line is −2.5.

using FFTs. (c) The calculation of **Q** can be easily organized so that it scales as $nL^2\ln(L)$, where n is the number of terms kept in the Taylor expansion [Eq. (255)]. The result is a stable accelerated algorithm which scales essentially as the volume of the system.

Figure 40 shows the force-displacement curve for a system of size 128×128 and elastic constant $e=10$. Whether we control the applied force F or the displacement D, the system will eventually suffer catastrophic collapse. However, this is not so when $e=100$ as shown in Fig. 41. In this case, only control of the force will lead to catastrophic failure. In the limit when $e\to\infty$, the model becomes the equal-load-sharing fiber bundle model, where $F=(1-D)D$. In this limit there are no spatial correlations and the force instability is due to the decreasing total elastic constant of the system making the force on each surviving bond increase faster than the typical spread of threshold values. No such effect exists when controlling displacement D. However, when the elastic constant e is small, spatial correlations in the form of localization, where fibers that are close in space have a tendency to fail consecutively, do develop, and these are responsible for the displacement instability seen in Fig. 40.

We now turn to the study of the burst distribution. Figures 42 and 43 show the burst distribution for $e=10$ and 100. In both cases we find that the burst distribution follows a power law with an exponent $\xi=2.6\pm0.1$. It was argued by Batrouni *et al.* (2002) that the value of ξ in this case is indeed 5/2 as in the global load-sharing model. These two figures should be compared with Fig. 37 showing the burst distribution in the variable-range fiber bundle model of Hidalgo, Moreno, *et al.* (2002), where $\xi=5/2$ is recovered as long as the range exponent γ is small, rendering the forces long range among the fibers.

As the failure process proceeds, there is an increasing competition between local failure due to stress enhancement and local failure due to local weakness of material. When the displacement D is the control parameter and e is sufficiently small (for example, $e=10$), catastrophic failure eventually occurs due to localization. The onset of this localization, i.e., the catastrophic regime, occurs

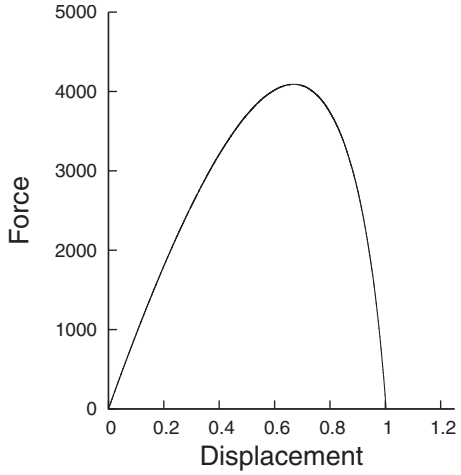

FIG. 41. Force-displacement curve, 128×128 systems with $e=100$.

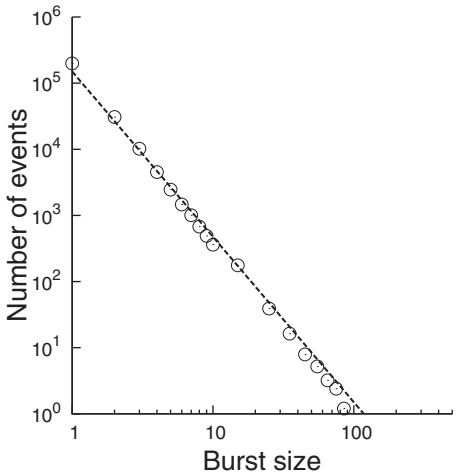

FIG. 43. Burst distribution for 128×128, $e=100$. The slope of the straight line is −2.5.

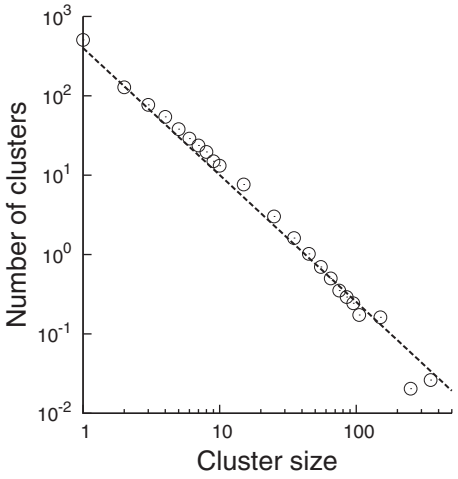

FIG. 44. Area distribution of zones where glue has failed for systems of size 128×128 and elastic constant $e=10$. The straight line is a least-squares fit and indicates a power law with exponent −1.6.

when the two mechanisms are equally important. This may be due to self-organized criticality (Bak *et al.*, 1987) occurring at this point. In order to test whether this is the case, Batrouni *et al.* (2002) measured the size distribution of broken bond clusters at the point when D reaches its maximum point on the F-D characteristics, i.e., the onset of localization and catastrophic failure. The analysis was performed using a Hoshen-Kopelman algorithm (Stauffer and Aharony, 1994). The result is shown in Fig. 44 for 56 disorder realizations, $L=128$, and $e=10$. The result is consistent with a power-law distribution with exponent −1.6 and consequently with self-organization. If this process were in the universality class of percolation, the exponent would have been 2.05. Hence, we are dealing with a new universality class in this system. This behavior should be contrasted to the one seen in the variable-range fiber bundle model studied by Hidalgo, Moreno, *et al.* (2002) where no power-law distribution was found (see Fig. 38 in Sec. IV.B).

V. FIBER BUNDLES IN MATERIALS SCIENCE AND OTHER APPLICATIONS

The aim of this section is to demonstrate how the fiber bundle model may be used as a tool for studying both important phenomena occurring in materials, such as fatigue, and important classes of materials, notably fiber-reinforced composites. A general review has recently been written by Mishnaevsky and Brøndsted (2009) on this subject. We also discuss applications of fiber bundle models in other contexts, ranging from traffic modeling to earthquake dynamics.

A. Time-dependent failure: Fatigue or creep phenomena

Materials may undergo time-dependent deformation under steady load. Sometimes when a load is applied, though the system survives at first stage, it fails after a long time. This type of failure is referred to as fatigue failure or creep rupture (Lawn, 1993; Chakrabarti, 1994; Kun *et al.*, 2006). Fatigue failure is basically a thermally activated process (Phoenix and Tierney, 1983) and originates at the atomic level of the fibers where the molecules are in random thermal vibrations. Eventually a molecule acquires sufficient thermal energy to overcome the local energy barrier and slips relative to other molecules. The frequency of such events is greatly enhanced by increases in temperature, stress, and impurity level. After a molecular slip or rupture, neighboring molecules become overloaded and the failure rate increases. These molecular failures accumulate locally and produce microcracks within the material. Also, microcracks can grow with time at the crack tips due to chemical diffusion in the atmosphere (Lawn, 1993), which helps the growth of fractures. These failures nucleate around the defects in the solid, and the failure behavior and its statistics therefore crucially depend on the disorder or impurity distribution within the sample. The system then fails under a stress less than its normal strength (σ_c) and the failure time (τ) depends on both the applied load and the impurity level.

Fatigue failure in the fiber bundle model was first studied by Coleman (1956, 1957a, 1957b) considering different classes of fibers and several breakdown rules. The probabilistic analysis gives the lifetime distribution under various loading conditions: constant load, loads proportional to time, and periodic loads. "Time dependent fatigue" and "cycle-dependent fatigue" are both addressed in this work, introducing the concept of a "memory" effect, i.e., the load history can affect the failure of fibers. Such time-dependent failure in fiber bundles has been considerably extended and generalized by Phoenix *et al.* (Phoenix, 1978, 1979; Phoenix and Tierney, 1983; Newman and Phoenix, 2001) for equal load-sharing (ELS) and local-load sharing (LLS) bundles. The approximate fatigue lifetime distributions have been achieved through probabilistic analysis introducing the power-law and exponential breakdown rules at the molecular level (Phoenix and Tierney, 1983).

When dry fibers are replaced by viscoelastic elements having-time dependent deformation properties, the fiber bundle model exhibits creep behavior (Moral *et al.*, 2001; Hidalgo, Kun, *et al.*, 2002; Kun *et al.*, 2003) in terms of the macroscopic response under constant external load. There exists a critical load (or stress) below which the deformation attains a constant value (infinite lifetime) and, above the critical load, deformation increases monotonically, resulting is global failure (finite lifetime). Another extension of the classical fiber bundle model, the continuous damage model (Hidalgo *et al.*, 2001; Kun *et al.*, 2003), captures similar creep behavior, assuming that a fiber can fail more than once and at each failure its stiffness is reduced by a constant factor. In both of these models the lifetime of the bundle diverges at the critical load, following robust power-law variation with the applied load.

Also, a few experiments (Pauchard and Meunier, 1993; Banerjee and Chakrabarti, 2001; Kun *et al.*, 2007),

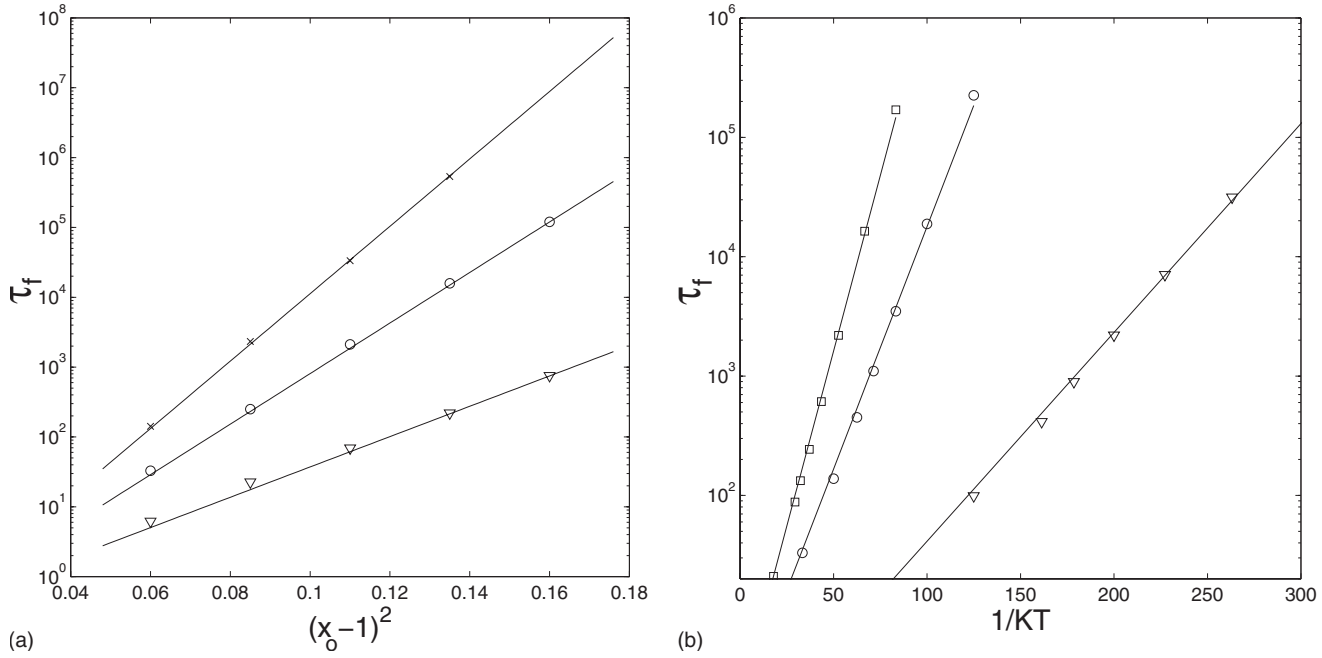

FIG. 45. Failure time τ_f of a homogeneous bundle ($kT_d=0$) in a creep test. (a) τ_f as a function of the normalized force $(1-x_0)^2$ for several values of thermal noise variance kT: $kT=0.0045$ (cross); 0.006 (circle); and 0.01 (triangle). (b) τ_f as a function of $1/kT$ for several values of x_0: $x_0=0.45$ (box); 0.54 (circle); and 0.7 (triangle). Continuous lines in (a) and (b) are the fits with Eqs. (259) and (260), respectively. Adapted from Ciliberto *et al.*, 2001.

have been performed to observe the failure time of materials and its statistics. The effect of thermal activation and disordered noise on the failure have recently been measured for material breakdown and approximate fatigue behavior has been obtained (Guarino, Garcimartín, and Ciliberto, 1999; Guarino, Scorretti, and Ciliberto, 1999; Roux, 2000; Scorretti *et al.*, 2001; Guarino *et al.*, 2002; Pradhan and Chakrabarti, 2003b; Kun *et al.*, 2007), using fiber bundle models.

In this section, we discuss several approaches to achieving fatigue-failure behavior in equal-load-sharing fiber bundle models. The approaches differ basically in the way time dependence has been incorporated in the failure process.

1. Thermally induced failure in fiber bundles

The influence of noise on macroscopic failure in the fiber bundle model has been studied numerically (Guarino, Garcimartín, and Ciliberto, 1999; Guarino, Scorretti, and Ciliberto, 1999; Ciliberto *et al.*, 2001; Scorretti *et al.*, 2001; Guarino *et al.*, 2002) using both disorder noise and thermal noise. The strength of each fiber is characterized by a critical stress $x_i^{(c)}$, which is a random variable that follows a normal distribution of mean $x^{(c)}$ and variance kT_d:

$$x_i^{(c)} = x^{(c)} + N_d(kT_d), \tag{256}$$

where k is the Boltzmann constant and N_d is the disorder noise. Again each fiber is subjected to an additive time-dependent random stress $\Delta x_i(t)$, which follows a zero mean normal distribution of variance kT:

$$\Delta x_i(t) = N_T(t,kT). \tag{257}$$

Here N_T is the thermal noise.

Due to the equal-load-sharing scheme, if a number $n(t)$ of fibers are broken at time t after force F is applied on the bundle, the local force on each of the remaining fibers will be

$$x_i(t) = \frac{x_0 N}{N - n(t)} + \Delta x_i(t), \tag{258}$$

where N is the total number of fibers in the intact bundle and $x_0=F/N$ is the initial force per fiber. If $kT=0$, the model reduces to the static one. In that case the applied force is increased linearly from zero to the critical value F_c above which the whole bundle breaks. Therefore, at a constant force F, the bundle breaks in a single avalanche only if $F>F_c$, otherwise it will never break. If $kT\neq 0$ then the system can break at an applied force $F<F_c$ due to the thermal effect. Such thermal failure of the model has been studied numerically as a function of x_0, kT, and kT_d (Guarino, Garcimartín, and Ciliberto, 1999; Guarino, Scorretti, and Ciliberto, 1999; Ciliberto *et al.*, 2001).

When $kT\neq 0$, the failure time τ_f as a function of $(1-x_0)^2$ follows an exponential law for any fixed value of kT_d,

$$\tau_f \sim \exp[\alpha(1-x_0)^2], \tag{259}$$

where α is a fitting parameter [Fig. 45(a)], which is a function of kT. At constant stress, the failure time depends on thermal noise kT as

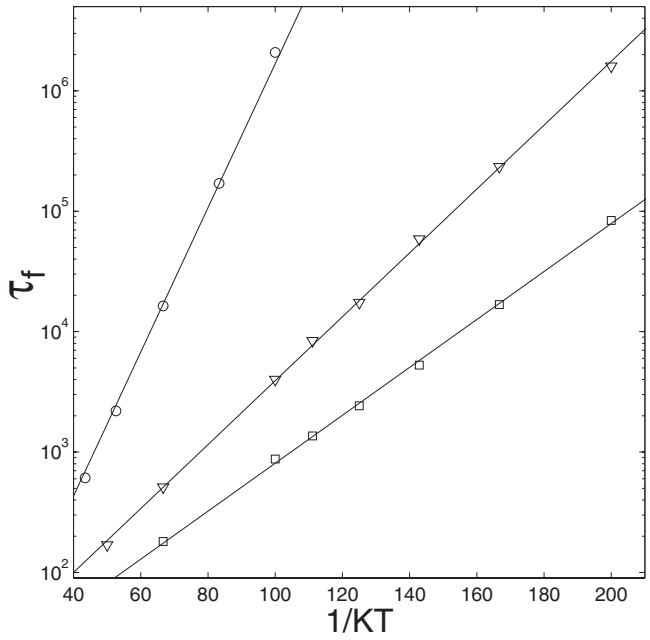

FIG. 46. Failure time τ_f of a heterogeneous bundle ($kT_d \neq 0$) in creep test. The lifetime τ_f is plotted as a function of $1/kT$ at $x_0=0.45$. Different symbols correspond to different values of kT_d: $kT_d=0$ (circle); 0.02 (triangle); and 0.04 (box). Adapted from Ciliberto *et al.*, 2001.

$$\tau_f \sim \tau_0 \exp\left(\frac{A}{kT}\right), \tag{260}$$

where A is a function of x [Fig. 45(b)]. A similar result has also been observed in the case of a heterogeneous fiber bundle (Fig. 46).

One can compare these results with Pomeau's theory (Pomeau, 1992) for the failure time of solids,

$$\tau_f = \tau_0 \exp\left(\alpha_g \frac{\Gamma_s^d Y^{(d-1)}}{kT_{\text{eff}} P_s^{(2d-2)}}\right), \tag{261}$$

where P_s is the imposed stress, τ_0 is a constant, Γ_s is the surface energy, Y is the Young modulus, α_g is a constant which depends on the geometry, T_{eff} is an effective temperature, and d is the dimensionality of the system. This theory is based on the physical argument that thermal activation of microcracks (Golubović and Feng, 1991; Pomeau, 1992), is responsible for the macroscopic failure of the material. Note that the functional dependence of τ_f on stress is different for the fiber bundle model and for solids, the main reason being the different geometries of the stress distribution in the fiber bundle and the solids.

These numerical studies suggest that disorder noise amplifies the effect of thermal noise and reduces the dependence of τ_f on the temperature and this can explain recent experimental observations on microcrystals (Pauchard and Meunier, 1993), gels (Bonn *et al.*, 1998), and macroscopic composite materials (Guarino, Garcimartín, and Ciliberto, 1999; Guarino, Scorretti, and Ciliberto, 1999).

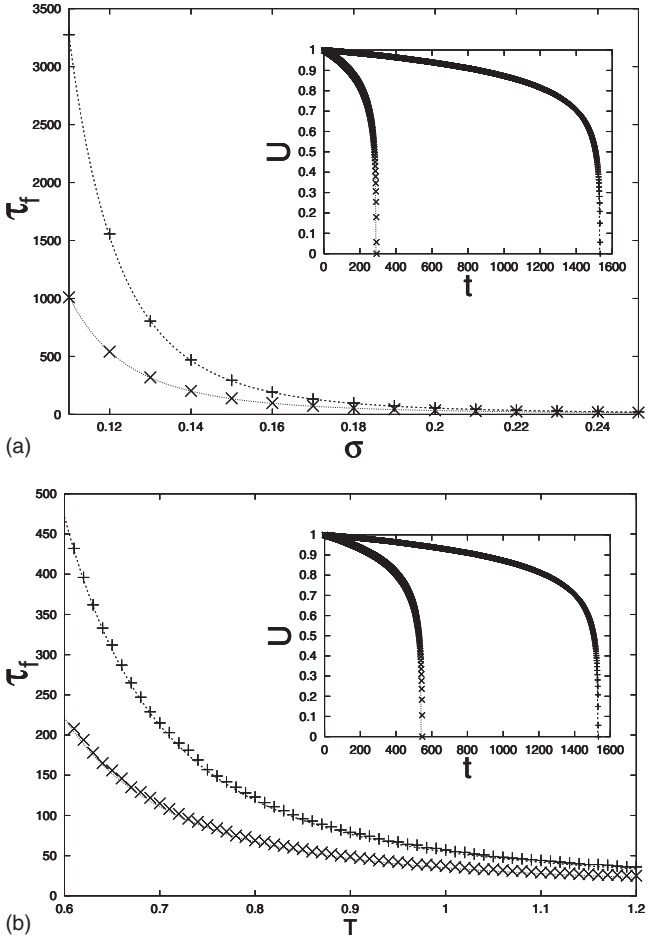

FIG. 47. The simulation results showing variation of average failure time τ_f against (a) external stress σ and (b) noise T ($k=1$ here) for a homogeneous bundle containing $N=10^5$ fibers. The insets show the variation of the fraction U of unbroken fibers with time t for different T values [1.2 (cross) and 1.0 (plus)] in (a) and different σ values [0.15 (cross) and 0.12 (plus)] in (b). The dotted and dashed lines represent the theoretical result [Eq. (277)].

The numerical observations described above have been confirmed later through an analytic investigation by Roux (2000). In a homogeneous (no disorder in fiber strengths) fiber bundle model, the force or stress on each fiber is

$$x = x_0 + \eta, \tag{262}$$

where $x_0=F/N$ and η is the random noise with a Gaussian distribution

$$p(\eta) = \frac{1}{\sqrt{2\pi kT}} \exp\left(-\frac{\eta^2}{2kT}\right), \tag{263}$$

with zero mean and variance kT. Now the probability that one fiber survives after time step t is

$$p_1(t) = [1 - P(1 - x_0)]^t, \tag{264}$$

where P is the cumulative probability. Then the probability that the entire bundle can survive after time step t time is

$$p_N(t) = [1 - P(1 - x_0)]^{Nt}. \tag{265}$$

Therefore the average failure time is

$$\langle \tau_1 \rangle = \frac{-1}{N \ln[1 - P(1 - x_0)]}. \tag{266}$$

After the first fiber breaks, the situation remains the same with a smaller bundle and larger stress. Thus the average failure time after $i-1$ broken fibers is

$$\langle \tau_i \rangle = \frac{-1}{(N-i)\ln\{1 - P[1 - Nx_0/(N-i)]\}}. \tag{267}$$

Now the total failure time can be obtained by taking the sum over all i as

$$\langle \tau_f \rangle = \sum_{i=1}^{N} \frac{-1}{(N-i)\ln\{1 - P[1 - Nx_0/(N-i)]\}}. \tag{268}$$

When N is large, one can replace the sum by a continuous integral,

$$\langle \tau_f \rangle = N^{-1} \int_0^N \frac{-N}{(N-y)\ln\{1 - P[1 - Nx_0/(N-y)]\}} dy$$
$$= \int_{x_0}^{\infty} \frac{-1}{\ln[1 - P(1-z)]} \frac{dz}{z}.$$

To achieve a closed-form equation it has been considered that the above sum is dominated by the time required for breaking the first fiber when x_0 is much smaller than the maximum load x_c and when $kT \ll 1$. Then P can be considered to be much smaller than 1. Now the derivative of the average time with respect to x_0 gives

$$\frac{\partial \langle \tau_f \rangle}{\partial x_0} = \frac{1}{x_0 \ln[1 - P(1 - x_0)]} \approx \frac{1}{x_0 P(1 - x_0)}. \tag{269}$$

When $(1-x_0)^2 \gg kT$ the error function can be expanded as

$$P(1 - x_0) = \frac{\sqrt{kT}\exp[-(1-x_0)^2/2kT]}{\sqrt{2\pi}(1-x_0)}[1 + O(kT)]. \tag{270}$$

Finally, taking into account the dominating terms, one gets

$$\langle \tau_f \rangle = \frac{\sqrt{2\pi kT}}{x_0} \exp\left(-\frac{(1-x_0)^2}{2kT}\right). \tag{271}$$

These analytic expressions are identical to those observed earlier (Guarino, Garcimartín, and Ciliberto, 1999; Guarino, Scorretti, and Ciliberto, 1999; Ciliberto *et al.*, 2001; Scorretti *et al.*, 2001; Guarino *et al.*, 2002) in numerical simulations. A similar analysis (Roux, 2000) showed that when fiber strengths are distributed (heterogeneous case), the average first failure time can be expressed as

$$\langle \tau_1 \rangle = \frac{\sqrt{2\pi}}{N} \frac{(1-x_0)}{\sqrt{k(T+\Theta)}} \exp\left(-\frac{(1-x_0)^2}{2k(T+\Theta)}\right), \tag{272}$$

where Θ is an effective temperature that is added to the temperature T due to the disorder. Hence, the disorder leads to an effective temperature $T_{\text{eff}} = T + \Theta$, and this is what Scorretti *et al.* (2001) proposed: time-independent heterogeneities of the system modify the effective temperature.

Politi *et al.* (2002) estimated the total time to failure for the thermally activated fiber bundle model and found the same behavior as in Eq. (272): the disorder adds a constant to the temperature of the fiber bundle. Guarino *et al.* (2006), generalized these results to the two-dimensional fuse model.

2. Noise-induced failure in fiber bundles

Not only the temperature but several other factors can result in fatigue failure in materials: weather effects, chemical effects, etc. (Lawn, 1993; Chakrabarti, 1994). Recently, there has been an attempt (Pradhan and Chakrabarti, 2003b) to incorporate all the noise effects through a single parameter kT (k is the Boltzmann constant), which can directly influence the failure probability of the individual elements. Such a failure probability $p(\sigma, kT)$ at any applied stress σ, induced by a nonzero noise kT, has been formulated as

$$p(\sigma, kT) = \begin{cases} \dfrac{\sigma}{x} \exp\left[-\dfrac{1}{kT}\left(\dfrac{x}{\sigma} - 1\right)\right], & 0 \leqslant \sigma \leqslant x \\ 1, & \sigma > x, \end{cases} \tag{273}$$

where x is the failure strength of an element. Clearly, the failure probability increases as σ and kT increase. Without any noise ($kT=0$) the model is trivial: the bundle remains intact for stress $\sigma < \sigma_c$ and it fails completely for $\sigma \geqslant \sigma_c$, where σ_c is the critical stress value.

At $kT \neq 0$ and under any stress σ ($< \sigma_c$) some fibers (weaker fibers) fail and the total load has to be supported by the surviving fibers, which in turn enhances their stress value, inducing further failure. The bundle therefore fails at $\sigma < \sigma_c$ after a finite time τ_f.

In the case of the homogeneous bundle (all fibers have the same strength x), the critical stress value for the bundle is $\sigma_c = x$. Then the time dynamics at an applied stress σ can be written (Pradhan and Chakrabarti, 2003b) as

$$U_{t+1} = U_t\left[1 - p\left(\frac{\sigma}{U_t}, kT\right)\right], \tag{274}$$

where U_t is the fraction of total fibers that remains intact after time step t. In the continuum limit, we can write the above recursion relation in a differential form,

$$-\frac{dU}{dt} = \frac{\sigma}{\sigma_c} \exp\left[-\frac{1}{kT}\left(\frac{\sigma_c}{\sigma}U - 1\right)\right]. \tag{275}$$

The solution gives the failure time

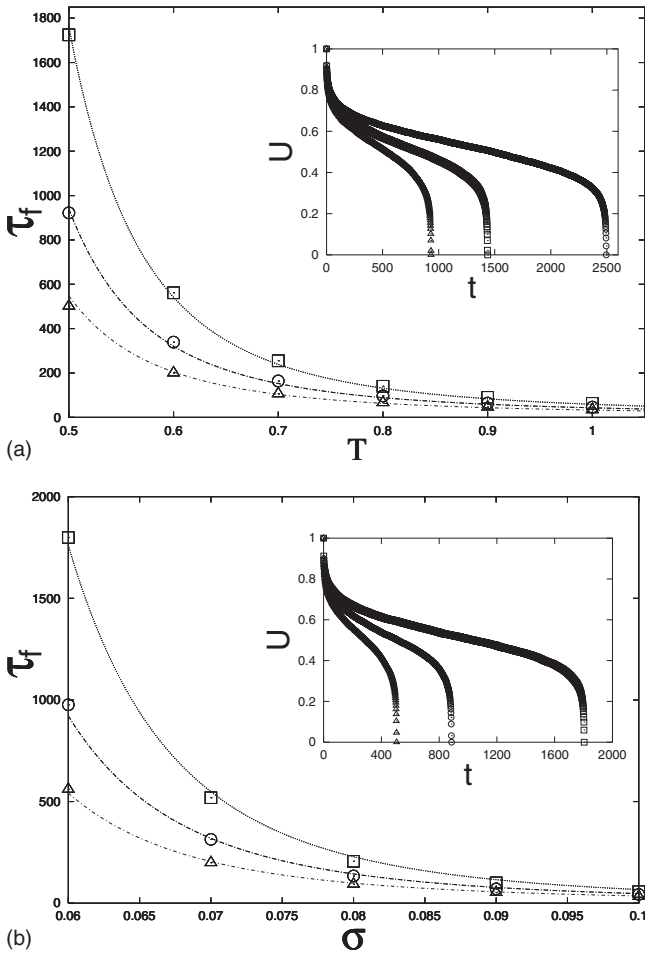

FIG. 48. Simulation results of fatigue behavior: (a) average failure time τ_f vs noise T ($k=1$ here) for three different stress values and (b) τ_f vs σ for three different noise values. The bundle contains $N=10^5$ fibers with uniformly distributed strength thresholds. The time variations of a fraction of surviving fibers are shown in the insets. The dotted lines in (a) and (b) correspond to the fit with expression [Eq. (278)] where $\sigma_c \simeq 0.245$ [exact value $=1/4$ (Pradhan *et al.*, 2002; Bhattacharyya *et al.*, 2003)].

$$\tau_f = \int_0^{\tau_f} dt = \frac{\sigma_c}{\sigma} \exp\left(-\frac{1}{kT}\right) \int_0^1 \exp\left[\frac{1}{kT}\left(\frac{\sigma_c}{\sigma}\right) U\right] dU. \tag{276}$$

Hence, for $\sigma < \sigma_c$,

$$\tau_f = kT \exp\left(-\frac{1}{kT}\right)\left[\exp\left(\frac{\sigma_c}{\sigma kT}\right) - 1\right]. \tag{277}$$

Again, for $\sigma \geqslant \sigma_c$, one gets $U_{t+1}=0$ from Eq. (274), giving $\tau_f=0$. For small kT and as $\sigma \to \sigma_c$, $\tau_f \simeq kT \exp[(\sigma_c/\sigma - 1)/kT]$ (see Fig. 47). These results agree qualitatively with recent experimental observations (Banerjee and Chakrabarti, 2001; Guarino *et al.*, 2002).

In order to investigate the fatigue behavior in heterogeneous fiber bundles, uniform distribution of fiber strengths has been considered (Pradhan and Chakrabarti, 2003b). The noise-induced failure probability has the similar form $p(\sigma,kT)=\exp[-(1/kT)(x/\sigma-1)]$ for $0 < \sigma \leqslant x$ and $p(\sigma,kT)=1$ for $\sigma > x$, where x denotes the strength of the individual fibers in the bundle. Now it is difficult to tackle the problem analytically. However, Monte Carlo simulations (Pradhan and Chakrabarti, 2003b) showed (Fig. 48) the variations of average failure time (τ_f) with noise (kT) and stress level (σ):

$$\tau_f = kT \exp\left(-\frac{1}{kT}\right)\left[\exp\left(\frac{\sigma_c}{\sigma kT} + \frac{1}{kT}\right) - 1\right], \tag{278}$$

where σ_c is the critical stress. This phenomenological form [Eq. (278)] is indeed very close to the analytic result [Eq. (276)] for the homogeneous fiber bundle.

Newman and Phoenix (2001) considered the breaking dynamics in a fiber bundle where each fiber has a failure probability p determined by the loading time t and the load σ on it as $p(t,\sigma)=1-\exp(-t\sigma^\rho)$ and analyzed the life time (t_f) distribution. For $1/2 \leqslant \rho \leqslant 1$, ELS and LLS models have identical Gaussian distribution for t_f. For $\rho > 1$, LLS shows extreme statistics, while ELS gives Gaussian behavior [see, e.g., Curtin and Scher (1997)]. Yoshioka *et al.* (2008) also studied similar t_f distributions and their scaling properties with load and temperature variations.

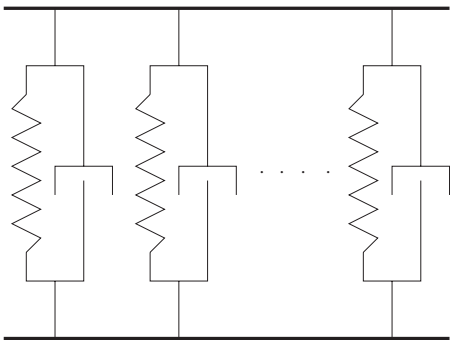

FIG. 49. The viscoelastic fiber bundle: intact fibers are modeled by Kelvin-Voigt elements which consist of a spring and a dashpot in parallel. From Kun *et al.*, 2003.

3. Creep rupture in viscoelastic fiber bundles

Creep behavior has been achieved (Hidalgo, Kun, *et al.*, 2002; Kun *et al.*, 2003) in a bundle of viscoelastic fibers, where a fiber is modeled by a Kelvin-Voigt element (see Fig. 49) and results in the constitutive stress-strain relation

$$\sigma_0 = \beta_0 \dot{\varepsilon} + Y\varepsilon. \tag{279}$$

Here σ_0 is the applied stress, ε is the corresponding strain, β_0 denotes the damping coefficient, and Y is the Young modulus of the fibers.

In the equal-load-sharing mode, the time evolution of the system under a steady external stress σ_0 can be described by

$$\frac{\sigma_0}{1-P(\varepsilon)} = \beta_0 \dot{\varepsilon} + Y\varepsilon. \tag{280}$$

As one can expect intuitively, there is a critical load σ_c for the system and Eq. (280) suggests two distinct regimes depending on the value of the external load σ_0: when σ_0 is below the critical value σ_c, Eq. (280) has a fixed-point solution ε_s, which can be obtained by setting $\dot{\varepsilon}=0$ in Eq. (280),

$$\sigma_0 = Y\varepsilon_s[1 - P(\varepsilon_s)]. \tag{281}$$

In this case the strain value converges to ε_s when $t\to\infty$, and no macroscopic failure occurs. But, when $\sigma_0 > \sigma_c$, no fixed-point solution exists. Here $\dot{\varepsilon}$ remains always positive, which means in this case that the strain of the system $\varepsilon(t)$ monotonically increases until the system fails globally at a finite time t_f (Hidalgo, Kun, *et al.*, 2002).

The solution of the differential equation [Eq. (280)] gives a complete description of the failure process. By separation of variables, the integral becomes

$$t = \beta_0 \int d\varepsilon \frac{1 - P(\varepsilon)}{\sigma_0 - Y\varepsilon[1 - P(\varepsilon)]} + C, \tag{282}$$

where C is the integration constant.

Below the critical point $\sigma_0 \leqslant \sigma_c$ the bundle slowly relaxes to the fixed-point value ε_s. The characteristic time scale of such a relaxation process can be obtained by analyzing the behavior of $\varepsilon(t)$ in the vicinity of ε_s. After introducing a new variable δ_0 as $\delta_0(t)=\varepsilon_s-\varepsilon(t)$, the differential equation can be written as

$$\frac{d\delta_0}{dt} = -\frac{Y}{\beta_0}\left(1 - \frac{\varepsilon_s p(\varepsilon_s)}{1 - P(\varepsilon_s)}\right)\delta_0. \tag{283}$$

Clearly, the solution of Eq. (283) has the form $\delta_0 \sim \exp[-t/\tau]$, with

$$\tau = \frac{\beta_0}{Y}\frac{1}{\left(1 - \frac{\varepsilon_s p(\varepsilon_s)}{1 - P(\varepsilon_s)}\right)}, \tag{284}$$

where τ is the characteristic time of the relaxation process.

The variation of the relaxation time τ with the external driving near the critical point σ_c is crucial for any dynamical system. Since $\sigma_0(\varepsilon_s)$ has a maximum of the value σ_c at ε_c, in the vicinity of ε_c one can use the approximation

$$\sigma_0 \approx \sigma_c - A(\varepsilon_c - \varepsilon_s)^2, \tag{285}$$

where the multiplication factor A depends on the cumulative distribution P. Using the approximation (285), it can be shown from Eq. (284) that

$$\tau \sim (\sigma_c - \sigma_0)^{-1/2} \quad \text{for } \sigma_0 < \sigma_c. \tag{286}$$

Therefore, the relaxation time diverges following a universal power law with an exponent $-1/2$. Note that a dry fiber bundle model, under constant load, shows similar power-law divergence (see Sec. III.A).

How does the system behave above the critical point? The behavior can be analyzed in the same way when σ_0 is close to σ_c. Then one can write $\sigma_0=\sigma_c+\Delta\sigma_0$, where

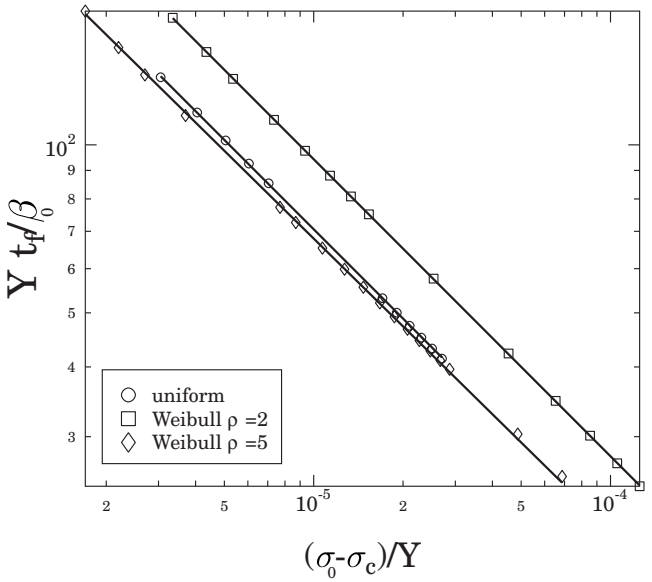

FIG. 50. The behavior of the time to failure t_f for uniform and Weibull distributions with two different Weibull indices for the ELS case. All three curves are parallel to each other on a double logarithmic plot with an exponent close to 0.5, in agreement with the general result [Eq. (288)]. From Hidalgo, Kun, *et al.*, 2002.

$\Delta\sigma_0 \ll \sigma_c$. It is obvious that the relaxation steps are too many when $\varepsilon(t)$ becomes close to ε_c. Therefore, the integral in Eq. (282) is dominated by the region close to ε_c. Using Eq. (285) the integral in Eq. (282) becomes

$$t_f \approx \beta_0 \int d\varepsilon \frac{1 - P(\varepsilon)}{\Delta\sigma_0 - A(\varepsilon_c - \varepsilon)^2}. \tag{287}$$

Evaluating the integration over a small ε interval in the vicinity of ε_c, one gets

$$t_f \approx (\sigma_0 - \sigma_c)^{-1/2} \quad \text{for } \sigma_0 > \sigma_c. \tag{288}$$

Thus, t_f has a two-sided power-law divergence at σ_c with a universal exponent $-\frac{1}{2}$ independent of the specific form of the disorder distribution $P(\varepsilon)$, similar to τ in the case of the dry fiber bundle (see Sec. III.A).

To check the validity of the universal power-law behavior of t_f, simulations were performed (Hidalgo, Kun, *et al.*, 2002) with various disorder distributions, i.e., a uniform distribution and the Weibull distribution of the form $P(\varepsilon)=1-\exp[-(\varepsilon/\lambda)^\rho]$, where λ is the characteristic strain and ρ is the shape parameter. The simulation results (Fig. 50) are in good agreement with the analytic results.

4. Creep rupture in a bundle of slowly relaxing fibers

A slow relaxation following fiber failure can also lead to creep behavior (Hidalgo *et al.*, 2001; Kun *et al.*, 2003). In this case, the fibers are linearly elastic until they break, but after breaking they undergo a slow relaxation process. Therefore when a fiber breaks, its load does not drop to zero instantaneously. Instead it undergoes a slow

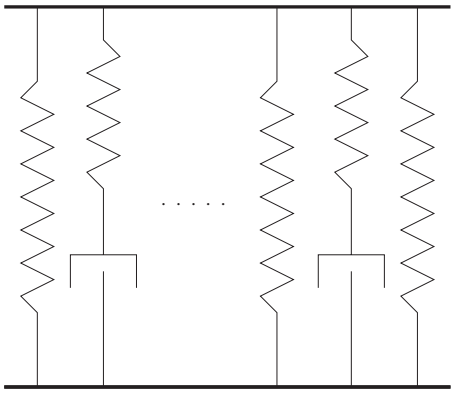

FIG. 51. The fibers are modeled by Maxwell elements. From Kun *et al.*, 2003.

relaxation process and thus introduces a time scale into the system. As the intact fibers are assumed to be linearly elastic, the deformation rate is

$$\dot{\varepsilon}_f = \frac{\dot{x}}{Y}, \tag{289}$$

where x denotes the stress, ε_f denotes the strain, and Y is the Young modulus of the fibers. In addition, to capture the slow relaxation effect, the broken fibers with the surrounding matrix material are modeled by Maxwell elements (Fig. 51), i.e., they are assumed as a serial coupling of a spring and a dashpot. Such arrangement results in the following nonlinear response:

$$\dot{\varepsilon}_b = \frac{\dot{x}_b}{S_b} + B x_b^m, \tag{290}$$

where x_b is the time-dependent stress and ε_b is the time-dependent deformation of a broken fiber. The relaxation of broken fibers is characterized by few parameters: S_b B, and m, where S_b is the effective stiffness of a broken fiber, the exponent m characterizes the strength of nonlinearity, and B is a constant.

In equal-load-sharing mode, when external stress σ_0 is applied, the macroscopic elastic behavior of the composite can be represented by the constitutive equation (Hidalgo *et al.*, 2001; Kun *et al.*, 2003),

$$\sigma_0 = x(t)[\dot{1} - P(x(t))] + x_b(t)P(x(t)). \tag{291}$$

Here $x_b(t)$ is the amount of stress carried by the broken fibers and $P(x(t))$ and $1-P(x(t))$ denote the fraction of broken and intact fibers at time t, respectively.

By construction (Fig. 51), the two time derivatives have to be always equal,

$$\dot{\varepsilon}_f = \dot{\varepsilon}_b. \tag{292}$$

Now the differential equation for the time evolution of the system can be obtained, using Eqs. (291), (290), and (292) as

$$\dot{x}\left\{\frac{1}{Y} - \frac{1}{S_b}\left[1 - \frac{1}{P(x)} + \frac{p(x)}{P(x)^2}(x-\sigma_0)\right]\right\} = B\left[\frac{\sigma_0 - x[1-P(x)]}{P(x)}\right]^m. \tag{293}$$

As in the viscoelastic model, two different regimes of $x(t)$ can be distinguished depending on the value of σ_0: if the external load is below the critical value σ_c a fixed-point solution x_s exists which can be obtained by setting $\dot{x}=0$ in Eq. (293),

$$\sigma_0 = x_s[1 - P(x_s)]. \tag{294}$$

This means that the solution $x(t)$ of Eq. (293) converges asymptotically to x_s resulting in an infinite lifetime t_f of the system. When the external load is above the critical value, the deformation rate $\dot{\varepsilon}=\dot{x}/Y$ always remains positive, resulting in a macroscopic failure in a finite time t_f. Now we focus on the universal behavior of the model in the vicinity of the critical point. Below the critical point the relaxation of $x(t)$ to the stationary solution x_s can be presented by a differential equation of the form

$$\frac{d\delta_0}{dt} \sim \delta_0^m, \tag{295}$$

where δ_0 denotes the difference $\delta_0(t)=x_s-x(t)$. Hence, the characteristic time scale τ of the relaxation process emerges only if $m=1$. Also, in this case relaxation time varies as $\tau \sim (\sigma_c-\sigma_0)^{-1/2}$ when the critical point is approached from below. However, for $m>1$ the situation is different: the relaxation process is characterized by $\delta_0(t)=at^{1/1-m}$, where $a\to 0$ with $\sigma_0\to\sigma_c$.

Again, close to the critical point, it can also be shown that the lifetime t_f shows power-law divergence when the external load approaches the critical point from above,

$$t_f \sim (\sigma_0 - \sigma_c)^{-(m-1/2)} \quad \text{for } \sigma_0 > \sigma_c. \tag{296}$$

The exponent is universal in the sense that it does not depend on the disorder distribution. However, it depends on the exponent m, which characterizes the nonlinearity of broken fibers.

As a check, numerical simulations have been performed (Hidalgo *et al.*, 2001; Kun *et al.*, 2003) for several different values of the exponent m (Fig. 52). The slope of the fitted straight lines agrees well with the analytic predictions [Eq. (296)].

5. Fatigue-failure experiment

An interesting experimental and theoretical study of fatigue failure in asphalt was performed by Kun *et al.* (2007). The experimental setup is shown in Fig. 53. The cylindrical sample was subjected to cyclic diametric compression at constant load amplitude σ_0, and the deformation ϵ as a function of the number of cycles N_{cycle} was recorded together with the number of cycles N_f at which catastrophic failure occurs.

Figure 54 shows deformation ϵ as a function of the number of cycles N_{cycle} for two different load amplitudes

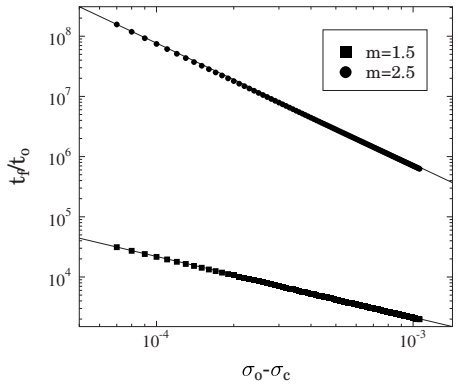

FIG. 52. Lifetime t_f as a function of the distance from the critical point, $\sigma_o - \sigma_c$, for two different values of the parameter m. The number of fibers in the bundle is $N=10^7$. From Kun *et al.*, 2003.

$\sigma_0/\sigma_c=0.3$ and 0.4. Here σ_c is the tensile strength of the asphalt. Figure 55 shows the number of cycles to catastrophic failure as a function of the load amplitude σ_0/σ_c. This curve shows three regimes, the middle one being characterizable by a power law,

$$N_f \sim \left(\frac{\sigma_0}{\sigma_c}\right)^{-\alpha'}. \tag{297}$$

This is the Basquin regime (Suresh, 1991; Sornette *et al.*, 1992; Li and Metcalf, 2002; Si *et al.*, 2002). Kun *et al.* (2007) found $\alpha'=2.2\pm0.1$ for the asphalt system.

In order to model the behavior found in Figs. 54 and 55, Kun *et al.* (2007) introduced the equal-load-sharing fiber bundle model as shown in Fig. 53(a). Each fiber $1 \leqslant i \leqslant N$ is subjected to a time-dependent load $x_i(t)$. There are two failure mechanisms present. Fiber i fails instantaneously at time t when $x_i(t)$ for the first time reaches its failure threshold t_i. However, there is also a damage accumulation mechanism characterized by the parameter $c_i(t)$. In the time interval dt, fiber i accumulates a damage

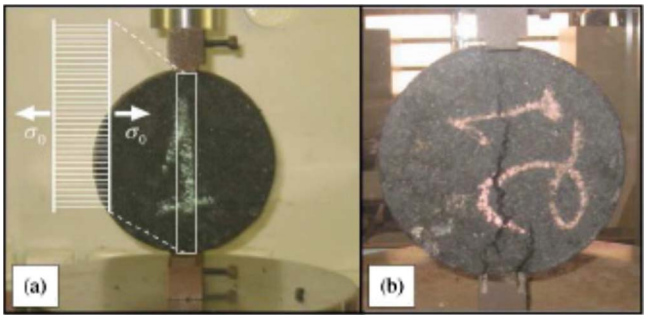

FIG. 53. (Color online) Asphalt samples set up for experimental testing of fatigue failure. (a) shows how fatigue failure under these experimental conditions is modeled using a fiber bundle model and (b) shows a postfailure sample. From Kun *et al.*, 2007.

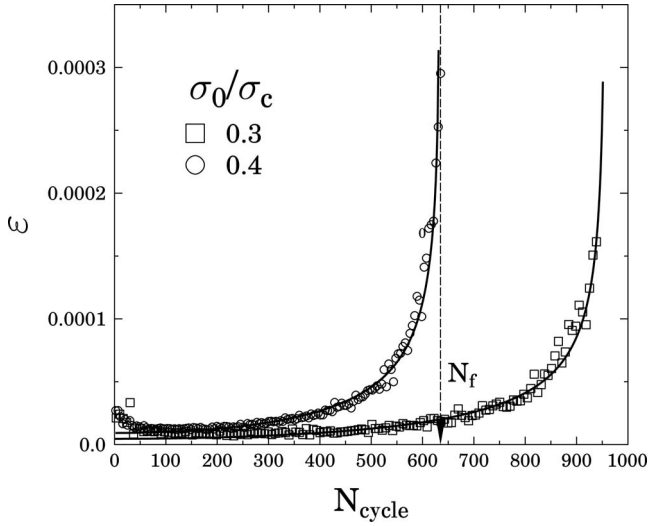

FIG. 54. Deformation ε as a function of number of cycles N_{cycle}, showing both experimental data and theoretical curves based on the fiber bundle model. From Kun *et al.*, 2007.

$$dc_i(t) = a x_i(t)^\gamma \, dt, \tag{298}$$

where $a>0$ is a scale parameter and $\gamma>0$ is an exponent to be determined. Hence, the accumulated damage is

$$c_i(t) = a \int_0^t x_i(t')^\gamma \, dt'. \tag{299}$$

When $c_i(t)$ for the first time exceeds the damage accumulation threshold s_i, fiber i fails. The thresholds t_i and s_i are chosen from a joint probability distribution $p_{t,s}(t,s)$. Kun *et al.* (2007) made the assumption that this distribution may be factorized, $p_{t,s}(t,s)=p_t(t)p_s(s)$.

In addition to damage accumulation, there is yet another important mechanism that needs to be incorporated in the model: damage *healing* (Si *et al.*, 2002; Jo *et al.*, 2008). A time scale τ is associated with this mechanism, and the ELS average force-load equation

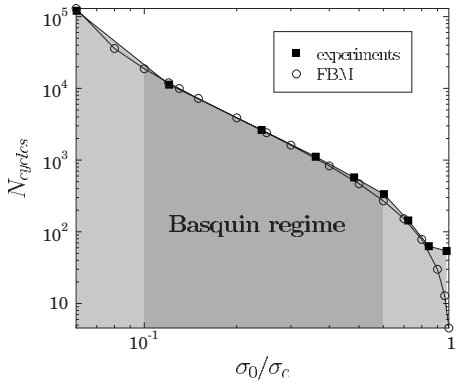

FIG. 55. Number of cycles at catastrophic failure N_f as a function of load amplitude σ_0/σ_c. The two curves show experimental and fiber bundle model data. From Kun *et al.*, 2007.

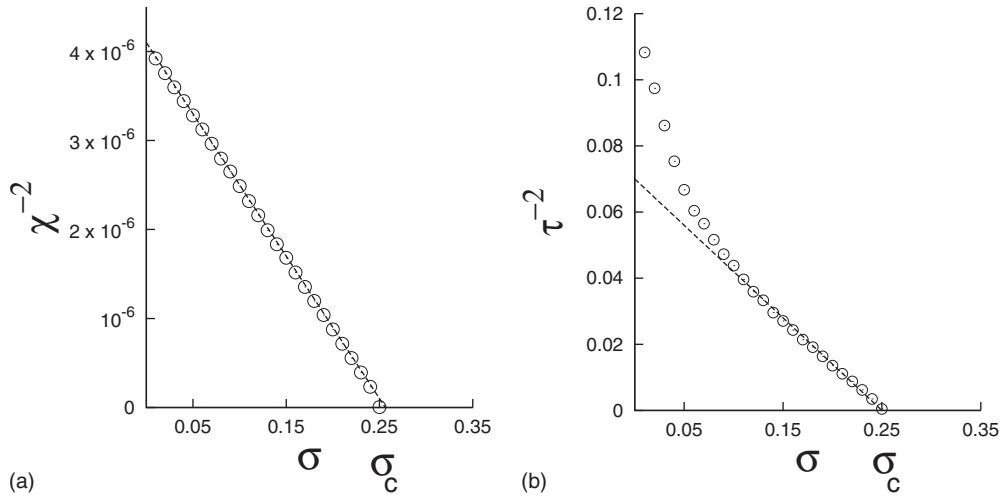

FIG. 56. Variation of χ^{-2} and τ^{-2} with applied stress for a bundle having $N=50\,000$ fibers. Uniform distribution of fiber thresholds is considered and averages are taken over 1000 samples. The dotted straight lines are the best linear fits near the critical point.

$$\sigma_0(t)[1 - P_t(x(t))]x(t), \tag{300}$$

where $P_t(t)=\int_0^t p_t(t')dt'$ is the cumulative instantaneous breaking threshold probability, is generalized to

$$\sigma_0(t) = \left[1 - P_s\left(a\int_0^t e^{-(t-t')/\tau}x(t')^\gamma\, dt'\right)\right] \times[1 - P_t(x(t))]x(t), \tag{301}$$

where $P_s(s)=\int_0^s p_s(s')ds'$. Kun *et al.* (2007) showed that the Basquin law (297) may be derived analytically from Eq. (301) leading to $\alpha'=\gamma$. The solid curves in Fig. 54 are fits of the theoretical curves based on Eq. (301) to the experimental data for the ϵ vs N_{cycle}. Likewise, Fig. 55 shows the fit of the theoretical N_f vs σ_0/σ_c to the experimental data. For this fit, $\gamma=2.0$ and $\tau=15\,000$.

B. Precursors of global failure

There is a fundamental question in strength considerations of materials: when does the material fail? Are there signals that can warn of imminent failure? This is of uttermost importance in, e.g., the diamond mining industry where sudden failure of the mine can be extremely costly in terms of lives. These mines are under continuous acoustic surveillance, but at present there is no tell-tale acoustic signature of imminent catastrophic failure. The same type of question is of course also central to earthquake prediction and initiates the search for precursors of global (catastrophic) failure events [see, e.g., Sahimi and Arbabi (1992, 1996) and Pradhan and Chakrabarti (2005, 2006)]. The precursor parameters essentially reflect the growing correlations within a dynamic system as it approaches the failure point. As we show, sometimes it is possible to predict the global failure points in advance. It is needless to mention that the existence of any such precursors and detailed knowledge about their behavior for major catastrophic failures, such as earthquakes, landslides, and mine or bridge collapses, would be of supreme value for our civilization. In this section we discuss some precursors of global failure in ELS models. We also comment on how one can predict the critical point (global failure point) from the precursor parameters.

1. Divergence of susceptibility and relaxation time

As discussed earlier (Sec. III.A) in the case of ELS fiber bundles the susceptibility (χ) and the relaxation time (τ) follow power laws (exponent $=-1/2$) with external stress and both diverge at the critical stress. Therefore, if we plot χ^{-2} and τ^{-2} with external stress, we expect a linear fit near the critical point, and the straight lines should touch the X axis at the critical stress. We indeed found similar behavior (Fig. 56) in simulation experiments after taking averages over many samples.

For applications, it is always important that such a prediction can be made on a single sample. For a single bundle having a very large number of fibers, similar responses of χ and τ have been observed. The estimation (through extrapolation) of the failure point is also quite satisfactory (Fig. 57).

2. Pattern of breaking rate

When we apply load on a material body, it is important to know whether the body can support that load or not. A similar question can be asked in the fiber bundle model. We found that if we record the breaking rate, i.e., the amount of failure in each load redistribution, then the pattern of the breaking rate clearly shows whether the bundle is going to fail or not. For any stress below the critical state, the breaking rate follows exponential decay (Fig. 58) with the step of load redistribution and for stress values above critical stress it is a power law followed by a gradual rise (Fig. 58). Clearly, at critical stress it follows a robust power law with an exponent value –2 that can be obtained analytically from Eq. (20). As we can see from Fig. 59, when the applied stress value is above the critical stress, the breaking rate initially goes down with step number, then at some point it

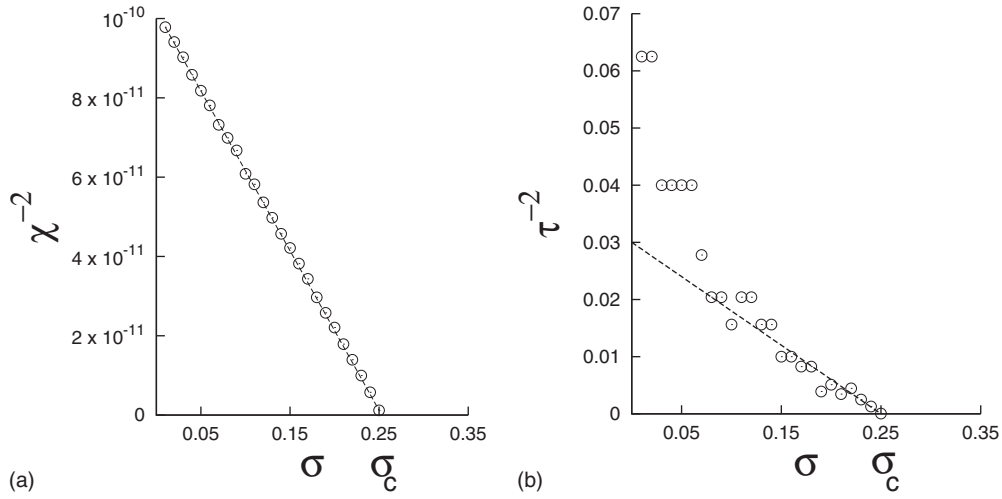

FIG. 57. Variation of χ^{-2} and τ^{-2} with applied stress for a single bundle having $N=10\,000\,000$ fibers with uniform distribution of fiber thresholds. Straight lines represent the best linear fits near the critical point.

starts going up and continues until the complete breakdown. That means if the breaking rate changes from a downward to an upward trend, the bundle will surely fail, but not immediately after the change occurs; it takes a few more steps and the number of these steps decreases as we apply larger external stress (above the critical value). Therefore if we can locate this minimum in the breaking-rate pattern, we can save the system (bundle) from breaking down by withdrawing the applied load immediately. We have another important question here: is there any relation between the breaking-rate minimum and the failure time (time to collapse) of the bundle? There is indeed a universal relationship, which has been explored recently (Pradhan and Hemmer, 2009) through numerical and analytical studies: for a slightly overloaded bundle we can rewrite Eq. (81) as

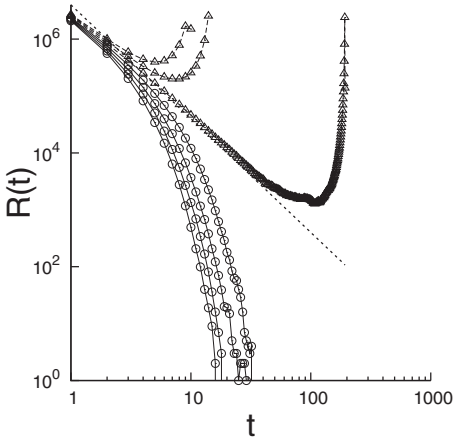

FIG. 58. Log-log plot of breaking rate with step of load redistribution for seven different stress values. Circles are for stresses below the critical stress and triangles are for stresses above the critical stress. The simulation has been performed for a single bundle with $N=10\,000\,000$ fibers having uniform distribution of fiber thresholds. The dotted straight line has a slope –2.

$$U_t = \frac{1}{2} - \sqrt{\epsilon}\tan(A^*t - B^*), \tag{302}$$

where

$$A^* = \tan^{-1}(2\sqrt{\epsilon}) \quad \text{and} \quad B^* = \tan^{-1}(1/2\sqrt{\epsilon}). \tag{303}$$

From Eq. (302) follows the breaking rate

$$R(t) = -\frac{dU_t}{dt} = \sqrt{\epsilon}A^*\cos^{-2}(A^*t - B^*). \tag{304}$$

$R(t)$ has a minimum when

$$0 = \frac{dR}{dt} \propto \sin(2A^*t - 2B^*), \tag{305}$$

which corresponds to

$$t_0 = \frac{B^*}{A^*}. \tag{306}$$

When criticality is approached, i.e., when $\epsilon \to 0$, we have $A^* \to 0$ and thus $t_0 \to \infty$ as expected.

We see from Eq. (302) that $U_t=0$ for

$$t_f = [B^* + \tan^{-1}(1/2\sqrt{\epsilon})]/A^* = 2B^*/A^*. \tag{307}$$

This is an excellent approximation to the integer value at which the fiber bundle collapses completely. Thus with good approximation we have the simple connection $t_f=2t_0$. When the breaking rate starts increasing we are halfway (see Fig. 59) to complete collapse.

3. Crossover signature in avalanche distribution

The bursts or avalanches can be recorded from outside, without disturbing the ongoing failure process. Therefore, any signature in burst statistics that can warn of imminent system failure would be useful in the sense of wide scope of applicability. As discussed in Sec. III.B, when the avalanches are recorded close to the global failure point, the distribution shows (Fig. 60) a different power law ($\xi=3/2$) than the one ($\xi=5/2$) characterizing

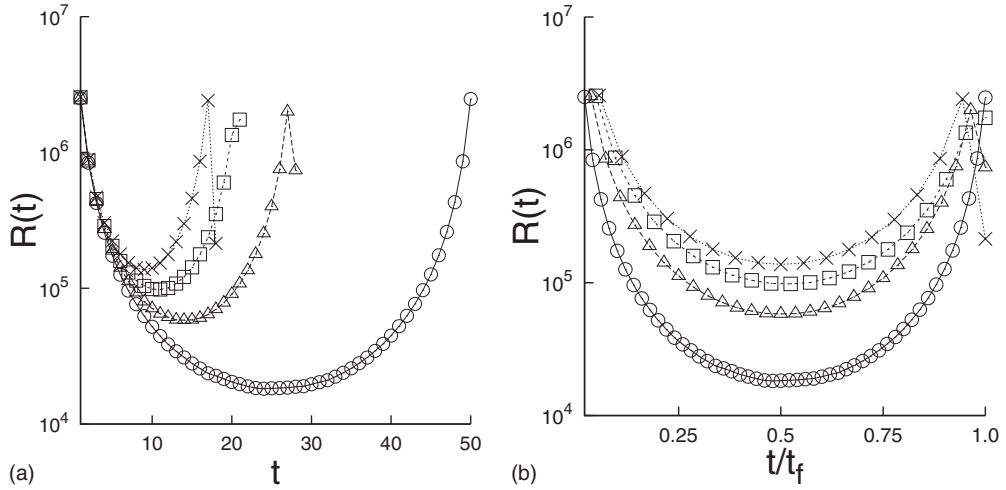

FIG. 59. The breaking rate $R(t)$ vs step t (upper plot) and vs the rescaled step variable t/t_f (lower plot) for the uniform threshold distribution for a bundle of $N=10^7$ fibers. Different symbols are used for different excess stress levels $\sigma-\sigma_c$: 0.001 (circles), 0.003 (triangles), 0.005 (squares), and 0.007 (crosses).

the size distribution of all avalanches. This crossover behavior has been analyzed analytically in the case of the ELS fiber bundle model and similar crossover behavior is also seen (Pradhan, Hansen, and Hemmer, 2006) in the burst distribution and energy distribution of the fuse model, which is an established model for studying fracture and breakdown phenomena in disordered systems. The crossover length becomes larger and larger as the failure point is approached and it diverges at the failure point [Eq. (192)]. In some sense, the magnitude of the crossover length tells us how far the system is from the global failure point. Most important is that this crossover signal does not hinge on observing rare events and is seen also in a single system (see Fig. 19). Therefore, such a crossover signature has a strong potential to be a useful detection tool. It should be mentioned that a recent observation (Kawamura, 2006) suggested a clear change in exponent values of the local magnitude distributions of earthquakes in Japan before the onset of a mainshock (Fig. 61). This observation has definitely strengthened the possibility of using crossover signals in burst statistics as a criterion for imminent failure.

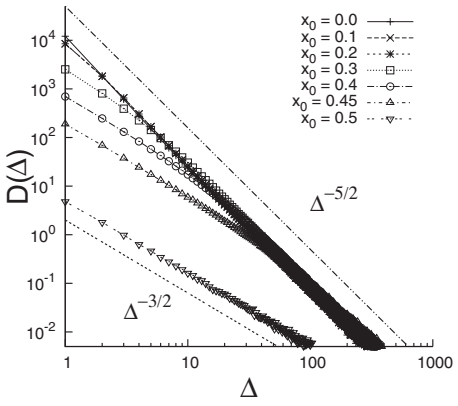

FIG. 60. The avalanche size distributions for different values of x_0 in the ELS model with uniform fiber strength distribution. Here bundle size $N=50\,000$ and averages are taken over 10 000 samples. Two power laws (dotted lines) have been drawn as reference lines to compare the numerical results.

C. Fiber-reinforced composites

As we have seen, fiber bundle models provide a fertile ground for studying a wide range of breakdown phenomena. In some sense, they correspond to the Ising model in the study of magnetism. In this section, we review how the fiber bundle models are generalized to describe composites containing fibers. Such composites are of increasing practical importance (see, e.g., Fig. 62).

The status of modeling fiber-reinforced composites has recently been reviewed (Mishnaevsky, 2007; Mishnaevsky and Brøndsted, 2009). These materials consist of fibers embedded in a matrix. During tensile loading the main part of the load is carried by the fibers and the strength of the composite is governed to a large extent by the strength of the fibers themselves. The matrix material is chosen so that its yield threshold is lower than

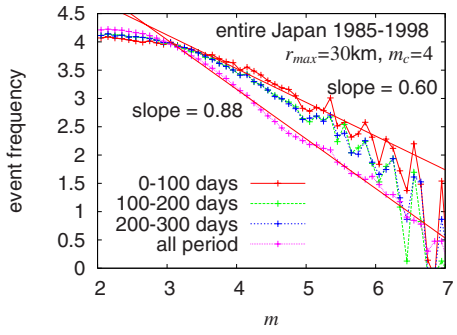

FIG. 61. (Color online) Crossover signature in the local magnitude distributions of earthquakes in Japan. The exponent of the distribution during 100 days before a mainshock is about 0.60; much smaller than the average value of 0.88. From Kawamura, 2006.

FIG. 62. (Color online) This dental bridge is made from a fiber-reinforced composite with braided fibers made from polyethylene. Due to the braided structure, this composite is four times tougher than a composite made from the same materials but without the braiding (Karbhari and Strassler, 2007). Courtesy of H. Strassler, University of Maryland Dental School and V. Karbhari, University of Alabama, Huntsville.

that of the fibers which are embedded in it. Common materials used for the fibers are aluminum, aluminum oxide, aluminum silica, asbestos, beryllium, beryllium carbide, beryllium oxide, carbon (graphite), glass (E glass, S glass, and D glass), molybdenum, polyamide (aromatic polyamide, aramid), Kevlar 29 and Kevlar 49, polyester, quartz (fused silica), steel, tantalum, titanium, tungsten, or tungsten monocarbide. Most matrix materials are resins as a result of their wide variation in properties and relatively low cost. Common resin materials are epoxy, phenolic, polyester, polyurethane, and vinyl ester. When the composite is to be used under adverse conditions such as high temperature, metallic matrix materials such as aluminum, copper, lead, magnesium, nickel, silver, or titanium or nonmetallic matrix materials such as ceramics may be used. When the matrix material is brittle, cracks open up in the matrix perpendicular to the fiber direction at roughly equal spacing. In metallic matrix materials, plasticity sets in at sufficient load. Lastly, in polymer matrix composites, the matrix typically responds linearly, but the fibers still carry most of the load due to the large compliance of the matrix. When a fiber fails, the forces it carried are redistributed among the surviving fibers and the matrix. If the matrix-fiber interface is weak compared to the strength of the fibers and the matrix itself, fractures develop along the fibers. When the matrix is brittle, the fibers bridging the developing crack in the matrix will, besides binding the crack together, lead to stress alleviation at the matrix crack front. Thus, the energy necessary to propagate a crack further increases with the length of the crack (Sørensen and Jacobsen, 1998, 2000), i.e., so-called *R-curve behavior* (Lawn, 1993). When the bridging fibers fail, they typically do so through debonding at the fiber-matrix interface. This is followed by pull out (see Fig. 63).

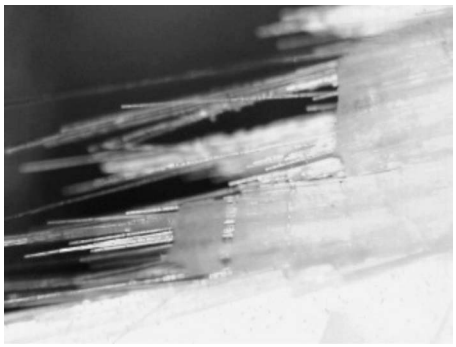

FIG. 63. Postmortem micrograph showing a fiber-reinforced composite where the matrix has undergone brittle failure followed by failure of the bridging fibers through debonding. From Karbhari and Strassler, 2007.

The Cox shear lag model forms the basis for the standard tools used for analyzing breakdown in fiber-reinforced composites (Cox, 1952; Chou, 1992). It considers the elastic response of a single fiber in a homegeous matrix only capable of transmitting shear stresses. By treating the properties of the matrix as effective and due to the self-consistent response by the matrix material and the rest of the fibers, the Cox model becomes a mean-field model (Räisänen *et al.*, 1997). Extensions of the Cox single-fiber model to debonding and slip at the fiber-matrix interface have been published (Aveston and Kelly, 1973; Budiansky *et al.*, 1986; Hsueh, 1990, 1992). In 1961 the single-fiber calculation of Cox was extended to two-dimensional unidirectional fibers in a compliant matrix, i.e., a matrix incapable of carrying tensile stress, by Hedgepeth (1961). In 1967, this calculation was followed up by Hedgepeth and Dyke (1967) for three-dimensional unidirectional fibers placed in a square or hexagonal pattern. They found the average stress intensity factor (i.e., the ratio between local stress in an intact fiber and the applied stress) to be

$$K_k = \prod_{i=1}^{k} \frac{2i+2}{2i+1} \tag{308}$$

after failure of k fibers. Fichter (1969) extended these calculations to aligned arrays of broken fibers mixed with intact fibers. This approach was subsequently generalized to systems where the matrix has a nonzero stiffness and hence is able to transmit stress (Beyerlein and Landis, 1999; Landis and McMeeking, 1999). Viscoelasticity of the matrix has been included by Lagoudas *et al.* (1989) and Beyerlein and Phoenix (1998).

Curtin (1991) demonstrated that when the fibers respond under global load-sharing conditions, a mean-field theory may be constructed where the breakdown of the composite is reduced to that of the failure of a single fiber in an effective matrix (Curtin, 1993; Hild *et al.*, 1994; Hild and Feillard, 1997; Roux and Hild, 2002). Wagner and Eitan (1993) studied the redistribution of forces onto the neighbors of a single failing fiber within

a two-dimensional unidirectional composite using the shear-lag model, finding that within this scheme the stress enhancement is less pronounced than earlier calculations had shown. Zhou and Wagner (1999, 2000) introduced a multifiber failure model including debonding and frictional effects at the fiber-matrix interface, finding that the stress intensity factor decreased with increasing interfiber distance. An important calculational principle, the *break influence superposition technique*, was introduced by Sastry and Phoenix (1993) based on the method of Kachanov (1985) in order to handle models with multiple fiber failures. The technique consists in determining the transmission factors, which give the load at a given position along a given fiber due to a unit negative load at the single break point in the fiber bundle. The multiple failure case is then constructed through superposition of these single-failure transmission factors. This method has proven efficient from a numerical point of view and has been later generalized [see Beyerlein *et al.* (1996), Beyerlein and Phoenix (1997a, 1997b), Landis *et al.* (2000), and Li *et al.* (2006)].

Ibnabdeljalil and Curtin (1997a, 1997b), Curtin (1998), Xia and Curtin (2001), and Xia *et al.* (2002) analyzed the interaction between multiple breaks in unidirectional fibers embedded in a matrix using a lattice Green's function technique (Zhou and Curtin, 1995) to calculate the load transfer from broken to unbroken fibers including fiber-matrix sliding with a constant interfacial shear resistance τ, given either by a debonded sliding interface or by matrix shear yielding. The differential load-carrying capacity of the matrix is assumed to be negligible. In the following we describe the Zhou-Curtin approach in some detail. The load-bearing fibers have a strength distribution given by the cumulative probability

$$P(\sigma,L) = 1 - e^{-\phi(\sigma,L)} \tag{309}$$

of failure over a length of fiber L experiencing a stress σ, where

$$\phi(\sigma,L) = \frac{L}{L_0}\left(\frac{\sigma}{\sigma_0}\right)^{\rho}, \tag{310}$$

and ρ is the Weibull index. When a fiber breaks, the load is transferred to the unbroken fibers. We return to the details henceforth. The newly broken fiber slides relative to the matrix. The shear resistance τ provides an average axial fiber stress along the single broken fiber,

$$\sigma(z) = \min\left(\frac{2\tau z}{r}, \sigma^0(z)\right) \equiv p(z), \tag{311}$$

at a distance z from the break, where r is the radius of the fibers and $\sigma^0(z)$ is the axial fiber stress prior to the failure at point z. This defines a length scale

$$l_s = \frac{r\sigma^0(l_s)}{2\tau}. \tag{312}$$

The total stress change within a distance $\pm l_s$ of the break is distributed to the other fibers. A key assumption in what now follows is that the total stress in each plane z is conserved: the stress difference $\sigma^0(z)-\sigma(z)$ is distributed among the other intact fibers at the same z level.

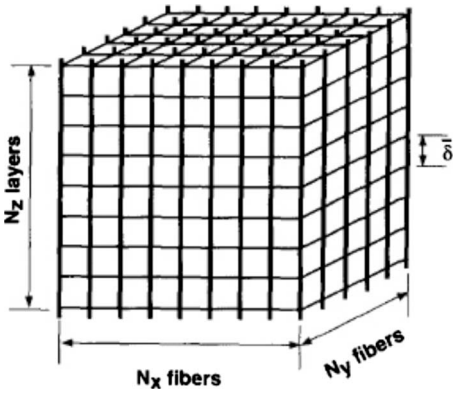

FIG. 64. The discretization of a three-dimensional unidirectional fiber-reinforced composite used by Zhou and Curtin (1995).

In order to set up the lattice Green's function approach, the system must be discretized. Each fiber, oriented in the z direction, of length L_z is divided into N_z elements of length $\bar{\delta}=L_z/N_z$. The fibers are arranged on the nodes of a square lattice in the x-y plane so that there is a total of $N_f=N_x\times N_y$ fibers. The lattice constants in the x and y directions are a_x and a_y, respectively. Each fiber is labeled by n where $1\leqslant n\leqslant N_f$. This is shown in Fig. 64. The stress on fiber n in layer m along the z direction is given by $\sigma_{n,m}$. Fiber n at layer m may be intact. It then acts as a Hookean spring with spring constant k_t responding to the stress $\sigma_{n,m}$. If fiber n has broken at layer m, it carries a stress equal to zero. The third possibility is that fiber n has broken elsewhere at m' and layer m is within the slip zone. It then carries a stress

$$\sigma_{n,m} = \min\left(\frac{2\tau\bar{\delta}}{r}|m-m'|, \sigma^0_{n,m}\right) \equiv p_{n,m}, \tag{313}$$

which is the discretization of Eq. (311) with zero spring constant.

Each element m of fiber n has two end nodes associated with it. At all such nodes, springs parallel to the x-y plane are placed linking fiber n with its nearest neighbors. These springs have spring constant k_s. The displacement of the nodes is assumed confined to the z direction only. Zhou and Curtin denoted the displacement of node connecting element m with element $m+1$ of fiber n, $u^+_{n,m}$, and the displacement of node linking element m with element $m-1$ of fiber n, $u^-_{n,m}$. The force on element m of fiber n from element m of fiber $n+1$ is

$$f_m(n;n+1) = k_s(u^+_{n+1,m} - u^+_{n,m}) + k_s(u^-_{n+1,m} - u^-_{n,m}). \tag{314}$$

The reader should compare the following discussion with that presented in Sec. IV.C. We now assume that it is only layer $m=0$ that carries any damaged or slipped

elements; the rest of the layers $m \neq 0$ are perfect. Let $\mathbf{u} = \{u^{\pm}_{n,m}\}$. If a force $\mathbf{f} = \{f^{\pm}_{n,m}\}$ is applied to the nodes, the response is

$$\mathbf{u} = \mathbf{G}\mathbf{f}, \tag{315}$$

where $\mathbf{G}$ is the lattice Green's function. Given the displacements from solving this equation combined with Eq. (314), the force carried by each broken element is found. The inverse of the lattice Green's function is $\mathbf{D} = \mathbf{G}^{-1}$. The elements of $\mathbf{D}$ are either zero, k_s or k_t, reflecting the status of the springs: undamaged, slipping, or broken. When there are no breaks in layer $m=0$, we define $\mathbf{D}^0 = (\mathbf{G}^0)^{-1}$ and $\delta\mathbf{D} = \mathbf{D}^0 - \mathbf{D}$. Hence, $\delta\mathbf{D}$ plays a role somewhat similar to the matrix $\mathbf{K}$ defined in Eq. (252). By combining these definitions, Zhou and Curtin found

$$\mathbf{G} = (\mathbf{1} - \mathbf{G}^0\delta\mathbf{D})^{-1}\mathbf{G}^0. \tag{316}$$

The matrices $\mathbf{G}$ and $\mathbf{D}$ have dimension $N \times N$, where $N = N_x \times N_y \times N_z$. By appropriately labeling the rows and columns, the matrices $\mathbf{D}$ and $\mathbf{G}$ may be written

$$\mathbf{G} = \begin{pmatrix} G_{dd} & G_{dp} \\ G_{pd} & G_{pp} \end{pmatrix}, \tag{317}$$

where the $(2N_xN_y) \times (2N_xN_y)$ matrix G_{dd} couples elements within the layer $m=0$, where all the damage is located. The matrix G_{pp} couples elements within the rest of the layers. These are undamaged—"perfect." The two matrices G_{dp} and G_{pd} provide the cross couplings. The matrix $\delta\mathbf{D}$ becomes in this representation

$$\delta\mathbf{D} = \begin{pmatrix} \delta D_{dd} & 0 \\ 0 & 0 \end{pmatrix}. \tag{318}$$

Combination of this equation with Eq. (316) gives

$$G_{dd} = (I - \delta D_{dd})^{-1} G^0_{dd}, \tag{319}$$

where the intact Green's function G^0_{dd} may be found analytically by solving Eq. (315) for the intact lattice in Fourier space $\{\vec{q}\}$,

$$\mathbf{F}\mathbf{G}^0\mathbf{F}^{-1}(\vec{q}) = \frac{1}{4}\left[k_s \sin^2\left(\frac{q_x a_x}{2}\right) + k_s \sin^2\left(\frac{q_y a_y}{2}\right) + k_t \sin^2\left(\frac{q_z \bar{\delta}}{2}\right)\right]^{-1}. \tag{320}$$

Using that $f^+_{n,0} = -f^-n,0$, Zhou and Curtin found that

$$u^+_{n,0} - u^-_{n,0} = \sum_{n'} [G_{dd}(n'^+;n^+) - G_d d(n'^+;n^-)] f^+_{n',0}, \tag{321}$$

where n^+ and n^- refer to the upper and lower nodes, respectively, attached to element n is layer $m=0$. Before completing the model, the Weibull strength distribution [Eqs. (309) and (310)] must be discretized. Each element (n,m) is given a maximum sustainable load $s_{n,m}$ from the cumulative probability

$$P_f(s) = 1 - e^{-(s/\bar{\sigma})^{\rho}}, \tag{322}$$

where $\bar{\sigma} = (L_0/\bar{\delta})^{1/\rho}\sigma_0$.

The breakdown algorithm proceeds as follows:

(1) Apply a force per fiber set equal to the smallest breaking threshold, $f_0 = \min_{n,m} s_{n,m}$, to the system.

(2) Break the weakest fiber or fibers by setting their spring constants to zero.

(3) Decrease the stresses in the elements below and above the just broken fibers according to Eq. (313).

(4) Solve Eq. (319) for the layers in which the breaks occurred.

(5) Calculate the spring displacements in the layers where the breaks occurred using Eq. (321) and an effective applied force $f^+_{n,m} = f_0 - p_{n,m}$. The force on each intact spring in such a layer is then $\sigma_{n,m} = k_t(u^+_{n,m} - u^-_{n,m})$.

(6) With the new stresses, search for other springs that carry a force beyond their thresholds $s_{n,m}$. If such springs are found, break these and return to (2). Otherwise proceed.

(7) Search for the spring that is closest to its breaking threshold. This spring is the one with $\lambda = \min_{n,m}(s_{n,m}/f_{n,m})$. Increase the load by a factor $\lambda\eta$, where η is equal to or somewhat larger than unity. This factor is present to take into account the nonlinearities introduced in the system due to the slip of the fibers.

(8) Proceed until the system can no longer sustain a load.

By a change in the ratio k_t/k_s between the moduli of the springs in the discretized lattice, it is possible to go from fiber bundle behavior essentially evolving according to equal load sharing to local load sharing.

Whereas the computational cost of finite-element calculations on fiber-reinforced composites scales with the volume of the composite, the break influence superposition technique and the lattice Green's function technique scale with the number of fiber breaks in the sample. This translates into systems studied by the latter two techniques that can be orders of magnitude larger than the former (Ibnabdeljalil and Curtin, 1997a).

After this rather sketchy tour through the use of fiber bundle models as tools for describing the increasing important fiber-reinforced composite materials, we now turn to the use of fiber bundle models in nonmechanical settings.

D. Failure phenomena in networks, traffic, and earthquakes

The typical failure dynamics of the fiber bundle model captures quite faithfully the failure behavior of several multicomponent systems such as communication or traffic networks. As in the elastic networks considered here, as the local stress or load (transmission rate or traffic

currents) at any part of the network goes beyond the sustainable limit, that part of the system or the network fails or gets jammed and the excess load gets redistributed over the other intact parts. This, in turn, may induce further failure or jamming in the system. Because of the tectonic motions stresses develop at the crust–tectonic plate resting (contact) regions and the failure at any of these supports induces additional stresses elsewhere. Apart from the healing phenomena in geological faults, the fiber bundle models have built-in features to capture the earthquake dynamics. Naturally, the statistically established laws for earthquake dynamics can be easily recast into the forms derived here for the fiber bundle models.

We consider here in more detail specifically these three applications specifically.

1. Modeling network failures

The fiber bundle model has been applied (Kim *et al.*, 2005) to study the cascading failures of network structures, such as Erdös-Rényi (ER) networks (Erdös and Rényi, 1959) and Watts-Strogatz (WS) networks (Watts and Strogatz, 1994) to model the overloading failures in power grids, etc. Here the nodes or the individual power stations are modeled as fibers and the transmission links between these nodes are utilized to transfer the excess load (from one broken fiber or station to another).

The load transfer of broken fibers or nodes through the edges or links of the underlying network is governed by the LLS rule (Harlow and Phoenix, 1978; Phoenix, 1978b; Smith and Phoenix, 1981). Under a nonzero external load $N\sigma$, the actual stress σ_i of the intact fiber i is given by the sum of σ and the transferred load from neighboring broken fibers. The local load transfer, from broken fibers to intact fibers, depends on the load concentration factor $K_i \equiv \sigma_i/\sigma$ with $K_i = 1 + \Sigma_j' m_j/k_j$, where the primed summation is over the cluster of broken fibers directly connected to i, m_j is the number of broken fibers in the cluster j, and k_j is the number of intact fibers directly connected to j.

Let the external stress σ be increased by an infinitesimal amount $\delta\sigma$ starting from $\sigma=0$. Fibers for which the strength is less than $K_i\sigma$ break iteratively until no more fibers break. For each increment of σ, the size $s(\sigma)$ of the avalanche is defined as the number of broken fibers triggered by the increment. The surviving fraction $U(\sigma)$ of fibers can be written as

$$U(\sigma) = 1 - \frac{1}{N}\sum_{\sigma' < \sigma} s(\sigma'). \tag{323}$$

One can also measure directly the response function χ or the generalized susceptibility, denoted as

$$\chi(\sigma) = \left|\frac{dU}{d\sigma}\right|. \tag{324}$$

The critical value σ_c of the external load can be defined from the condition of the global breakdown $U(\sigma_c)=0$.

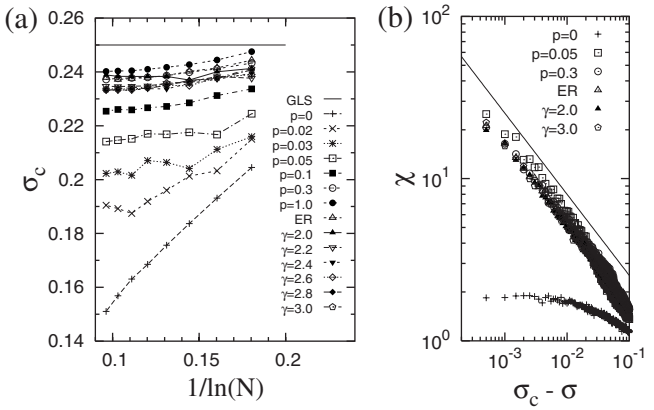

FIG. 65. Fiber bundle model on networks: (a) The system size (N) dependence of critical points (σ_c) for various networks with $N=2^8, 2^9, \ldots, 2^{15}$ vertices. (b) The susceptibility for the networks with $N=2^{14}$. p and γ are the rewiring probability in the WS networks and the exponent of degree distribution $P(k) \sim k^{-\gamma}$, respectively. The data points are obtained from the averages over 10^4 (10^3 for $N=2^{15}$) ensembles. From Kim *et al.*, 2005.

The critical value σ_c and the susceptibility χ have been calculated numerically for the model under the LLS rule on various network structures, such as the local regular network, the WS network, the ER network, and scale-free networks (Fig. 65). The results suggest that the critical behavior of the model on complex networks is completely different from that on a regular lattice. More specifically, while σ_c for the FBM on a local regular network vanishes in the thermodynamic limit and is described by $\sigma_c \sim 1/\ln(N)$ for finite-sized systems (see the curve for $p=0$ in Fig. 65, corresponding to the WS network with the rewiring probability $p=0$), σ_c for all networks except for the local regular one does not diminish but converges to a nonzero value as N is increased. Moreover, the susceptibility diverges at the critical point as $\chi \sim (\sigma_c - \sigma)^{-1/2}$, regardless of the networks, which is again in sharp contrast to the local regular network [see Fig. 65(b)]. The critical exponent $1/2$ clearly indicates that the FBM under the LLS rule on complex networks belongs to the same universality class as that of the ELS regime (Pradhan *et al.*, 2002) although the load-sharing rule is strictly local. The observed variation for σ_c is only natural for the LLS model. In LLS model if n successive fibers fail (each with a finite probability ρ_f), then the total probability of such an event is $N\rho_f^n(1-\rho_f)^2$ as the probability is proportional to the bundle size N. If this probability is finite, then $n \sim \ln N$ (for any finite ρ_f, the failure probability of any fiber in the bundle). For a failure of n successive fibers, the neighboring intact fibers get the transferred load $\sim n\sigma$, which, if it becomes greater than or equal to their strength, surely fails giving $\sigma_c \sim 1/n \sim 1/\ln N$ (see Sec. IV.A).

The evidence that the LLS model on complex networks belongs to the universality class of the ELS model is also found (Kim *et al.*, 2005) in the avalanche size distribution $D(\Delta)$: the unanimously observed power-law

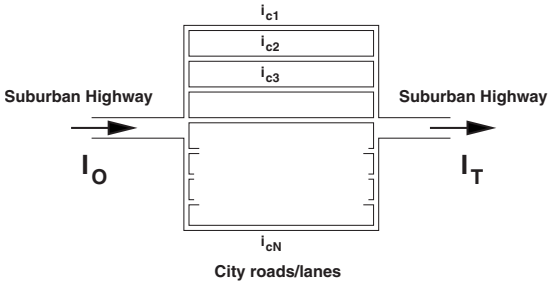

FIG. 66. The highway traffic current I_O gets fragmented into uniform currents i in each of the narrower roads and the roads having threshold current $i_{c_n} \leq i$ get congested or blocked. This results in extra load for the uncongested roads. We assume that this extra load per uncongested roads gets equally redistributed and gets added to the existing load, causing further blocking of some more roads.

behavior $D(\Delta) \sim \Delta^{-5/2}$ for all networks except for the local regular one (the WS network with $p=0$) is in perfect agreement with the behavior for the ELS case (Hemmer and Hansen, 1992). On the other hand, the LLS model for a regular lattice has been shown to exhibit completely different avalanche size distribution (Hemmer and Hansen, 1994b; Kloster *et al.*, 1997). Also, one can observe a clear difference in terms of the failure probability $F(\sigma)$ defined as the probability of failure of the whole system at an external stress σ. While $F(\sigma)$ values for LLS on complex networks fall on a common line, LLS on a regular network shows a distinctly different trend (Kim *et al.*, 2005) [see also Divakaran and Dutta (2007c)].

2. Modeling traffic jams

One can apply the equal-load-sharing fiber bundle model to study the traffic failure in a parallel road network in a city. For some special distributions, such as the uniform distribution, of traffic handling capacities (thresholds) of the roads, the critical behavior of the jamming transition can be studied analytically. This, in fact, is exactly comparable with the asymmetric simple exclusion process in a single channel or road (Chakrabarti, 2006).

Traffic jams or congestion occur essentially due to the excluded volume effects (among the vehicles) in a single road and due to the cooperative (traffic) load sharing by the (free) lanes or roads in multiply connected road networks [see, e.g., da Silveira (1999) and Chowdhury *et al.* (2000)]. Using FBM for the traffic network, it has been shown (Chakrabarti, 2006) that the generic equation for the approach of the jamming transition in FBM corresponds to that for the asymmetric simple exclusion processes (ASEPs) leading to transport failure transition in a single channel or lane [see, e.g., Stinchcombe (2005)].

Let the suburban highway traffic, on entering the city, get fragmented equally through the various narrower streets within the city and become combined again outside the city (see Fig. 66). If I_O denotes the input traffic current and I_T is the total output traffic current, then at the steady state, without any global traffic jam, $I_T=I_O$. If I_T falls below I_O, a global jam starts, and soon I_T drops to zero. This occurs if $I_O > I_c$, the critical traffic current of the network, beyond which a global traffic jam occurs. Let the parallel roads within the city have different thresholds for traffic handling capacity: $i_{c_1}, i_{c_2}, \ldots, i_{c_N}$ for the N different roads (the nth road gets jammed if the traffic current i per road exceeds i_{c_n}). Initially $i=I_O/N$ and increases as some of the roads get jammed and the same traffic load I_O has to be shared equally by a lower number of unjammed roads. Next, we assume that the distribution $p(i_c)$ of these thresholds is uniform up to a maximum threshold current (corresponding to the widest road traffic current capacity), which is normalized to unity (sets the scale for I_c).

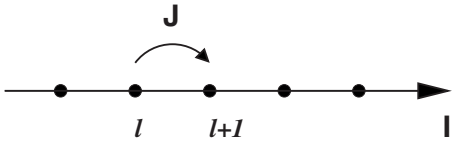

FIG. 67. The transport current I in the one-dimensional lane or road is possible if, say, the lth site is occupied and the $(l+1)$th site is vacant. The intersite hopping probability is indicated by J.

The jamming dynamics in this model starts from the nth road (say, in the morning) when the traffic load i per city roads exceeds the threshold i_{c_n} of that road. Due to this jam, the total number of uncongested roads decreases and the rest of these roads have to bear the entire traffic load in the system. Hence the effective traffic load or stress on the uncongested roads increases and this compels some more roads to get jammed. These two sequential operations, namely, the stress or traffic load redistribution and further failure in service of roads, continue until an equilibrium is reached, where either the surviving roads are strong (wide) enough to share equally and carry the entire traffic load on the system (for $I_O < I_c$) or all the roads fail (for $I_O \geq I_c$) and a (global) traffic jam occurs in the entire road network system.

This jamming dynamics can be represented by recursion relations in discrete time steps. Let $U_t(i)$ be the fraction of uncongested roads in the network that survive after (discrete) time step t, counted from the time $t=0$ when the load (at the level $I_O=iN$) is put in the system (time step indicates the number of stress redistributions). As such, $U_t(i=0)=1$ for all t and $U_t(i)=1$ for $t=0$ for any i; $U_t(i)=U^*(i)\neq 0$ for $t\to\infty$ if $I_O<I_c$, and $U_t(i)=0$ for $t\to\infty$ if $I_O>I_c$.

Here $U_t(i)$ follows a simple recursion relation

$$U_{t+1} = 1 - i_t, \quad i_t = \frac{I_O}{U_t N}$$

$$\text{or } U_{t+1} = 1 - \frac{i}{U_t}. \tag{325}$$

The critical behavior of this model remains the same as discussed in Sec. III.A in terms of i and the exponent

values remain unchanged: $\alpha=1/2=\beta=\theta$, $\eta=1$ for all these equal (traffic) load-sharing models.

In the simplest version of the asymmetric simple exclusion process transport in a chain (see Fig. 67), the transport corresponds to movement of vehicles, which is possible only when a vehicle at site l, say, moves to the vacant site $l+1$. The transport current I is then given by (Stinchcombe, 2005)

$$I = J\rho_l'(1-\rho_{l+1}'), \tag{326}$$

where ρ_l' denotes the site occupation density at site l, and J denotes the intersite hopping probability. The above equation can be easily recast in the form

$$\rho_{l+1}' = 1 - \frac{\sigma}{\rho_l'}, \tag{327}$$

where $\sigma=I/J$. Formally it is the same as the recursion relation for the density of uncongested roads in the FBM model discussed above; the site index here in the ASEP plays the role of time index in FBM. Such exact correspondence indicates identical critical behavior in both the cases. The same universality for different cases (different threshold distributions) in FBM suggests similar behavior for other equivalent ASEP cases as well (Bhattacharjee, 2007). For extension of the model to scale-free traffic networks, see Zheng *et al.* (2008).

3. Modeling earthquake dynamics

The Earth's outer crust, several tens of kilometers in thickness, rests on tectonic shells. Due to the high temperature-pressure phase changes and consequent ionizations of the metallic ores, powerful magnetohydrodynamic convective flows occur in the Earth's mantle at several hundreds of kilometers in depth. The tectonic shells, divided into about ten mobile plates, have relative velocities of the order of a few centimeters per year [see, e.g., Scholz (2002)]. The stresses developed at the interfaces between the crust and the tectonic shells during the (long) *sticking* periods get released during the (very short) *slips*, causing the releases of the stored elastic energies (at the fault asperities) and consequent earthquakes.

Two well-known phenomenologically established laws governing the earthquake statistics are (a) the Gutenberg-Richter law

$$\mathcal{N}(E) \sim E^{-\xi'}, \tag{328}$$

relating the number density ($\mathcal{N}$) of earthquakes with the released energy greater than or equal to E, and (b) the Omori law

$$d(\tilde{\mathcal{N}}(t))/dt = 1/t^{\eta'}, \tag{329}$$

where $\tilde{\mathcal{N}}$ denotes the number of aftershocks having magnitude or released energy larger than a preassigned small but otherwise arbitrary threshold value.

As mentioned, because of the tectonic motions, stresses develop at the crust–tectonic plate contact regions and the entire load is supported by such regions. Failure at any of these supports necessitates load redistributions and induces additional stresses elsewhere. In fact, the avalanche statistics discussed in Sec. III.B can easily explain the Gutenberg-Richter law [Eq. (328)] with the identification $\xi'=\xi-1$. Similarly, the decay of the number of failed fibers $N(t)=N(1-U_t)$ at the critical point, given by $N(t)\sim t^{-\eta}$ [see, e.g., Eq. (20)], crudely speaking, gives in turn the Omori law behavior [Eq. (329)] for the fiber bundle model, with the identification $\eta'=1+\eta$.

For some recent discussions on further studies along these lines, see, e.g., Moreno, Correig, *et al.* (2001) and Turcotte and Glassco (2004). The stick-slip motion in the Burridge-Knopoff model [see, e.g., Carlson *et al.* (1994)], where the blocks (representing a portion of the solid crust) connected with springs (representing the elastic strain developed due to tectonic motion) are pulled uniformly on a rough surface, has the same feature of stress redistribution as one or more blocks slip and the dynamics was mapped onto a ELS fiber bundle model by Sornette (1992). The power-law distributions of the fluctuation-driven bursts around the critical points have been interpreted as the above two statistical laws for earthquakes.

VI. SUMMARY AND CONCLUDING REMARKS

The fiber bundle model enjoys a rare double position in that it is both useful in a practical setting for describing a class of real materials under real working conditions and at the same time is abstract enough to function as a model for exploring fundamental breakdown mechanisms from a general point of view. Very few models are capable of such a double life. This means that a review of the fiber bundle model may take on a very different character depending on the point of view. In this review we have emphasized the fiber bundle model as a model for exploring fundamental breakdown mechanisms.

Failure in loaded disordered materials is a collective phenomenon. It proceeds through a competition between disorder and stress distribution. The disorder implies a distribution of local strength. If the stress distribution were uniform in the material, it would be the weakest spot that would fail first. Suppose now that there has been a local failure at a given spot in the material. The further away we go from this failed region, the weaker the weakest region within this distance will be. Hence, the disorder makes local failures repel each other: they will occur as far as possible from each other. However, as the material fails locally, the stresses are redistributed. This redistribution creates hot spots where local failure is likely due to high stresses. Since these hot spots occur at the boundaries of the failed regions, the effect of the stress field is an attraction between the local failures (Roux and Hansen, 1990). Hence, disorder and stress have opposite effects on the breakdown process, repulsion versus attraction, and this leads to competition between them. Since the disorder in the strength of the material, leading to repulsion, diminishes throughout

the breakdown process, whereas the stresses create increasingly important hot spots, it is the stress distribution that ends up dominating toward the end of the process.

The fiber bundle model catches this essential aspect of the failure process. Depending on the load redistribution mechanism, the quantitative aspects change. However, qualitatively it remains the same. In the ELS case, there are no *localized* hot spots; all surviving fibers are loaded the same way. Geometry does not enter into the redistribution of forces, and we may say that the "hot spots" include all surviving fibers. This aspect gives the ELS fiber bundle model its mean-field character, even though all other fluctuations are present, such as those giving rise to bursts.

As shown in Sec. III, the lack of geometrical aspects in the redistribution of forces in the ELS model enables us to construct the recursion relations [e.g., Eq. (8)], which capture well the failure dynamics. We find that the eventual statistics, governed by the fixed points for $\sigma < \sigma_c$, the average strength of the bundle, essentially shows a normal critical behavior: order parameter $O \sim (\sigma_c - \sigma)^{\alpha}$, breakdown susceptibility $\chi \sim (\sigma_c - \sigma)^{-\beta}$, and relaxation time $\tau = \kappa |\sigma_c - \sigma|^{-\theta}$ with $\alpha = 1/2 = \beta = \theta$ and $\kappa_- / \kappa_+ = \ln N / 2\pi$ for a bundle of N fibers, where the subscripts + and − refer to postcritical and precritical cases, respectively. The statistics of fluctuations over these average behaviors is given by the avalanche size distributions $D(\Delta) \sim \Delta^{-\xi}$ with $\xi = 3$ for discrete load increment and $=5/2$ for quasistatic load increment in such ElS cases. The critical stress σ_c of the bundle is of course nonuniversal and its magnitude depends on the fiber strength distribution.

For the LLS model, we essentially find (see Sec. IV.A) the critical strength of the fiber bundle $\sigma_c \sim 1/\ln N$, which vanishes in the macroscopic system size limit. The avalanche size distribution is exponential for such cases. For range-dependent redistribution of load (see Sec. IV.B) one recovers the finite value of σ_c and the ELS-like mean-field behavior for its failure statistics.

Extensions of the model to capture creep and fatigue behavior of composite materials are discussed in Sec. V.A Precursors of global failure are discussed in Sec. V.B. It appears that detailed knowledge of the critical behavior of the model can help precise determination of the global failure point from the well-defined precursors. Section V.C provides a rather cursory review of models of fiber-reinforced composites. These models go far beyond the simple fiber bundle model in complexity and represent the state of the art of theoretical approaches to this important class of materials. However, as complicated as these models are, the philosophy of the fiber bundle model is still very much present. Finally, we discussed a few extensions of the model to failures in communication networks, traffic jams, and earthquakes in Sec. V.D

As discussed here in detail, the fiber bundle model not only gives an elegant and profound solution of the dynamic critical phenomena of failures in disordered systems, with the associated universality classes, etc., but also offers the first solution to the entire linear and nonlinear stress-strain behaviors for any material up to its fracture or rupture point. Although the model was introduced at about the same time (1926) as the Ising model for static critical phenomena, it is only now that the full (mean-field) critical dynamics in the fiber bundle model is solved. Apart from these, as discussed, several aspects of the fluctuations in this model are now well understood. Even from this specific point of view, the model is not only intuitively very attractive, its behavior is extremely rich and intriguing. It would be surprising if it did not offer new profound insight into failure phenomena in the future also.

ACKNOWLEDGMENTS

We thank P. Bhattacharyya and P. C. Hemmer for important collaborations at different parts of this work. We acknowledge the financial support from Norwegian Research Council through Grant No. NFR 177958/V30. S.P. thanks SINTEF Petroleum Research for providing partial financial help and moral support toward this work.

REFERENCES

Aharony, A., 1976, in *Phase Transition and Critical Phenomena*, edited by C. Domb and M. Green (Academic, New York), Vol. 17, p. 357.
Alava, M. J., P. K. V. V. Nukala, and S. Zapperi, 2006, Adv. Phys. **55**, 349.
Andersen, J. V., D. Sornette, and K. Leung, 1997, Phys. Rev. Lett. **78**, 2140.
Aveston, J., and A. Kelly, 1973, J. Mater. Sci. **8**, 352.
Bak, P., C. Tang, and K. Wiesenfeld, 1987, Phys. Rev. Lett. **59**, 381.
Banerjee, R., and B. K. Chakrabarti, 2001, Bull. Mater. Sci. **24**, 161.
Batrouni, G. G., and A. Hansen, 1988, J. Stat. Phys. **52**, 747.
Batrouni, G. G., A. Hansen, and M. Nelkin, 1986, Phys. Rev. Lett. **57**, 1336.
Batrouni, G. G., A. Hansen, and J. Schmittbuhl, 2002, Phys. Rev. E **65**, 036126.
Bernardes, A. T., and J. G. Moreira, 1994, Phys. Rev. B **49**, 15035.
Beyerlein, I. J., and C. M. Landis, 1999, Mech. Mater. **31**, 331.
Beyerlein, I. J., and S. L. Phoenix, 1997a, Eng. Fract. Mech. **57**, 241.
Beyerlein, I. J., and S. L. Phoenix, 1997b, Eng. Fract. Mech. **57**, 267.
Beyerlein, I. J., and S. L. Phoenix, 1998, Int. J. Solids Struct. **35**, 3177.
Beyerlein, I. J., S. L. Phoenix, and A. M. Sastry, 1996, Int. J. Solids Struct. **33**, 2543.
Bhattacharjee, S. M., 2007, J. Phys. A: Math. Theor. **40**, 1703.
Bhattacharyya P., S. Pradhan, and B. K. Chakrabarti, 2003, Phys. Rev. E **67**, 046112.
Bonn D., H. Kellay, M. Prochnow, K. Ben-Djemiaa, and J. Meunier, 1998, Science **280**, 265.
Budiansky B., J. W. Hutchinson, and A. G. Evans, 1986, J. Mech. Phys. Solids **34**, 167.
Carlson J. M., J. S. Langer, and B. E. Shaw, 1994, Rev. Mod.

Phys. **66**, 657.
Chakrabarti, B. K., 1994, in *Nonlinearity and Breakdown in Soft Condensed Matter*, edited by K. K. Bardhan, B. K. Chakrabarti, and A. Hansen (Springer-Verlag, Heidelberg), p. 171.
Chakrabarti, B. K., 2006, Physica A **372**, 162.
Chakrabarti, B. K., and L. G. Benguigui, 1997, *Statistical Physics of Fracture and Breakdown in Disordered Systems* (Oxford University Press, Oxford).
Chou, T. W., 1992, *Microstructural Design of Fiber Reinforced Composites* (Cambridge University Press, Cambridge).
Chowdhury, D., L. Santen, and A. Schadschnider, 2000, Phys. Rep. **329**, 199.
Ciliberto, S., A. Guarino, and R. Scorretti, 2001, Physica D **158**, 83.
Coleman, B. D., 1956, J. Appl. Phys. **27**, 862.
Coleman, B. D., 1957a, J. Appl. Phys. **28**, 1058.
Coleman, B. D., 1957b, J. Appl. Phys. **28**, 1065.
Cox, H. L., 1952, Br. J. Appl. Phys. **3**, 72.
Curtin, W. A., 1991, J. Am. Ceram. Soc. **74**, 2837.
Curtin, W. A., 1993, J. Mech. Phys. Solids **41**, 217.
Curtin, W. A., 1998, Phys. Rev. Lett. **80**, 1445.
Curtin, W. A., and H. Scher, 1997, Phys. Rev. B **55**, 12038.
Daniels, H. E., 1945, Proc. R. Soc. London, Ser. A **183**, 405.
Daniels, H. E., 1989, Adv. Appl. Probab. **21**, 315.
Daniels, H. E., and T. H. R. Skyrme, 1985, Adv. Appl. Probab. **17**, 85.
da Silveira, R., 1998, Phys. Rev. Lett. **80**, 3157.
da Silveira, R., 1999, Am. J. Phys. **67**, 1177.
Diodati, P., F. Marchesoni, and S. Piazza, 1991, Phys. Rev. Lett. **67**, 2239.
Divakaran, U., and A. Dutta, 2007a, Phys. Rev. E **75**, 011109.
Divakaran, U., and A. Dutta, 2007b, Phys. Rev. E **75**, 011117.
Divakaran, U., and A. Dutta, 2007c, Int. J. Mod. Phys. **18**, 919.
Divakaran, U., and A. Dutta, 2008, Phys. Rev. E **78**, 021118.
Duxbury, P. M., and P. M. Leath, 1994, Phys. Rev. B **49**, 12676.
Erdös, P., and A. Rényi, 1959, Publ. Math. (Debrecen) **6**, 290.
Fazzini, P., 1991, *Basic Acoustic Emission*, Nondestructive Testing Monographs and Tracts Vol. 6, edited by W. J. McGonnagle (Gordon and Breach Science, New York).
Feller, W., 1966, *An Introduction to Probability Theory and Its Applications*, 2nd ed. (Wiley, New York), Vol. 1.
Fichter, W. B., 1969, Ph.D. Thesis (North Carolina State University).
Fisher, M. E., 1974, Rev. Mod. Phys. **46**, 597.
Garcimartín, A., A. Guarino, L. Bellon, and S. Ciliberto, 1997, Phys. Rev. Lett. **79**, 3202.
Golubović, L., and S. Feng, 1991, Phys. Rev. A **43**, 5223.
Gomez, J. B., D. Iniguesz, and A. F. Pacheco, 1993, Phys. Rev. Lett. **71**, 380.
Guarino, A., S. Ciliberto, A. Garcimartín, M. Zei, and R. Scorretti, 2002, e-print arXiv:cond-mat/0201257.
Guarino, A., A. Garcimartín, and S. Ciliberto, 1998, Eur. Phys. J. B **6**, 13.
Guarino, A., A. Garcimartín, and S. Ciliberto, 1999, Europhys. Lett. **47**, 456.
Guarino, A., R. Scorretti, and S. Ciliberto, 1999, e-print arXiv:cond-mat/9908329.
Guarino, A., L. Zei, R. Scorretti, and S. Ciliberto, 2006, J. Stat. Mech.: Theory Exp. **2006**, P06020.
Hansen, A., and P. C. Hemmer, 1994a, Trends Stat. Phys. **1**, 213.
Hansen, A., and P. C. Hemmer, 1994b, Phys. Lett. A **184**, 394.
Harlow, D. G., 1985, Proc. R. Soc. London, Ser. A **397**, 211.
Harlow, D. G., and S. L. Phoenix, 1978, J. Compos. Mater. **12**, 314.
Harlow, D. G., and S. L. Phoenix, 1981, Int. J. Fract. **17**, 601.
Harlow, D. G., and S. L. Phoenix, 1991, J. Mech. Phys. Solids **39**, 173.
Hedgepeth, J. M., 1961, Technical Report No. TND-882, NASA (unpublished).
Hedgepeth, J. M., and P. Van Dyke, 1967, J. Compos. Mater. **1**, 294.
Hemmer, P. C., and A. Hansen, 1992, ASME J. Appl. Mech. **59**, 909.
Hemmer, P. C., A. Hansen, and S. Pradhan, 2006, in *Modelling Critical and Catastrophic Phenomena in Geoscience: A Statistical Physics Approach*, edited by P. Bhattacharyya and B. K. Chakrabarti (Springer-Verlag, Berlin), Vol. 705, p. 27.
Hemmer, P. C., and S. Pradhan, 2007, Phys. Rev. E **75**, 046101.
Herrmann, H. J., and S. Roux, 1990, Eds., *Statistical Models for the Fracture of Disordered Media* (North-Holland, Amsterdam).
Hidalgo, R. C., K. Kovacs, I. Pagonbarraga, and F. Kun, 2008, Europhys. Lett. **81**, 54005.
Hidalgo, R. C., F. Kun, and H. J. Herrmann, 2001, Phys. Rev. E **64**, 066122.
Hidalgo, R. C., F. Kun, and H. J. Herrmann, 2002, Phys. Rev. E **65**, 032502.
Hidalgo, R. C., Y. Moreno, F. Kun, and H. J. Herrmann, 2002, Phys. Rev. E **65**, 046148.
Hidalgo, R. C., S. Zapperi, and H. J. Herrmann, 2008, J. Stat. Mech.: Theory Exp. **2008**, P01004.
Hild, F., J. M. Domergue, A. G. Evans, and F. A. Leckie, 1994, Int. J. Solids Struct. **31**, 1035.
Hild, F., and P. Feillard, 1997, Reliab. Eng. Syst. Saf. **56**, 225.
Hsueh, C. H., 1990, Mater. Sci. Eng., A **123**, 1.
Hsueh, C. H., 1992, Mater. Sci. Eng., A **154**, 125.
Ibnabdeljalil, M., and W. A. Curtin, 1997a, Acta Mater. **45**, 3641.
Ibnabdeljalil, M., and W. A. Curtin, 1997b, Int. J. Solids Struct. **34**, 2649.
Jo, J., H. Kang, M. Y. Choi, J. Choi, and B.-G. Yoon, 2008, J. Phys. A **41**, 145101.
Johnson, K. L., 1985, *Contact Mechanics* (Cambridge University Press, Cambridge).
Kachanov, M., 1985, Int. J. Fract. **28**, R11.
Karbhari, V., and H. Strassler, 2007, Dent. Mater. **23**, 960.
Kawamura, H., 2006, e-print arXiv:cond-mat/0603335.
Kim, B. J., 2004, Europhys. Lett. **66**, 819.
Kim, D.-H., B. J. Kim, and H. Jeong, 2005, Phys. Rev. Lett. **94**, 025501.
Kloster, M., A. Hansen, and P. C. Hemmer, 1997, Phys. Rev. E **56**, 2615.
Kun, F., M. H. Costa, R. N. Costa Filho, J. S. Andrade, Jr., J. B. Soares, S. Zapper, and H. J. Herrmann, 2007, J. Stat. Mech.: Theory Exp. **2007**, P02003.
Kun, F., R. C. Hidalgo, H. J. Herrmann, and K. F. Pal, 2003, Phys. Rev. E **67**, 061802.
Kun, F., R. C. Hidalgo, F. Raischel, and H. J. Herrmann, 2006, in *Modelling Critical and Catastrophic Phenomena in Geoscience: A Statistical Physics Approach*, edited by P. Bhattacharyya and B. K. Chakrabarti (Springer-Verlag, Berlin), Vol. 705, p. 57.
Kun, F., and S. Nagy, 2008, Phys. Rev. E **77**, 016608.
Kun, F., S. Zapperi, and H. J. Herrmann, 2000, Eur. Phys. J. B

17, 269.
Kuo, C. C., and S. L. Phoenix, 1987, J. Appl. Probab. **24**, 137.
Lagoudas, D. C., S. L. Phoenix, and C. Y. Hui, 1989, Int. J. Solids Struct. **25**, 45.
Landau, L., and E. M. Lifshitz, 1958, *Theory of Elasticity* (Clarendon, Oxford).
Landis, C. M., I. J. Beyerlein, and R. M. McMeeking, 2000, J. Mech. Phys. Solids **48**, 621.
Landis, C. M., and R. M. McMeeking, 1999, Compos. Sci. Technol. **59**, 447.
Lawn, B. R., 1993, *Fracture of Brittle Solids* (Cambridge University Press, Cambridge).
Layton, B. E., and A. M. Sastry, 2004, J. Biomech. Eng. **126**, 803.
Lee, W., 1994, Phys. Rev. E **50**, 3797.
Li, H., X. J. Jia, M. Geni, J. Wei, and L. J. An, 2006, Mater. Sci. Eng. **425**, 178.
Li, Y., and J. Metcalf, 2002, J. Mater. Civ. Eng. **14**, 303.
Lund, J. R., and J. P. Byrne, 2001, Civ. Eng. Environ. Syst. **18**, 243.
Måløy, K. J., and J. Schmittbuhl, 2001, Phys. Rev. Lett. **87**, 105502.
McCartney, L. N., and R. L. Smith, 1983, J. Appl. Mech. **50**, 601.
Mishnaevsky, L., Jr., 2007, *Computational Mesomechanics of Composites* (Wiley, New York).
Mishnaevsky, L., Jr., and P. Brøndsted, 2009, Comput. Mater. Sci. **44**, 1351.
Monette, L., 1994, Int. J. Mod. Phys. B **8**, 1417.
Moral, L., Y. Moreno, J. B. Gómez, and A. F. Pacheco, 2001, Phys. Rev. E **63**, 066106.
Moreno, Y., A. M. Correig, J. B. Gómez, and A. F. Pacheco, 2001, J. Geophys. Res. **106**, 6609.
Moreno, Y., J. B. Gómez, and A. F. Pacheco, 2000, Phys. Rev. Lett. **85**, 2865.
Moreno, Y., J. B. Gómez, and A. F. Pacheco, 2001, Physica A **296**, 9.
Moreno, Y., J. B. Gómez, and A. F. Pacheco, 2002, Europhys. Lett. **58**, 630.
Nechad, H., A. Helmstetter, R. El Guerjouma, and D. Sornette, 2005, J. Mech. Phys. Solids **53**, 1099.
Newman, W. I., and A. M. Gabrielov, 1991, Int. J. Fract. **50**, 1.
Newman, W. I., A. M. Gabrielov, T. A. Durand, S. L. Phoenix, and D. T. Turcotte, 1994, Physica D **77**, 200.
Newman, W. I., and S. L. Phoenix, 2001, Phys. Rev. E **63**, 021507.
Pauchard, L., and J. Meunier, 1993, Phys. Rev. Lett. **70**, 3565.
Peirce, F. T., 1926, J. Text. Ind. **17**, 355.
Petri, A., G. Paparo, A. Vespignani, A. Alippi, and M. Constantini, 1994, Phys. Rev. Lett. **73**, 3423.
Phoenix, S. L., 1978, Int. J. Fract. **14**, 327.
Phoenix, S. L., 1979, Adv. Appl. Probab. **11**, 153.
Phoenix, S. L., and R. L. Smith, 1983, Int. J. Solids Struct. **19**, 479.
Phoenix, S. L., and H. M. Taylor, 1973, Adv. Appl. Probab. **5**, 200.
Phoenix, S. L., and L. J. Tierney, 1983, Eng. Fract. Mech. **18**, 193.
Politi, A., S. Ciliberto, and R. Scorretti, 2002, Phys. Rev. E **66**, 026107.
Pomeau, Y., 1992, C. R. Acad. Sci., Paris **314**, 553.
Pradhan, S., P. Bhattacharyya, and B. K. Chakrabarti, 2002, Phys. Rev. E **66**, 016116.
Pradhan, S., and B. K. Chakrabarti, 2001, Phys. Rev. E **65**, 016113.
Pradhan, S., and B. K. Chakrabarti, 2003a, Int. J. Mod. Phys. B **17**, 5565.
Pradhan, S., and B. K. Chakrabarti, 2003b, Phys. Rev. E **67**, 046124.
Pradhan, S., and B. K. Chakrabarti, 2005, in *Nonequilibrium Phenomena in Plasmas*, edited by A. S. Sharma and P. K. Kaw (Springer, Dordrecht), p. 293.
Pradhan, S., and B. K. Chakrabarti, 2006, in *Modelling Critical and Catastrophic Phenomena in Geoscience: A Statistical Physics Approach*, edited by P. Bhattacharyya and B. K. Chakrabarti (Springer-Verlag, Berlin), Vol. 705, p. 459.
Pradhan, S., B. K. Chakrabarti, and A. Hansen, 2005, Phys. Rev. E **71**, 036149.
Pradhan, S., and A. Hansen, 2005, Phys. Rev. E **72**, 026111.
Pradhan, S., A. Hansen, and P. C. Hemmer, 2005, Phys. Rev. Lett. **95**, 125501.
Pradhan, S., A. Hansen, and P. C. Hemmer, 2006, Phys. Rev. E **74**, 016122.
Pradhan, S., and P. C. Hemmer, 2007, Phys. Rev. E **75**, 056112.
Pradhan, S., and P. C. Hemmer, 2008, Phys. Rev. E **77**, 031138.
Pradhan, S., and P. C. Hemmer, 2009, Phys. Rev. E **79**, 041148.
Press, W. H., S. A. Teukolsky, W. T. Vetterling, and B. P. Flannery, 1992, *Numerical Recipes in Fortran 77: The Art of Scientific Computing* (Cambridge University Press, Cambridge).
Räisänen, V. I., M. J. Alava, K. J. Niskanen, and R. M. Nieminen, 1997, J. Mater. Res. **12**, 2725.
Raischel, F., F. Kun, and H. J. Herrmann, 2006, Phys. Rev. E **74**, 035104.
Roux, S., 2000, Phys. Rev. E **62**, 6164.
Roux, S., and A. Hansen, 1990, Europhys. Lett. **11**, 37.
Roux, S., and F. Hild, 2002, Int. J. Fract. **116**, 219.
Sahimi, M., 2003, *Heterogeneous Materials II: Nonlinear and Breakdown Properties* (Springer-Verlag, Berlin).
Sahimi, M., and S. Arbabi, 1992, Phys. Rev. Lett. **68**, 608.
Sahimi, M., and S. Arbabi, 1996, Phys. Rev. Lett. **77**, 3689.
Sastry, A. M., and S. L. Phoenix, 1993, J. Mater. Sci. Lett. **12**, 1596.
Schmittbuhl, J., and K. J. Måløy, 1997, Phys. Rev. Lett. **78**, 3888.
Scholz, C. H., 2002, *The Mechanics of Earthquakes and Faulting* (Cambridge University Press, Cambridge).
Scorreti, R., S. Ciliberto, and A. Guarino, 2001, Europhys. Lett. **55**, 626.
Scott, I. G., 1991, *Basic Acoustic Emission*, Nondestructive Testing Monographs and Tracts Vol. 6, edited by W. J. McGonnagle (Gordon and Breach Science, New York).
Si, Z., D. N. Little, and R. L. Lytton, 2002, J. Mater. Civ. Eng. **14**, 461.
Smith, R. L., 1980, Proc. R. Soc. London, Ser. A **372**, 539.
Smith, R. L., and S. L. Phoenix, 1981, J. Appl. Mech. **48**, 75.
Sørensen, B. F., and T. K. Jacobsen, 1998, Composites, Part A **29**, 1443.
Sørensen, B. F., and T. K. Jacobsen, 2000, Plast. Rubber Compos. **29**, 119.
Sornette, D., 1989, J. Phys. A **22**, L243.
Sornette, D., 1992, J. Phys. I **2**, 2089.
Sornette, D., 2000, *Critical Phenomena in Natural Sciences* (Springer-Verlag, Berlin).
Sornette, D., T. Magnin, and Y. Brechet, 1992, Europhys. Lett. **20**, 433.
Stanley, H. E., 1987, *Introduction to Phase Transition and Criti-*

cal Phenomena (Oxford University Press, Oxford).
Stauffer, D., and A. Aharony, 1994, *Introduction to Percolation Theory* (Taylor & Francis, London).
Stinchcombe, R. B., 2005, Physica A **346**, 1.
Suresh, S., 1991, *Fatigue of Materials* (Cambridge University Press, Cambridge).
Toffoli, S. M., and R. L. Lehman, 2001, J. Am. Ceram. Soc. **84**, 123.
Turcotte, D. L., and M. T. Glassco, 2004, Tectonophysics **383**, 71.
Wagner, H. D., and A. Eitan, 1993, Compos. Sci. Technol. **46**, 353.
Watts, D. J., and S. H. Strogatz, 1998, Nature (London) **393**, 440.
Xia, Z. H., and W. A. Curtin, 2001, Compos. Sci. Technol. **61**, 2247.
Xia, Z. H., W. A. Curtin, and T. Okabe, 2002, Compos. Sci. Technol. **62**, 1279.
Yoshioka, N., F. Kun, and N. Ito, 2008, Phys. Rev. Lett. **101**, 145502.
Zapperi S., P. Ray, H. E. Stanley, and A. Vespignani, 1997, Phys. Rev. Lett. **78**, 1408.
Zapperi, S., P. Ray, H. E. Stanley, and A. Vespignani, 1999a, Phys. Rev. E **59**, 5049.
Zapperi, S., P. Ray, H. E. Stanley, and A. Vespignani, 1999b, Physica A **270**, 57.
Zhang, S. D., and E. J. Ding, 1994, Phys. Lett. A **193**, 425.
Zhang, S. D., and E. J. Ding, 1995, J. Phys. A **28**, 4323.
Zhang, S. D., and E. J. Ding, 1996, Phys. Rev. B **53**, 646.
Zheng, J. F., Z.-Y. Gao, X.-M. Zhao, and B.-B. Fu, 2008, Int. J. Mod. Phys. C **19**, 1727.
Zhou, S. J., and W. A. Curtin, 1995, Acta Metall. Mater. **43**, 3093.
Zhou, X. F., and H. D. Wagner, 1999, Compos. Sci. Technol. **59**, 1063.
Zhou, X. F., and H. D. Wagner, 2000, Compos. Sci. Technol. **60**, 367.